Effects of Duct Lip Shaping and Various Control Devices on the Hover and Forward Flight Performance of Ducted Fan UAVs

by

Will E. Graf

Thesis submitted to the faculty of
Virginia Polytechnic Institute and State University
in partial fulfillment of the requirements for the degree of

Master of Science
in
Aerospace Engineering

Approved by:

Wing F. Ng, Committee Co-Chairman
William H. Mason, Committee Co-Chairman
William J. Devenport

May 13, 2005
Blacksburg, Virginia

Keywords: ducted fan, UAV, duct lip shaping, control vanes, control effectors, stabilizer vanes, aerodynamics

Effects of Duct Lip Shaping and Various Control Devices on the Hover and Forward Flight Performance of Ducted Fan UAVs

by:

Will E. Graf

(ABSTRACT)

The military's desire for ducted fan vertical takeoff and landing (VTOL) unmanned aerial vehicles (UAVs) stems from the vehicles' relatively small size, safety in tight quarters, increased payload capacity for their size, and their ability to hover for surveillance missions. However, undesirable aerodynamic characteristics are associated with these vehicles in crosswinds, namely momentum drag and asymmetric duct lift.

Because the duct itself, and not the fan, is the root cause of these unfavorable aerodynamic attributes, various lip shapes were tested to determine the effects of leading edge radius of curvature and duct wall thickness. It was found that a lip with a small leading edge radius performed best in forward flight and crosswind conditions, while the performance of a lip with a large leading edge radius was enhanced in static conditions. Through tuft flow visualization and static pressure measurements it was determined that the reason for the difference in performance between the two lips was due to flow separation on the interior of the duct lip surface.

Control vanes positioned aft of the duct were tested as the primary attitude control for the vehicle. An empirical control vane model was created based on the static data for the control vanes, and it was applied to wind tunnel test results to determine the required control vane angle for trim. Wind tunnel testing showed the control vanes were capable of trimming out the adverse pitching moment generated by the duct, but at some flight speeds large vane deflections were necessary. Additional control devices placed at the lip of the duct and stabilizer vanes positioned aft of the duct were tested to reduce the amount of control vane deflection required for trim. It was found that the duct deflector control effector had the largest impact on the adverse pitching moment, while the stabilizer vanes were only effective at low crosswind velocities.

Acknowledgements

I would like to thank first my family, Mom, Dad, Ben, and Luke. Without your support through my life I would have never gotten as far as I have. I am forever in debt for the help you gave me, the lessons you taught me, and the love you showed me.

Just as important in my life is the one that will always have a special place in my heart, Liz. Though the past two years apart have been hard on both of us, you have supported and encouraged me, and even though I wish we could have spent more time together during the past two years, I feel we are stronger because of it.

I would also like to thank Jon Fleming for the tremendous amount of support and knowledge he has bestowed upon me. I consider my experiences at Techsburg invaluable, and I am grateful for the time he spent guiding me through this project. To Troy Jones, I also owe my thanks for his tremendous help in getting me started and teaching me the basics.

In addition, I would like to thank my advisors, Dr. Mason and Dr. Ng. Without their support and guidance, I would have been lost. Dr. Mason, your knowledge is endless, and I hope to be able to tap into it in the future. Dr. Ng, you knew all the right questions to ask to guide me through this project, and I cannot thank you enough for the opportunity to participate in such an exciting program as the ducted fan VTOL UAV.

Table of Contents

List of Figures

List of Tables

List of Symbols

A_e	Duct exit area; *ft^2*
C_T	Coefficient of thrust
C_{Tref}	Reference coefficient of thrust
c	Duct airfoil chord length; *ft*
D	Drag force, F_x in wind axis system; *lbs*
D_m	Momentum drag force; *lbs*
d	Duct inner diameter; *ft*
F_x, F_z	Vehicle forces in body axis system; *lbs*
J	Advance ratio
L	Lift force, F_z in wind axis system; *lbs*
$\dot{m}_{duct}$	Duct mass flow; *slugs/sec*
M_y	Vehicle pitching moment, referenced to duct lip; *ft-lbs*
n	Fan speed; *rpm*
n_{ref}	Fan speed at $T=T_{ref}$; *rpm*
P	Motor power; *hp*
P_{ref}	Reference motor power; *hp*
T	Vehicle thrust; *lbs*
T_{ref}	Vehicle reference thrust; *lbs*
t_w	Duct wall thickness; *ft*
V_e	Duct exit velocity; *ft/sec*
V_x, V_z	Air velocity in body axis system; *ft/sec*
x_b, y_b, z_b	Body coordinate system
x_w, y_w, z_w	Wind coordinate system
z_{cp}	Center of pressure location, positive above duct lip; *ft*
α	Vehicle angle of attack; *degrees*
β	Vehicle sideslip angle; *degrees*
θ	Vehicle pitch angle; *degrees*
ρ	Air density; *$slugs/ft^3$*
ρ_{LE}	Duct leading edge radius of curvature; *ft*
ψ	Vehicle heading angle; *degrees*

Chapter 1: Introduction

The Army's desire for improved awareness in combat situations has led to research into small, ducted fan, vertical takeoff and landing (VTOL) unmanned aerial vehicles (UAVs) that can provide a small group of soldiers with a bird's-eye view of the battlefield. As surveillance vehicles these UAVs can be sent into a hostile city or over the next hill to see what lies beyond and can be loaded with the latest in camera and sensing technology to report the most accurate information back to the soldier.

Currently the military is using many remotely-operated UAVs in fixed-wing aircraft configurations, but these lack the ability to hover in place and often require specialized launch and recovery techniques that may limit their mobility and readiness. Ducted fan UAVs can take off and land vertically, as well as hover in one location, providing surveillance data continuously over a single area or target. The use of a ducted fan has been selected as one of the preferred propulsion solutions for these aircraft because of safety in tight quarters as well as improved payload capacities for a given vehicle size.

The duct diameter of these vehicles currently ranges from less than 12 inches (small enough to fit in a soldier's backpack) to over 2.5 feet (transported in the back of a jeep). Although not a UAV, an early attempt at using a ducted fan in hover and forward flight for military operations was the Hiller Flying Platform[1]. The Hiller Flying Platform, shown in Figure 1-1a, was a response to a request from the Office of Naval Research for VTOL concepts in the mid-1950s. Designed to carry one soldier, it had a six-foot diameter duct with two counter-rotating propellers to eliminate torque, each driven by a 44-hp two-stroke piston engine. The pilot flew the craft by shifting his weight in the direction he wished to fly and varying the engine throttle. Despite successful hover test flights in calm weather conditions, the program ended because of limitations in the forward flight performance of the vehicle. Utilizing similar designs, research continued in the area of ducted fan aerodynamics, particularly striving for a solution to the adverse pitching moment that limited the vehicle's forward flight performance[1,2,3].

An early ducted fan VTOL UAV concept to have some success was the Airborne Remotely Operated Device (AROD). Built for the United States Marine Corps by Sandia National Laboratories in the 1980s, it was designed for short range surveillance without the need for a large communications tracking van. A 26-hp, 2-stroke, 2-cylinder, gasoline engine powered a

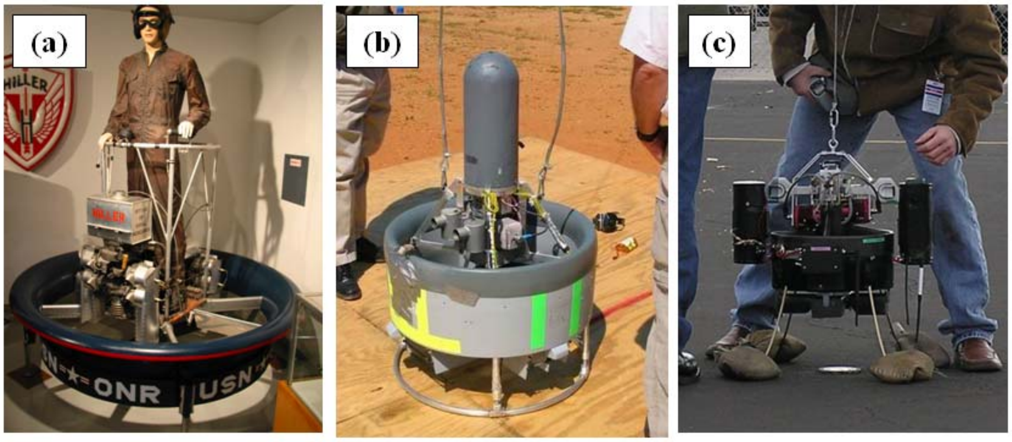

Figure 1-1: Examples of ducted fan vehicles: (a) Hiller Flying Platform, (b) iSTAR, (c) Honeywell MAV.

single 24-inch diameter, 3-bladed fan. Through its onboard attitude sensors and stabilization computer, AROD achieved stable hover, as well as multi-directional translation[2,4,5]. More information on stability control for AROD can be found in White, et. al.[6].

Another successful VTOL UAV utilizing a ducted fan was the Moller Aerobot. Various versions of the Aerobot have been built with duct diameters of 20 and 24 inches. Engines have ranged from a 10-hp, two-stroke engine with a 15- lb payload capacity to a 100-hp rotary engine capable of lifting 650 lb. Cameras and sensors can be attached to the UAV, giving the Aerobot a wide variety of mission profiles, one of which was in a proposed bridge inspection role[2,7,8,9].

Both the iSTAR (Figure 1-1b) and Honeywell MAV (Micro Air Vehicle) (Figure 1-1c) programs are similar to the AROD program in mission profile but are much more recent. The iSTAR was built by Allied Aerospace and Honeywell and was designed to hover as well as transition to forward flight. Lipera, et. al.[10]. provides more information on the iSTAR program, which is still in development by Allied Aerospace. The Honeywell MAV concept is still in the design and testing process, and it is this program, in cooperation with the Unites States Army, upon which the research presented here is based. The Honeywell MAV is designed to be small enough to be transported in a soldier's backpack, so not only does it need to be lightweight, it has to be durable enough to withstand the rigors of the battlefield. The duct provides protection for the soldier from the rotor blades as well as augmenting the thrust provided by the fan to allow a larger payload to be lifted with a smaller fan diameter. Its ability to hover gives the vehicle VTOL capabilities, which simplifies the soldier's role in operating one of these vehicles.

The above mentioned ducted fan VTOL aircraft are by no means the only vehicles in this category. Many other similar vehicles exist with similar goals in mind, such as the Sikorsky Cypher and the MASS Helispy. Only a few have been mentioned here to provide the reader with an idea of the use of ducted fans in past and present unmanned VTOL aircraft concepts.

Primarily designed to be autonomous aerial robots, ducted fan UAVs need to be capable of flight in a wide range of atmospheric conditions, especially gusty winds. Maintaining vehicle attitude and position control despite wind gusts is a key issue facing the designers of these aircraft, and current research is focused on improved understanding of ducted fan aerodynamics in forward flight. The research presented here investigates two key areas in the performance and control of ducted fan vehicles: duct lip aerodynamics and the effectiveness of various control devices on vehicle performance. More specifically, this research focuses on the pitch characteristics of the vehicle, as opposed to the roll and yaw characteristics, because of the large adverse pitching moment generated by the duct, as will be discussed in more detail later.

As Kruger[11] has explained, the duct lip geometry is very influential in the overall duct aerodynamic characteristics. Small changes in the lip design can determine if the lip flow remains attached, which could potentially cause a large adverse pitching moment, or separates, reducing the total thrust and increasing the required power. Grundwald, et. al.[12] has shown that most of the adverse pitching moment is carried by the duct as opposed to the fan, and so the emphasis should be placed on duct lip design. Graf, et. al.[13] summarized the results presented here for the duct lip testing.

Duct lip shaping alone is not sufficient to maintain controlled flight in adverse conditions. Control vanes placed in the duct jet aft of the duct perform the essential role of controlling vehicle attitude, both in forward flight and maintaining position in changing crosswinds. The location of the control vanes can be seen in Figure 1-2. Unfortunately, trimmed control vane deflection angles can become quite large during these two flight regimes, reducing the ability of the vehicle to react to further changes in environmental conditions.

As a result, additional control devices are necessary to alleviate the load placed on the control vanes and provide the vehicle with another means of attitude control. Due to the importance of the duct lip suction, these auxiliary control effectors are placed at or near the duct lip to influence the lift produced by the duct, as shown in Figure 1-2. However, that is not always the case. On the Aerobot, Moller[9] used troughs at the duct trailing edge to divert the airflow from the fan and

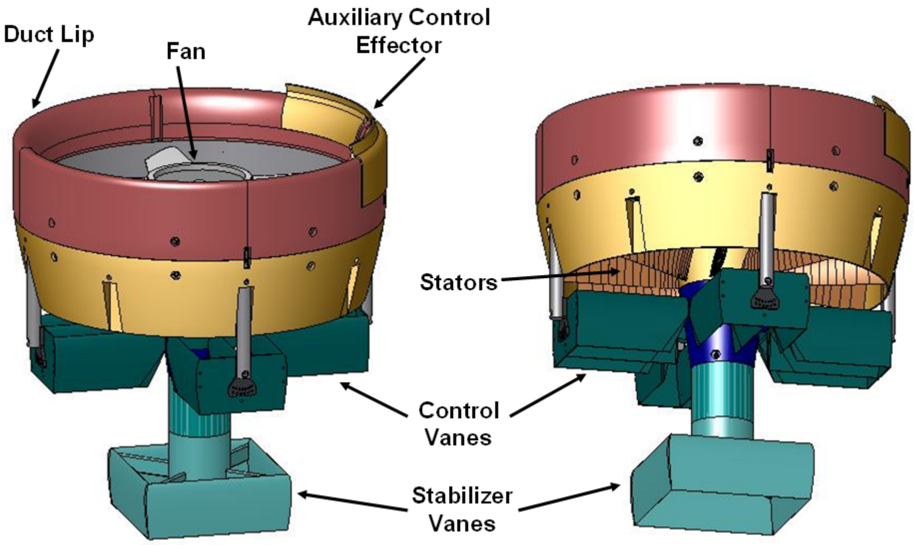

Figure 1-2: CAD image showing the location of the control vanes, auxiliary control effectors, and stabilizer vanes in relation to each other.

provide additional control. Depending on whether the goal of the device is to produce more lift or spoil the lift already being produced by the duct lip, the auxiliary control effectors can be placed on either the leeward or windward side of the duct to improve the aerodynamic characteristics. These devices would theoretically be actuated, similar to the control vanes, and only used when necessary. Unfortunately, the additional actuation components contribute to the overall weight of the vehicle, thus requiring the ducted fan to provide more thrust to maintain hover. This becomes more difficult when the vehicle is using the auxiliary control effectors to reduce lift on portions of the duct.

Therefore a passive (non-actuated) device placed aft of the duct could improve the controllability of the vehicle without adding excessive weight. This stabilizer vane (Figure 1-2) would work by utilizing the bending of the duct jet in a crosswind to generate an additional force to counter the adverse pitching moment. One of the major drawbacks, though, is the inability to adjust the amount of influence the stabilizer vane contributes as the aerodynamic conditions change.

Unfortunately, the effects of duct lip shaping and the various control effectors on the flight characteristics of ducted fans is not well understood. Therein lies the objective of the current research: to improve the design of ducted fan UAVs by gaining a better understanding of the effects of various components, including the duct lip, control vanes, auxiliary control effectors, and stabilizer vanes, on ducted fan aerodynamics. Further, based on the results presented here, a recommended configuration for a ducted fan VTOL UAV can be developed.

Chapter 2: Ducted Fan Aerodynamics

The following chapter provides the reader with a background in the aerodynamics of ducted fans and the purpose of this research. Even though ducted fans hold distinct advantages over free-air propellers, the adverse characteristics associated with ducted fans prevent them from being as widely incorporated in aircraft designs as conventional propellers.

2.1 Advantages of Ducted Fans Over Free-Air Propellers

Physically, the duct acts as a shroud to protect objects and personnel from the spinning blades of the fan[12,14]. This is particularly useful when launching and recovering the UAVs. The AROD in particular required assistance from military personnel to guide it to the ground when landing to prevent it from tipping over[5].

Aerodynamically, significant performance gains can be obtained by using a ducted fan. Assuming small tip gaps between the tips of the fan blades and the wall of the duct, the loading on the blades is allowed to extend to the tips, reducing tip losses associated with free-air propellers. The reduction in tip losses further reduces the noise level, which is particularly appealing to the military when using these vehicles in a surveillance role[2,5]. Depending on the duct lip shape, a significant amount of the load can be carried by the duct, reducing the load on the blades and allowing the fan to operate much more efficiently than if the duct was not present[15,16]. Even though the fan produces less thrust than one of the same diameter in free air, the combination of the duct and fan is capable of producing nearly twice the static thrust. This can be explained theoretically by examining the slipstream contractions of both a ducted fan and a free-air propeller. As shown in Figure 2-1, the presence of the duct significantly reduces the slipstream contraction, allowing a larger mass flow through the propeller disk and over the duct lip[16]. An open rotor relies on the pressure differential across the rotor to generate thrust, while the ducted fan relies on the amount of air moving through the duct. In fact, the pressure at the exit of the duct is very nearly atmospheric pressure, preventing the slipstream from contracting to the degree seen in open rotors. Because of the increased mass flow, the ducted fan inner diameter need be only 50% to 60% of an open rotor for the same static thrust requirements[16,17]. Unfortunately more power is required for a ducted fan than an open rotor[18].

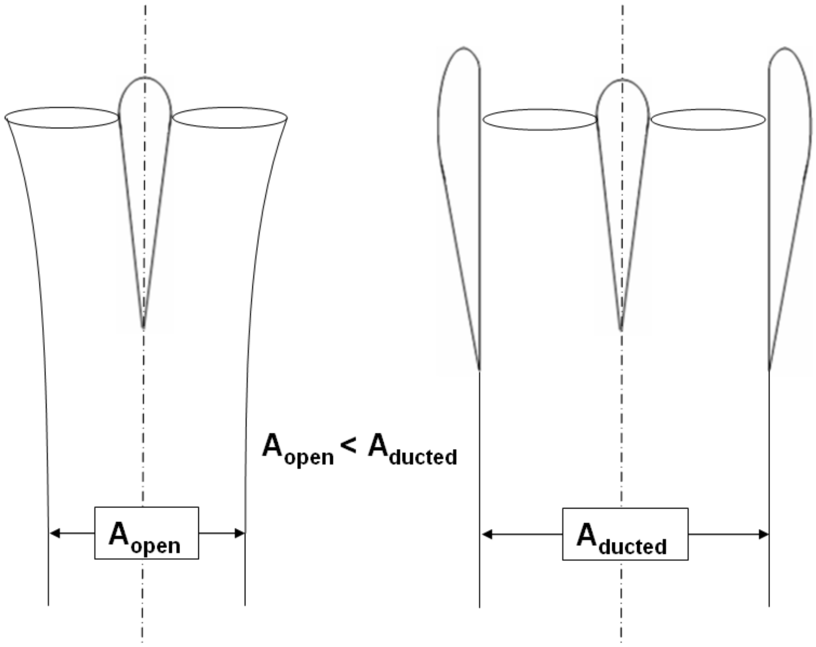

Figure 2-1: The slipstream contraction associated with open propellers is not nearly as large using ducted fans.

2.2 Adverse Characteristics of Ducted Fans

In order for a ducted fan UAV to be practical, it must be capable of hovering in place as well as pitching down to attain forward flight. Unfortunately, a ducted fan typically has atypical, adverse aerodynamic characteristics, such as momentum drag and asymmetric lift, that are particularly critical when hovering in windy conditions. Figure 2-2 shows a CAD image of the ducted fan model used for this testing and the coordinate systems that describe the forces and moments of interest. The body-axis coordinate system, which defines the thrust vector, remains

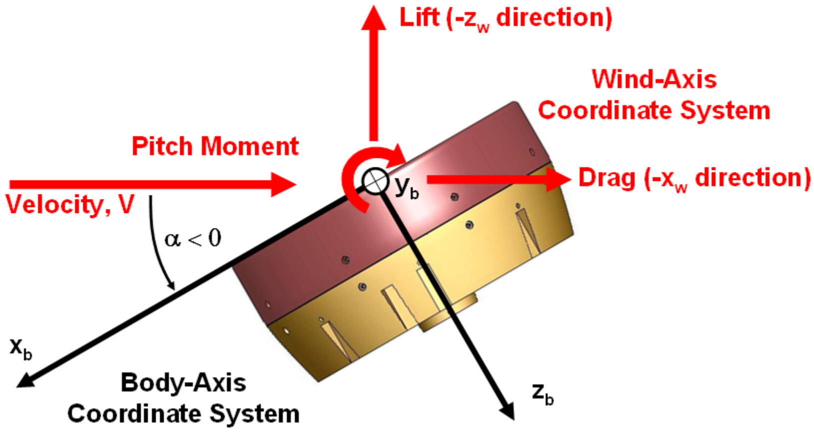

Figure 2-2: CAD image of baseline model with definitions of the coordinate systems used.

fixed to the duct, while the wind-axis coordinate system, which defines lift and drag, is associated with the direction of the freestream air, *V*. Note that $\alpha = 0°$ when the vehicle is in hover, and the angle of attack becomes negative as it transitions to forward flight. This convention is typical of other hovering aircraft, such as helicopters.

2.2.1 Momentum Drag

As described in Fleming, et. al.[19], momentum drag, also referred to as ram drag, is the result of the duct and rotor changing the direction, and thus momentum, of the freestream air, as shown in Figure 2-3. To conserve momentum, a force acting at the center of pressure of the turning stream of air must be applied. The ram drag center of pressure is most likely above the center of gravity of the vehicle, which is typically at or slightly below the lip of the duct, creating a positive pitching moment. It is important to reduce this component of the overall drag since it makes up a large percentage of the total drag generated by the vehicle. In addition, the positive pitching moment from the momentum drag force rotates the duct so the thrust vector points in the same direction the wind is blowing, further reducing the ability of the UAV to maintain position in windy conditions. This problem is minimized for open rotors because there is no duct to constrain the flow. For ducted fans the key to reducing the effect of the momentum drag on

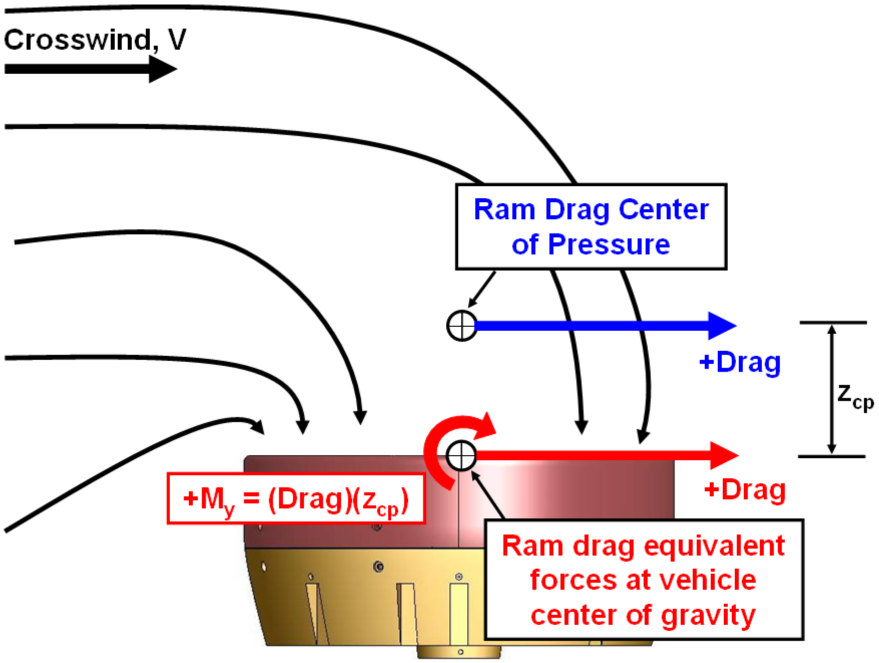

Figure 2-3: Ram drag force acting at the center of pressure in a crosswind, resulting in a positive pitching moment.

the pitching moment is to reduce the distance between the vehicle center of gravity and the center of pressure. By raising the center of gravity closer to the location of the center of pressure or vice versa, the moment arm is reduced and the momentum drag has less effect on the pitching moment. AVID LLC has performed an analysis on the effects of the center of pressure location on the vehicle trimmed tilt angle vs. velocity and the trimmed control vane deflection vs. velocity. A summary of the analysis can be found in Graf, et. al.[13]

In hover ($\alpha = 0^{o}$), the momentum drag can be estimated by considering the mass flow rate through the duct and the crosswind velocity, as shown in Equation (2-1)[13]. Naturally, in static conditions (no crosswind), the momentum drag is zero.

$$D_m = \dot{m}_{duct} V_x = \rho A_e V_e V_x \tag{2-1}$$

V_x represents the air velocity in the x-direction of the vehicle's body axis coordinate system. In hover ($\alpha = 0°$) the crosswind velocity and V_x are the same, but as the vehicle tilts into the wind ($\alpha < 0°$) V_x decreases as compared to the crosswind velocity. In the same manner as Equation (2-1) was derived, the total thrust generated by the vehicle in static conditions can be estimated using the momentum flux through the duct[13],

$$T = \rho A_e V_e^2 . \tag{2-2}$$

Solving for the duct exit velocity in Equation (2-2) and plugging into Equation (2-1) results in an equation to estimate the momentum drag,

$$D_m = V_x \sqrt{T \rho A_e} . \tag{2-3}$$

Note the dependence of the momentum drag on the crosswind velocity and the vehicle thrust.

2.2.2 Asymmetric Lift

The asymmetric lift distribution around the duct lip can be viewed as the physical mechanism behind the momentum drag effects. In hover and zero crosswind, the fan draws in air from all sides of the duct evenly, creating a symmetric pressure distribution around the lip (Figure 2-4a). However, in a crosswind or forward flight, the forces required to turn the flow into the duct generate a lower pressure region on the windward side of the duct as compared to the leeward side, resulting in more lift on the windward side, as shown schematically in Figure 2-4b. Figure 2-5 shows a CFD analysis of an isolated duct in a 20-knot crosswind, showing the velocity contours and the increase in flow speed on the windward lip, which corroborates the forces and

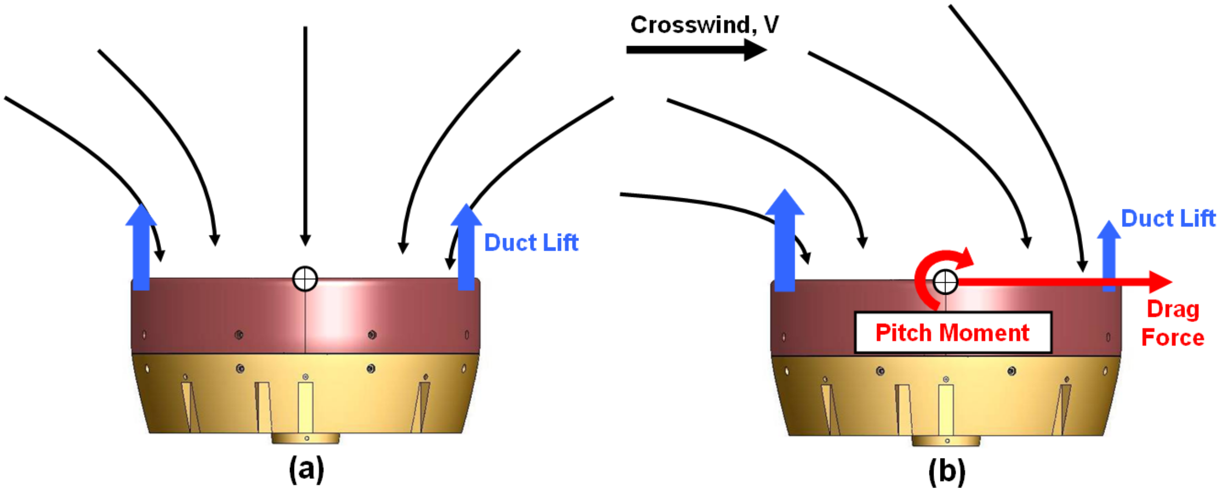

Figure 2-4: (a) Symmetric lift in zero crosswind. (b) Asymmetric lift in crosswind (V > 0) and resulting forces and moments.

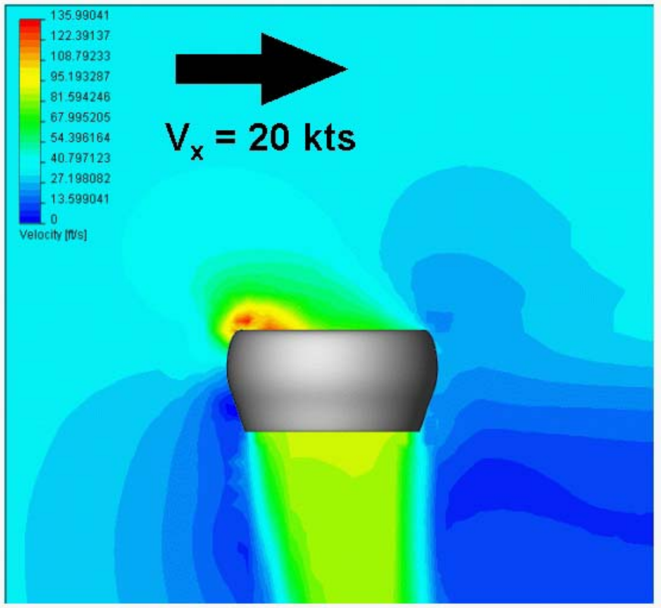

Figure 2-5: Results from simple CFD analysis (FloWorks) for an isolated ducted fan at α = 0° and V_x = 20 knots (~34 ft/s), showing velocity contours ranging from 0 to 136 ft/s.

moments shown in Figure 2-4. Also, if the vehicle is rotated into the wind, the asymmetric flow into the duct causes the windward side to be at a higher angle of attack than the leeward side, further increasing the asymmetry of the lift distribution[14]. The difference in lift on the windward and leeward sides creates a positive pitching moment and reduces the ability of the UAV to tilt downward and achieve steady forward flight despite the use of control vanes aft of the duct.

At this time, a note regarding the CFD analysis should be made. FloWorks and ADPAC were used to generate the CFD results presented here, but the analysis was not performed by this author. The CFD results are presented here only as a clarification to the reader as to the general flowfield around the ducted fan in a qualitative sense.

A common misconception with ducted fans is that the fan generates a favorable pressure gradient on the interior of the duct lip, preventing separation from occurring. However, a suction peak actually occurs on the interior of the duct lip near the leading edge, as shown by the velocity contours in Figure 2-6, after which the flow sees an adverse pressure gradient and has a greater tendency to separate, depending on the shape of the duct lip and the suction pressures that it can sustain. Flow separation is not necessarily undesirable because the decrease in lift caused by the flow separation reduces the asymmetry in the lift distribution around the duct lip, which reduces the pitching moment generated by the duct[14].

In summary, the ducted fan has some advantages over an open rotor, namely a reduction in tip losses and increased thrust for the same size rotor. However, the disadvantages of using a ducted fan include momentum drag and asymmetric lift, both of which generate a positive, adverse pitching moment, preventing the vehicle from achieving steady forward flight. Unfortunately these disadvantages keep the ducted fan from being widely accepted as a reliable means of propulsion of small VTOL aircraft. Therefore the development of methods to reduce the impact of momentum drag and asymmetric lift on the flight characteristics of ducted fans will allow the advantages of ducted fans to shine through, such as lifting a larger payload while maintaining a relatively small size. The methods that will be examined here are duct lip shaping and various control devices to gain a better understanding of their effects on the overall vehicle aerodynamics.

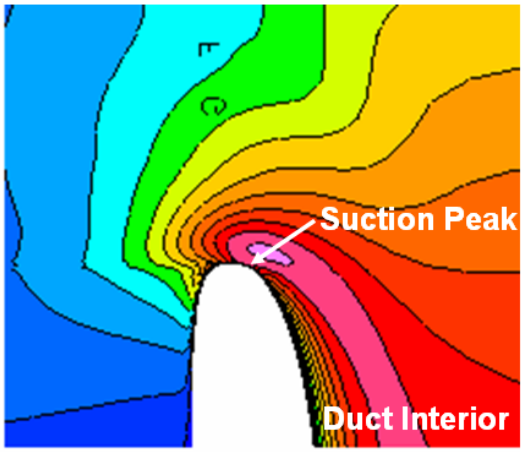

Figure 2-6: CFD results (ADPAC) showing air flow velocity magnitude contours for the Baseline lip in static conditions. The suction peak occurs on the interior of the lip near the leading edge.

Chapter 3: Experimental Methods

Descriptions of the model used during testing and the various duct lip geometries, control vanes, auxiliary control effectors, and stabilizer vanes tested specifically for this research are presented in this chapter. Also included are descriptions of the static and wind tunnel testing.

3.1 Model Description

The model used in this testing was from an existing model being used in the development of the Honeywell MAV UAV (Figure 1-1c). The model consisted of an aluminum ring frame, to which the duct components were attached, as shown in Figure 3-1. The duct was made using rapid prototyping from SLA resin to allow for quick fabrication and to keep the weight of the model low. The model had removable lip sections so that various geometries could be easily switched out and tested. The propulsion consisted of a 5-bladed fan designed by AVID LLC and built using rapid prototyping of a high tensile strength material. The fan was powered by a MOOG G402-1006A electric motor capable of spinning at 8500 rpm and providing 2.5 ft-lbs of torque (about 4 hp). It was controlled by a MOOG T200-610 controller. The tip clearance between the tips of the fan blades and the duct wall was about 0.050 in. to avoid rubbing problems caused by shaft vibration and blade elongation at maximum rpm settings.

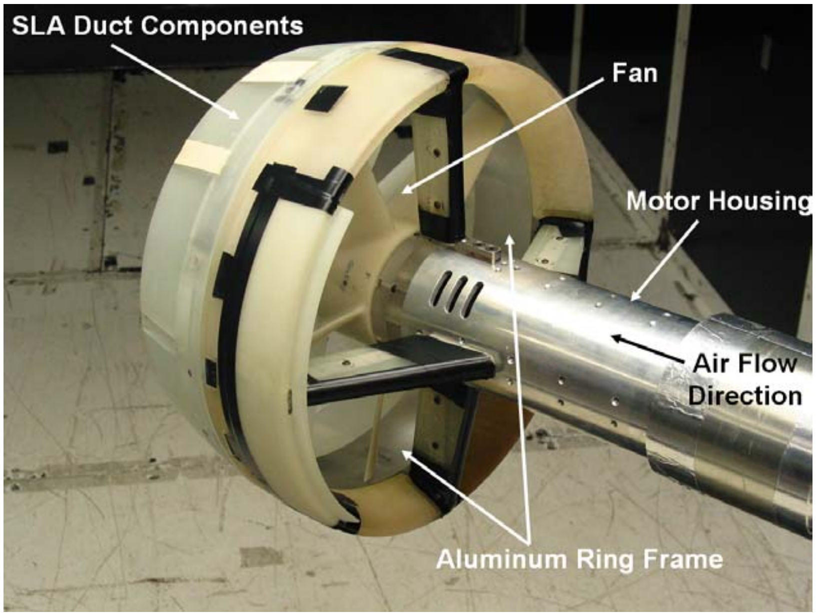

Figure 3-1: Ducted fan UAV model shown in wind tunnel setup.

3.2 Duct Lip Geometries

Five duct lip shapes were examined during testing, and their profiles can be seen in Figure 3-2. The geometries of the duct lip shapes can be described by two characteristics: wall thickness (t_w) and leading edge radius of curvature (ρ_{LE}). As Figure 3-3 illustrates, wall thickness is the maximum thickness of the airfoil shape used to make up the wall of the duct, and the leading edge radius of curvature describes the roundness of the duct lip. Table 1 shows the values of these geometry characteristics for each lip shape. The testing presented here is not a detailed optimization study of duct lip geometry. Instead, it examines relatively large changes in lip shape to determine, in a general sense, the effects of duct lip shaping on the flight characteristics of ducted fans.

The primary purpose of changing the duct lip geometry is to control flow separation on the interior of the lip. The Baseline lip shape was designed to have a relatively small leading edge radius with the leading edge near the exterior of the profile to allow more room for the pressure gradient to change gradually. The Enlarged lip was designed to increase the wall thickness without increasing the duct external dimensions, as well as increase the leading edge radius of curvature of the Baseline lip. The step was necessary to allow for the same physical diameter fan, and it was assumed the small reduction in effective fan diameter would not affect the results since the pitching moment is primarily generated by the duct and not the fan, as stated earlier. The Elliptical and Circular Arc lip shapes were designed to test the two extremes of leading edge

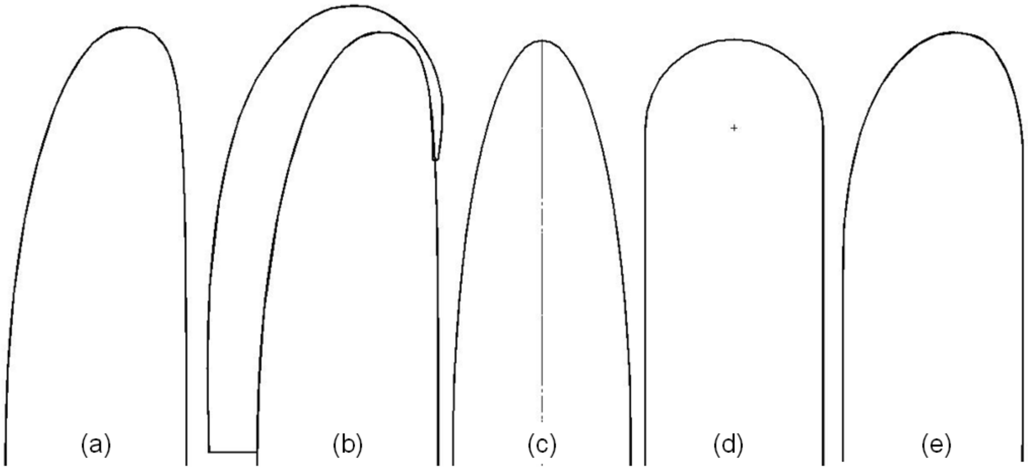

Figure 3-2: Duct lip shape profiles include (a) Baseline, (b) Enlarged, (c) Elliptical, (d) Circular Arc, and (e) Revised. The left side of each lip corresponds to the interior of the duct.

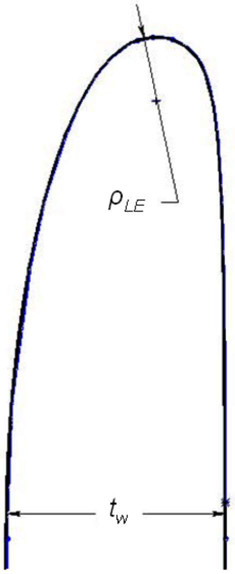

Figure 3-3: Duct lip geometry characteristics and their associated symbols.

Table 1: Duct lip geometry values for each lip shape. All dimensions presented in fraction of duct airfoil chord length

	t_w/c	ρ_{LE}/c
Baseline	0.125	0.0365
Enlarged	0.158	0.0553
Elliptical	0.125	0.0157
Circular Arc	0.125	0.0625
Revised	0.125	0.0375

radius of curvature. Finally, the Revised lip shape was designed to have a leading edge radius between the Baseline and Enlarged lips while maintaining the wall thickness of the Baseline lip.

3.3 Control Vanes

Four, 3-bladed control vanes were used as the primary attitude control devices on the vehicle. The 3 blades making up each control vane created a large amount of surface area to generate the required forces and moments to control the vehicle without reducing the spacing between the blades to the extent where interference and reduced effectiveness would occur. Positioned just aft of the trailing edge of the duct, as shown in Figure 3-4, they could be individually rotated from -30 degrees to +30 degrees in 5-degree increments. For the testing presented here, only the pitch vanes were used (the top and bottom vanes in Figure 3-4), and they were deflected collectively. Vane deflection angles were set manually and held in position with a pin that screwed in place. A NACA 0014 was used for the control vane cross-sectional geometry, and an

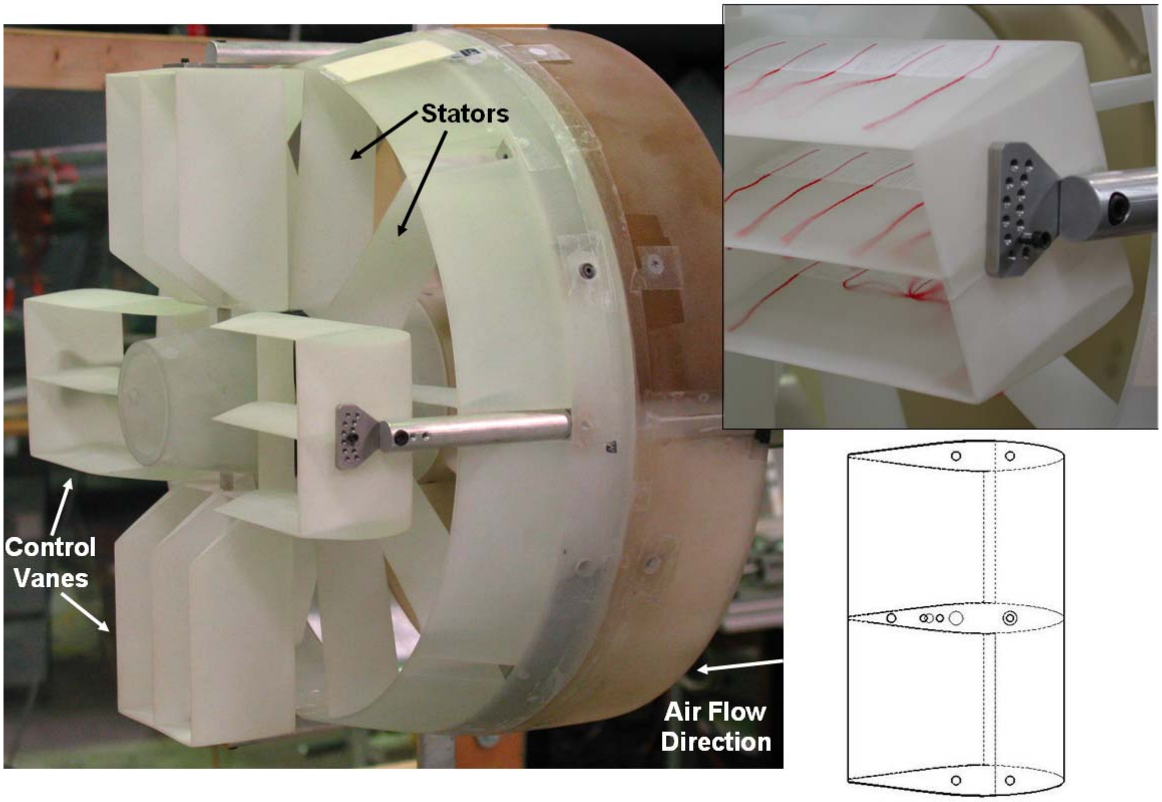

Figure 3-4: Control vane configuration as seen on the wind tunnel model. Top right figure shows the pin holding the vane at a +20 degree deflection, while the bottom right figure shows a side view of the vane geometry.

angled portion of each vane closest to the center of the duct was removed to prevent contact between the vanes when they were deflected towards each other. As with the duct components, the vanes were made using rapid prototyping from SLA resin. For this research, a positive vane deflection resulted in a negative moment. The Revised lip was used during the control vane testing because of its improved static performance over the other lip geometries, as will be shown later.

3.4 Auxiliary Control Effectors

Three auxiliary control effectors were tested, each having multiple configurations made from SLA resin. Because of the importance of the suction near the leading edge of the duct lip, all auxiliary control effectors were designed to influence the air flow near the duct lip. The first control effector, the lip spoiler, shown in Figure 3-5, was designed to induce separation on the interior of the lip, thus limiting the effects of the adverse pitching moment by reducing the lift generated by a portion of the duct lip. The spoiler swept 90 degrees around the leading edge of the lip and could be applied to both the windward and leeward sides of the duct. The other two sides of the duct were not tested with any auxiliary control effectors because the primary purpose of this research was to examine the influence of the control effectors on the pitch characteristics of the vehicle.

Figure 3-6 shows the leading edge slat auxiliary control effector in the base configuration. In this configuration, the leading edge slat was designed to augment the lift produced by the duct and so would best be suited for the leeward side to counter the adverse pitching moment. However, a ducted fan UAV utilizing this control effector would not experience wind gusts from one side only. Therefore, the leading edge slat was designed to rotate into a closed (Figure 3-7) and open (Figure 3-8) position in order to cancel its lift-augmenting effects when necessary. Both the closed and open configuration would theoretically disrupt the flow on the interior of the lip, reducing the amount of lift produced on that portion of the duct. All configurations of the leading edge slat swept 45 degrees around the duct lip.

The last auxiliary control effector, the duct deflector, shown in Figure 3-9, was designed to inhibit the flow of air into a portion of the duct, thus decreasing the lift from both the fan and duct in that region. Sweeping a 40-degree arc, it consisted of a flat plate on both sides of the engine strut and extended almost halfway from the lip to the motor housing. It was designed to

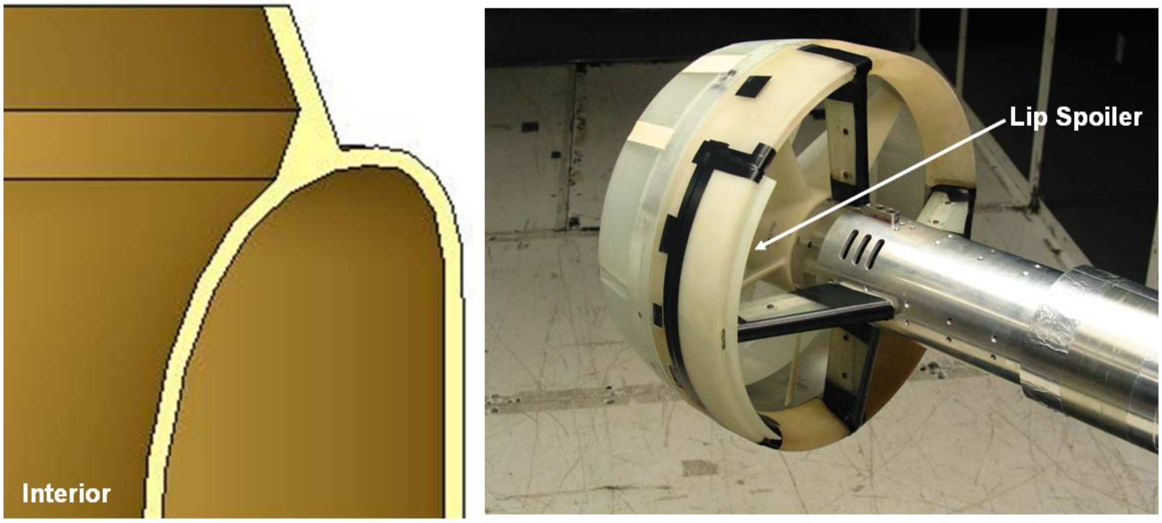

Figure 3-5: Lip spoiler auxiliary control effector profile and application on the wind tunnel model.

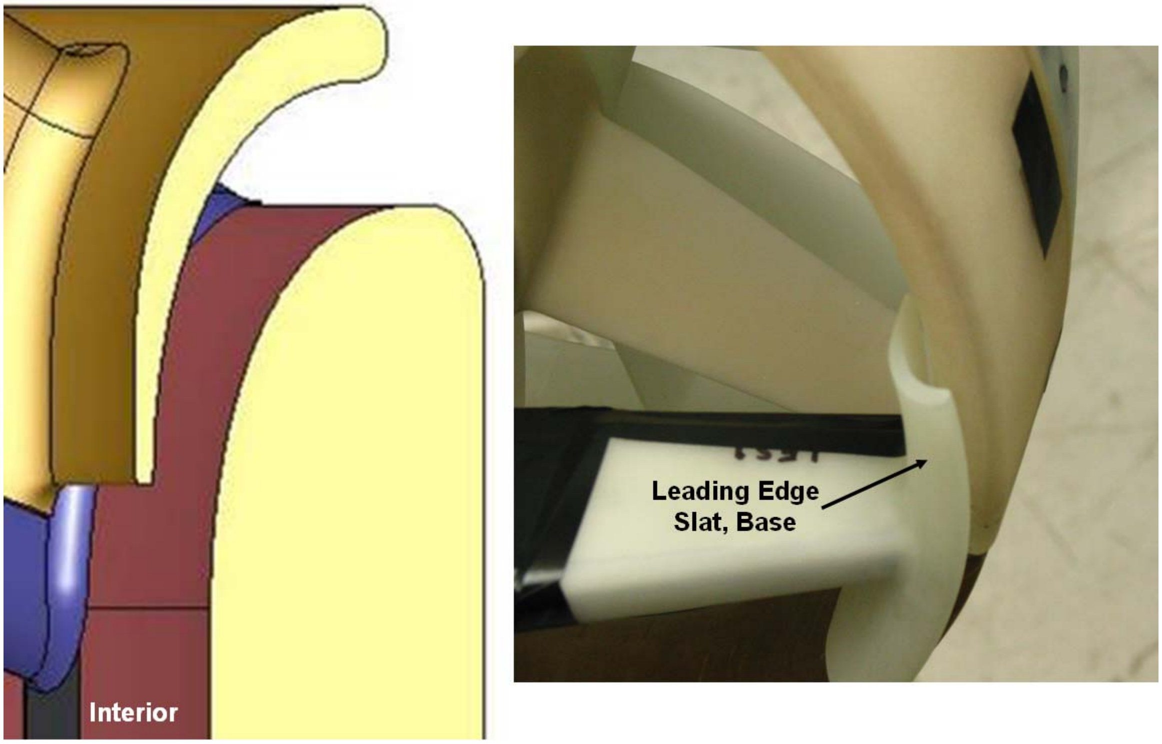

Figure 3-6: Leading edge slat (base configuration) auxiliary control effector profile and application on the wind tunnel model.

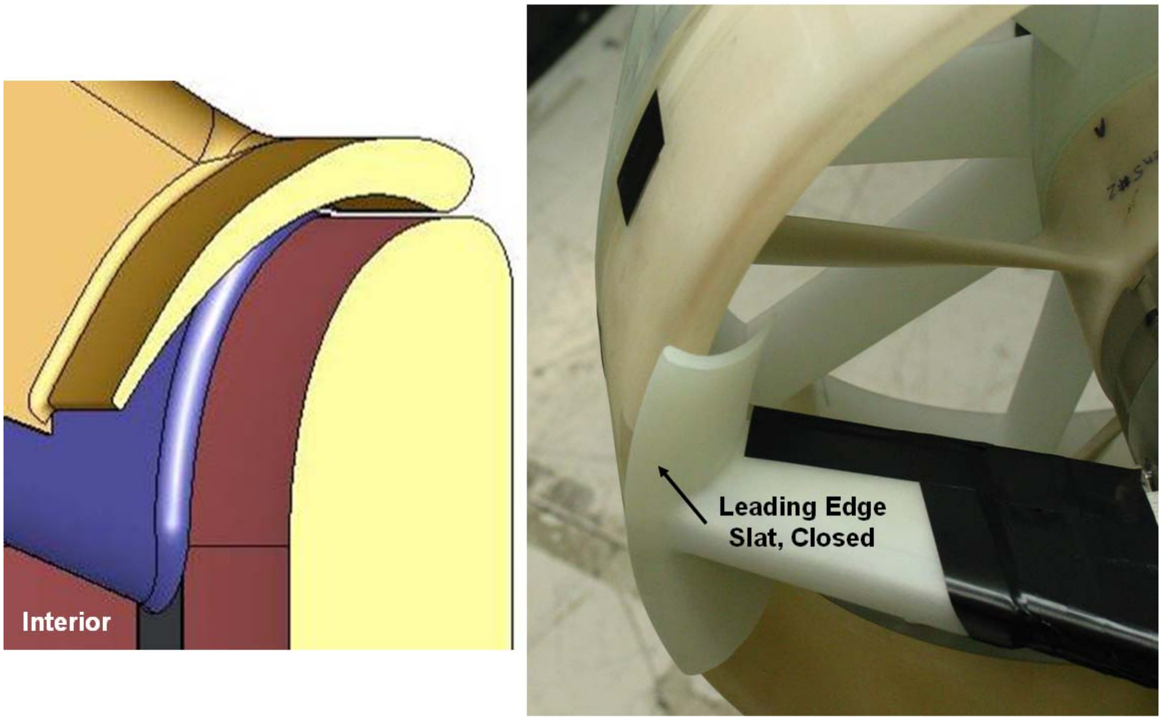

Figure 3-7: Leading edge slat (closed configuration) auxiliary control effector profile and application on the wind tunnel model.

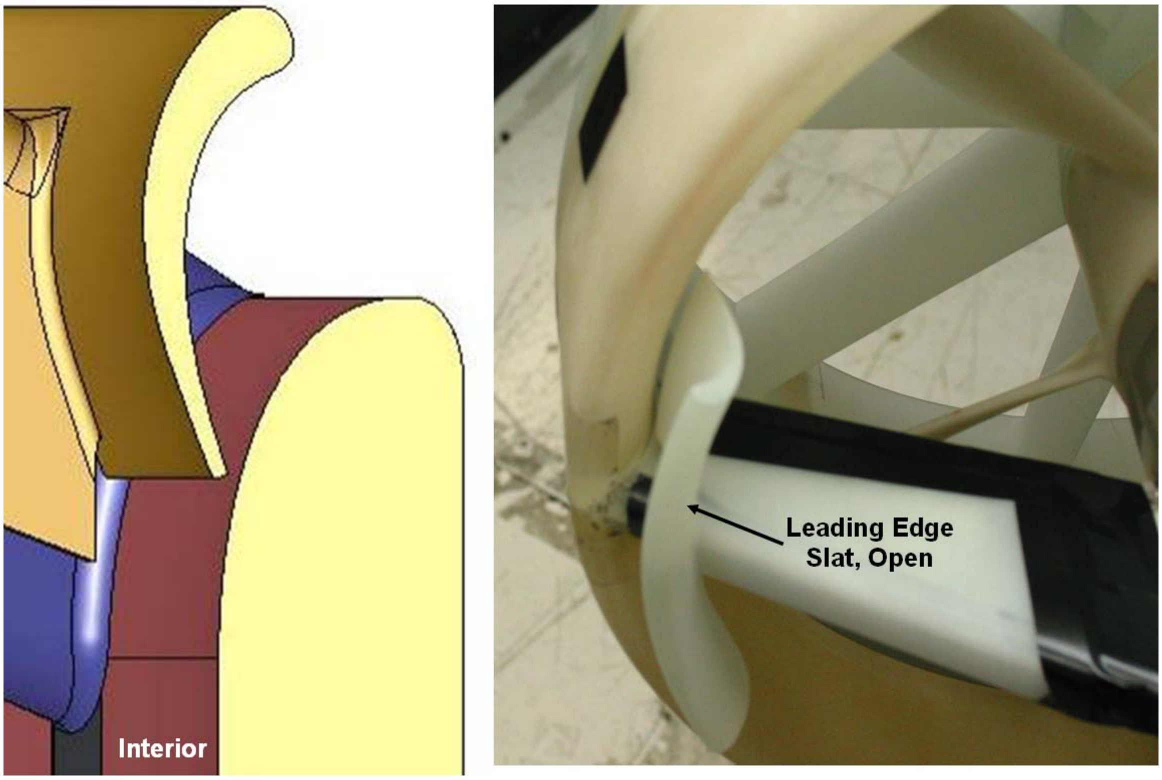

Figure 3-8: Leading edge slat (open configuration) auxiliary control effector profile and application on the wind tunnel model.

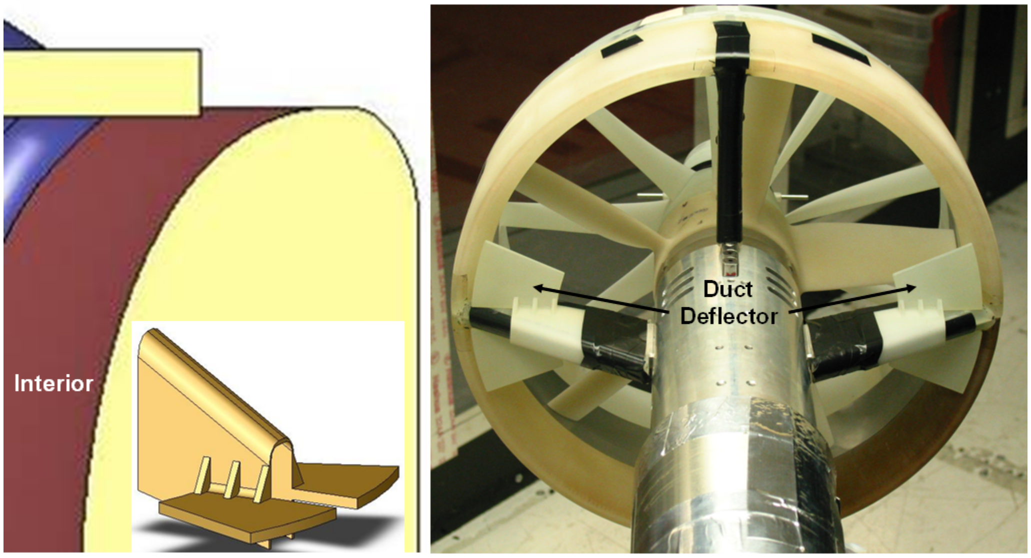

Figure 3-9: Duct deflector auxiliary control effector profile and application on the wind tunnel model.

theoretically be able to fold down onto the surface of the engine strut when its effects were not needed and could be applied to both sides of the duct.

3.5 Stabilizer Vanes

The passive stabilizer vanes can be seen in Figure 3-10. The geometry for both configurations was the same, but a 2-inch spacer was used in one configuration to extend the distance from the trailing edge of the duct to the leading edge of the vanes from 6 inches to 8 inches. The vanes consisted of four, 2.5-aspect ratio "wings" created using a NACA 0012 airfoil and arranged in a square shape. In a crosswind or forward flight, the freestream air bends the duct jet exiting the duct, as shown for a clean duct in Figure 3-11. The angle of attack seen by the vanes in the duct jet generates a force perpendicular to the jet flow to counter the adverse pitching moment. The long moment arm from the vanes to the duct lip allows for small forces at the vanes to have a much larger effect on the pitching moment.

For the most part, each control device was tested individually to determine their sole contribution to the duct aerodynamics. For example, when testing the auxiliary control effectors, the control vanes and the stabilizer vanes were not present in the vehicle configuration. However, control vanes were present when testing the stabilizer vanes (although the control vane deflections remained at 0 degrees throughout testing) because the "complete" vehicle configuration was used, which consisted of avionics pods and components simulating a two-

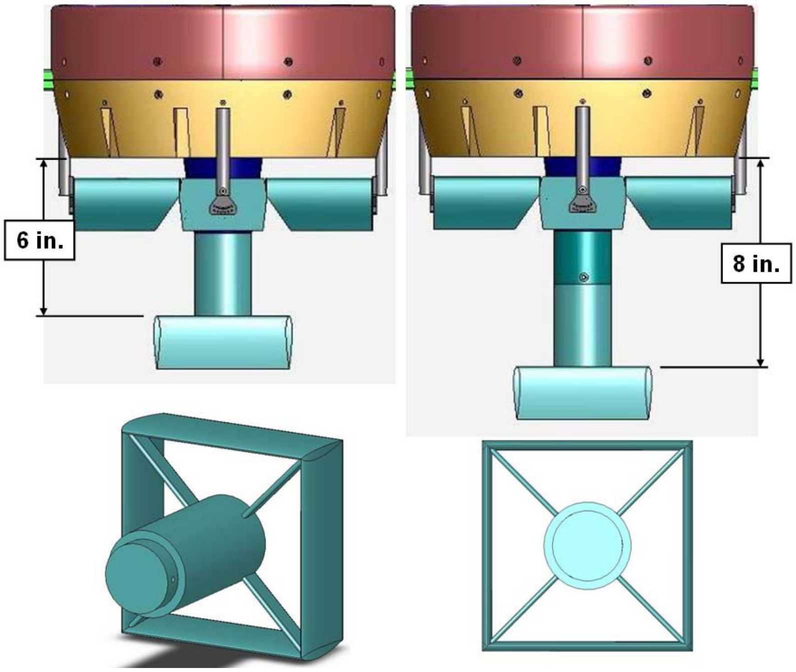

Figure 3-10: Square stabilizer vanes in the 6-inch (left) and 8-inch (right) configurations. Bottom portion of figure shows isometric and rear views of the square stabilizer vane design.

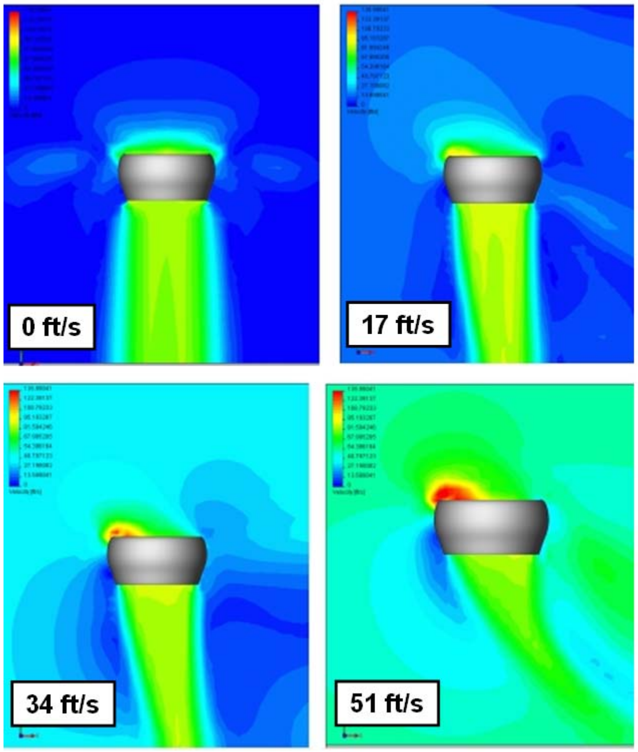

Figure 3-11: CFD results (FloWorks) showing duct jet turning with increasing crosswind at 12 lb/ft^2 for a different duct geometry. As a comparison, the disk loading for the vehicle tested in this research was approximately 21 lb/ft^2 at n/n$_{ref}$ = 1.00.

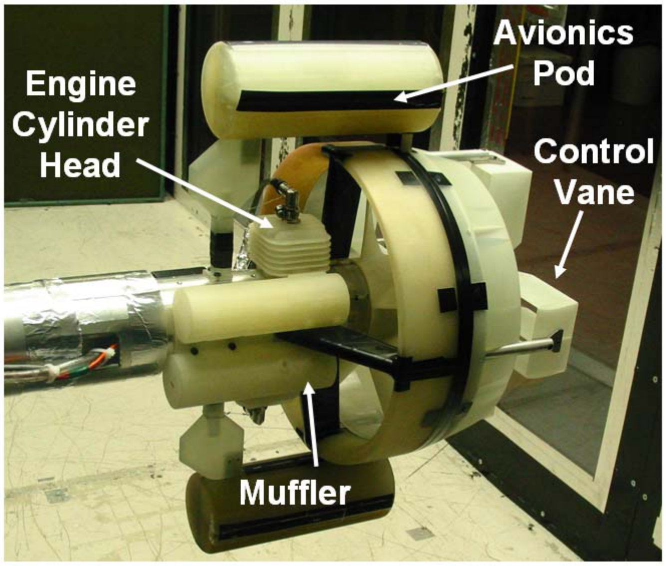

Figure 3-12: Wind tunnel model with additional components, as viewed from downstream.

cylinder engine and muffler, as shown in Figure 3-12. This was taken into account, though, in the data analysis for the stabilizer vanes, as will be described later.

3.6 Static Testing

Extensive static testing of the model and its components was performed using a thrust stand, shown in Figure 3-13. As the name suggests, the primary purpose of the thrust stand was to measure the thrust of the model configuration so the user could compare the effects of various components on the static thrust of the vehicle. The thrust stand utilized two load cells to measure the axial force and yawing moment generated by the duct and fan. Whereas the wind tunnel model was connected to the motor directly using four engine supports, the static model maintained a disconnect between the duct and the propulsive unit. The duct and motor were each mounted to their own support plate, which slid on linear bearings along two steel rods. When the support plates were connected to each other, the thrust load cell measured the thrust from both the fan and the duct. However, when the plates were split apart, the load cell only measured the thrust from the fan. By comparison, the user could determine the percentage of the total load carried by the duct and fan separately. Note that Figure 3-13 shows an early configuration for the thrust stand in which the thrust load cell is attached to the duct support plate directly. Most of the testing, though, was completed with the thrust load cell attached to the

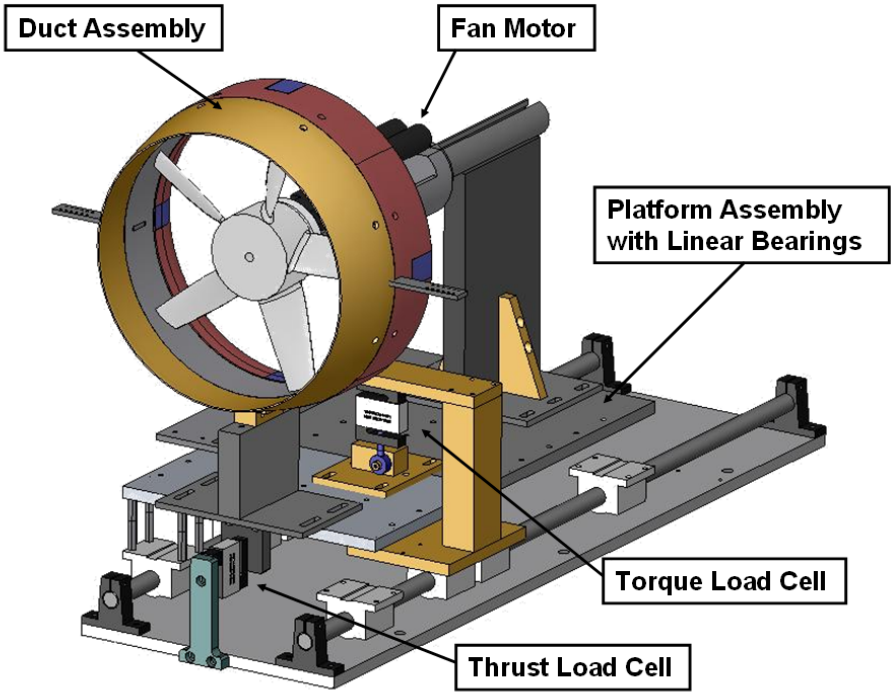

Figure 3-13: CAD image of static thrust stand with duct assembly and fan.

other side of the platform assembly where it measured the thrust from the fan when performing thrust split testing.

Data acquisition was handled by a NI-BNC-2110 8-channel DAC board and software developed by Techsburg using LabView. The software recorded the thrust and torque values from the load cells, as well as the motor speed and torque as reported by the motor controller.

3.7 Wind Tunnel Testing

The wind tunnel testing was performed in the Virginia Tech Stability Wind Tunnel, a continuous, closed-jet, subsonic wind tunnel with a 6 x 6 x 24-foot test section. The general design layout can be seen in Figure 3-14. A 600-hp d.c. motor with a 14-foot propeller provided a maximum tunnel speed of 275 ft/s (187 mph), although speeds in excess of 100 ft/s were rare during this testing. Turbulence levels in the tunnel were on the order of 0.05% or less due to the installation of seven anti-turbulence screens by the NACA before Virginia Tech acquired the tunnel in 1958[20].

Force and moment data was collected using a six-component, strain gauge, sting-mount balance (Figure 3-15a) mounted directly to the model centerbody such that the forces and moments were always measured relative to the body-axis coordinate system. The signals from

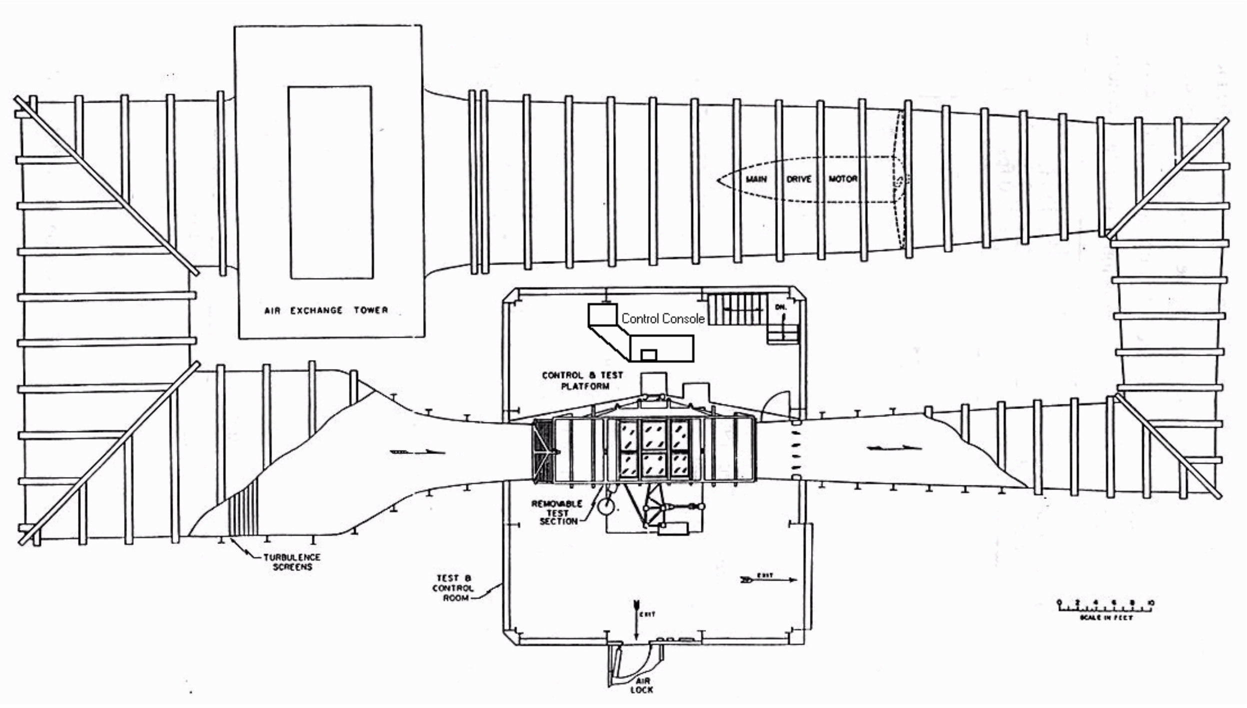

Figure 3-14: General layout of the Virginia Tech Stability Wind Tunnel.

the balance passed through six Measurements Group 2310 strain gauge amplifiers (Figure 3-15b) before passing through the data acquisition system (four SCXI-1120D isolation amplifiers and a AT-MIO-16-XE-10 DAC board) and finally ending up at the computer[21]. The pre-existing data acquisition software was developed by Techsburg using LabView. Each data point was an average of 2000 points taken over a 5 second period (400-Hz data rate), and the standard deviation of each data point was also recorded. In addition to recording the force and moment data for each test, the software also saved the model configuration and orientation information, tunnel dynamic pressure, temperature, and static pressure, and motor speed and torque. It also continuously monitored the forces and moments on the model, motor status, and tunnel properties, as well as displaying plots of the results at the end of each test. Several screen captures of the data acquisition software can be seen in Figure 3-15c.

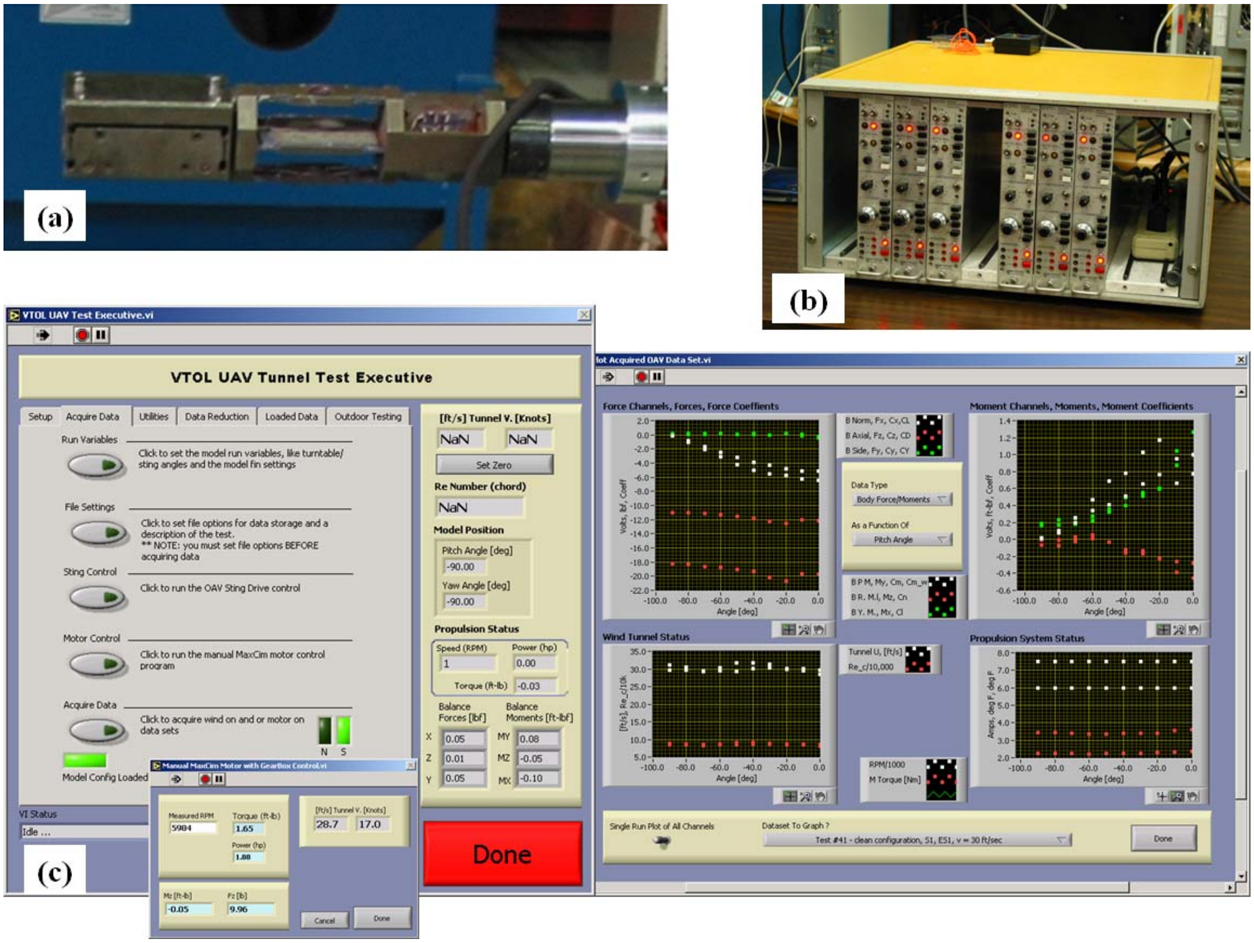

Click to set the model run variables, like turntable/ sting angles and the model fin settings

Click to set file options for data storage and a description of the test. ** NOTE: you must set file options BEFORE acquiring data

Click to run the OAV Sting Drive control

Click to run the manual MaxCim motor control program

Click to acquire wind on and or motor on data sets

VI Status: Idle ...

[ft/s] Tunnel V. [Knots]: NaN NaN

Re Number (chord): NaN

Model Position

Pitch Angle [deg]: -90.00

Yaw Angle [deg]: -90.00

Propulsion Status

Speed (RPM): 1

Power (hp): 0.00

Torque (ft-lb): -0.03

	Balance Forces [lbf]		Balance Moments [ft-lbf]
X	0.05	MY	0.08
Z	0.01	MZ	-0.05
Y	0.05	MX	-0.10

Measured RPM: 5984

Torque (ft-lb): 1.65

Power (hp): 1.88

[ft/s] Tunnel V. [Knots]: 28.7 17.0

Mz [ft-lb]: -0.05

Fz [lb]: 9.96

Data Type: Body Force/Moments

As a Function Of: Pitch Angle

Dataset To Graph ?: Test #41 - clean configuration, S1, ES1, v = 30 ft/sec

Figure 3-15: Wind tunnel test hardware and software, including (a) sting-mount balance, (b) strain gauge amplifiers, and (c) LabView data acquisition software.

Figure 3-16 shows the model configuration used in the wind tunnel and the custom strut used to support it. The model was mounted on its side and directly connected to the sting balance, which was shrouded from the oncoming airflow. This configuration, with the balance mounted in front of the duct, was chosen for multiple reasons. If the balance was mounted aft of the duct, it would have interfered with the duct jet flow, altering the results. Also, because the yawing moment of these vehicles tends to be relatively small, the model was configured so the balance would measure the yawing moment directly, reducing the amount of uncertainty in that measurement. Appendix A has more information on interference effects caused by this mounting configuration. The other end of the balance was connected to the support strut, which, in turn, was mounted to the wind tunnel's turntable in the floor of the test section. The pitch angle of the model was varied by rotating the turntable at the base of the support strut, and the heading angle could be changed by rotating the shroud either manually or with a stepper motor controlled using the LabView data acquisition software[22]. The majority of the tests were run with a wind tunnel velocity ranging from 10 to 85 ft/s and a fan motor speed between 5000 and 8000 rpm. The pitch angle was also varied between 0 and -90 degrees throughout testing.

The size of the model was comparable to the full-size vehicle, so no scaling factors were necessary for this testing. However, due to changes in vehicle design, two slightly different duct

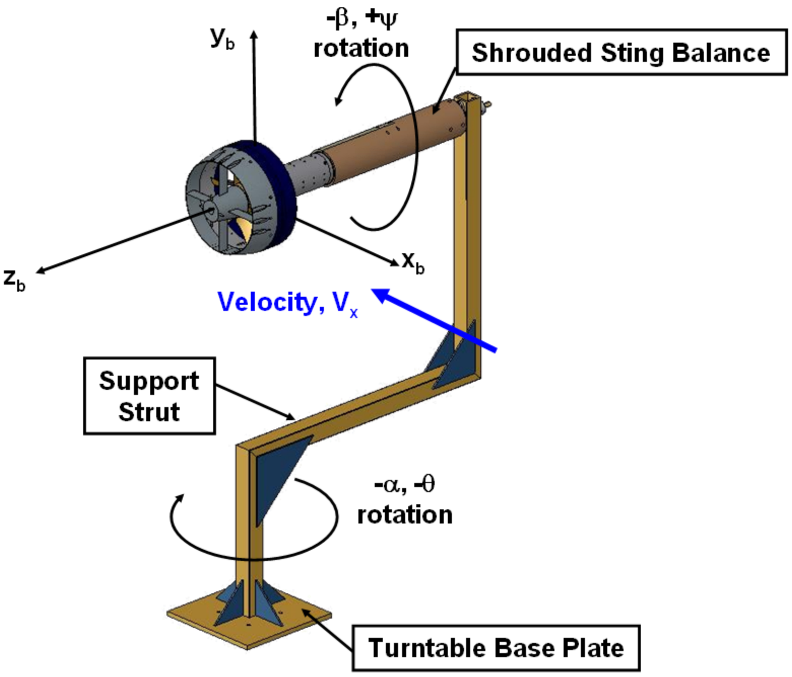

Figure 3-16: Wind tunnel model mounted on sting balance and support strut.

diameters were used in wind tunnel testing. The Baseline and Enlarged duct lips were tested with a 10-inch inner diameter duct, while the Revised duct lip was tested with an 11.5-inch inner diameter duct. Considering the different duct sizes, the wind tunnel data is still comparable as long as it is normalized with the duct diameter. The static data is directly comparable since the duct size remained constant during that testing. The control vane data, auxiliary control effector data, and the stabilizer vane data were all taken with the 11.5-inch inner diameter duct.

Chapter 4: Experimental Results

With the exception of a few plots, most of the data is presented in non-dimensional form using T_{ref} and n_{ref}. T_{ref} can be thought of as being roughly equivalent to the vehicle weight, and n_{ref} is the fan speed required to achieve T_{ref}. The alternative would have been to non-dimensionalize the data by converting it to coefficient form. However, by using T_{ref}, which is the same for each lip, the reader can more easily determine when the vehicle is generating enough lift or thrust to maintain hover. All data has been corrected to standard day, sea level density. In addition to the data presented in this chapter, supplementary data is presented in Appendix A. A detailed uncertainty analysis for the data presented here can be found in Appendix B, while average uncertainties are shown in parentheses throughout this chapter when the associated plots are discussed.

4.1 Duct Lip Results

Various forms of testing were performed on the duct lip. The first that will be presented is the diagnostic testing, in which methods were used to determine how the flow around the lip influenced the forces and moments experienced by the vehicle. These methods consisted of both static pressure data on the duct lip and tuft flow visualization. Secondly, static testing was performed to determine which lip generated the most static thrust with the least power input. Finally, the three lip shapes that performed best statically were tested in the wind tunnel to ascertain their forward flight characteristics.

4.1.1 Diagnostic Test Results

Although not the primary purpose of this research, some diagnostic testing was performed on the duct lip. In particular, static pressure data was taken on the Revised lip during wind tunnel testing. Two of the removable lip sections were replaced with similar sections with static pressure taps, spaced 10 degrees apart azimuthally, around the inner portion of the lip, as shown in Figure 4-1. The location of the pressure taps along the lip profile corresponded to a location near the hover suction peak for this lip shape, which was determined from a CFD analysis. Figure 2-6 illustrates similar CFD results but for the Baseline lip instead of the Revised lip.

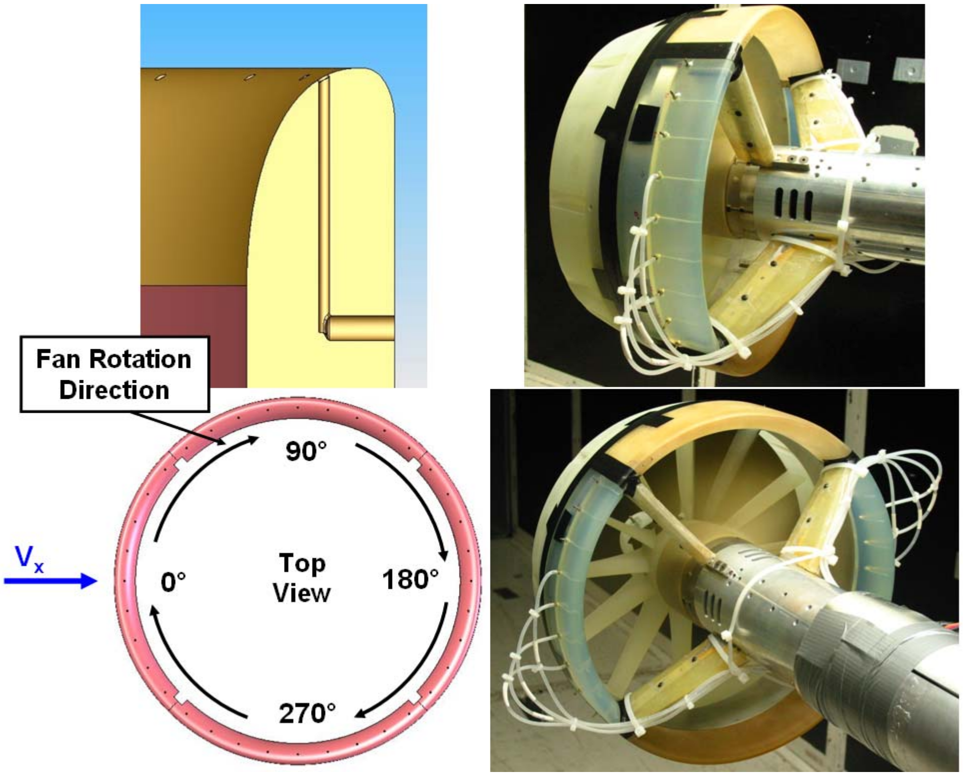

Figure 4-1: Wind tunnel model configured to acquire pressure data around the duct lip. Placement of pressure taps was dependent on profile peak pressure data from CFD results.

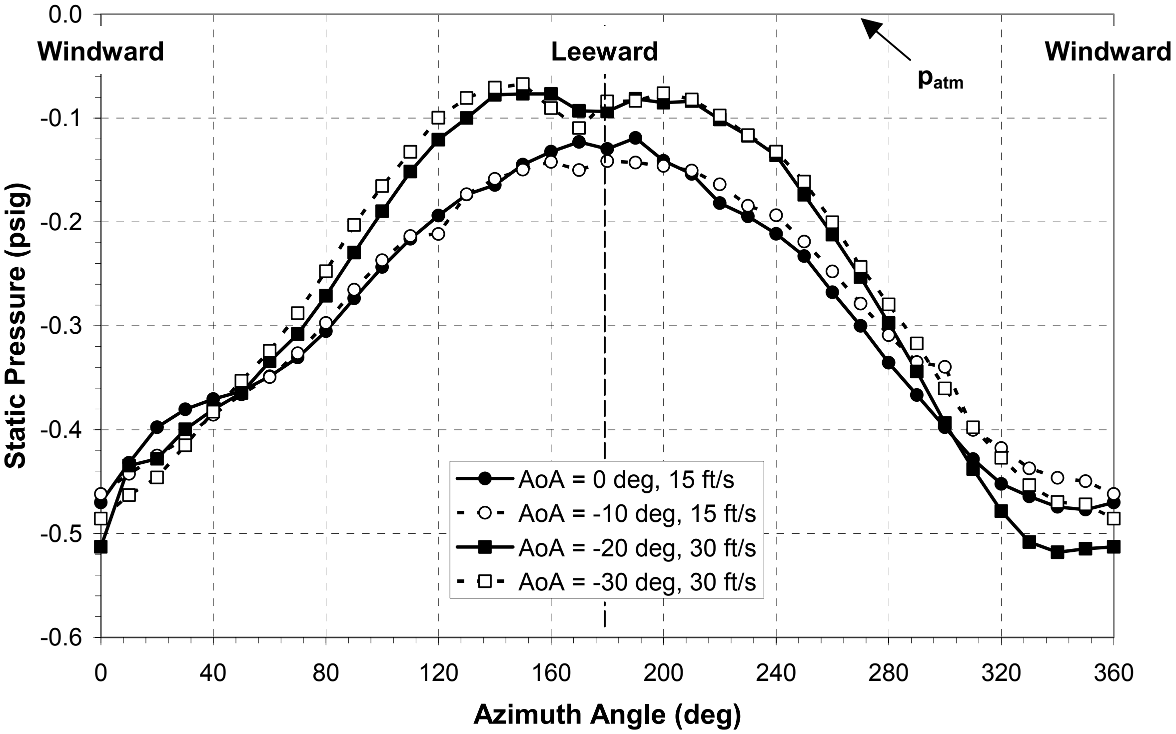

Figure 4-2: Static gage pressure data for each azimuth angle for various angles of attack and tunnel velocities with $n/n_{ref} = 1.00$.

Since only two of the four lip sections contained pressure taps, the model was rotated about its *z*-axis to obtain pressure data for the remaining azimuth angles.

Figure 4-2 shows the gage pressure ($p = \pm0.0125$ psig) at each azimuth angle for various angles of attack and tunnel velocities. Refer to Figure 4-1 for azimuth angle conventions. Again, the angle of attack is defined as 0 degrees in hover and negative as the vehicle tilts into the wind. The data is for an angle of attack range from 0 to -30 degrees and two tunnel velocities, 15 and 30 ft/s. The increase in tunnel velocity at the more negative angles of attack corresponds to higher crosswind velocities seen by the vehicle as its forward speed increases. The dip in the data at approximately 180 degrees azimuth is due to the influence of the motor housing on the flow on the leeward portion of the duct. Also, note that the data on either side of 0 degrees azimuth is asymmetric. Because the fan blades have a fixed pitch, the advancing blades generate more lift than the retreating blades, resulting in lower pressures at 350 degrees azimuth than at 10 degrees azimuth. The major result from Figure 4-2 is the difference in pressures between the windward and leeward lips. An increase in tunnel velocity further increases the pressure difference between the two sides of the duct. This accounts for the

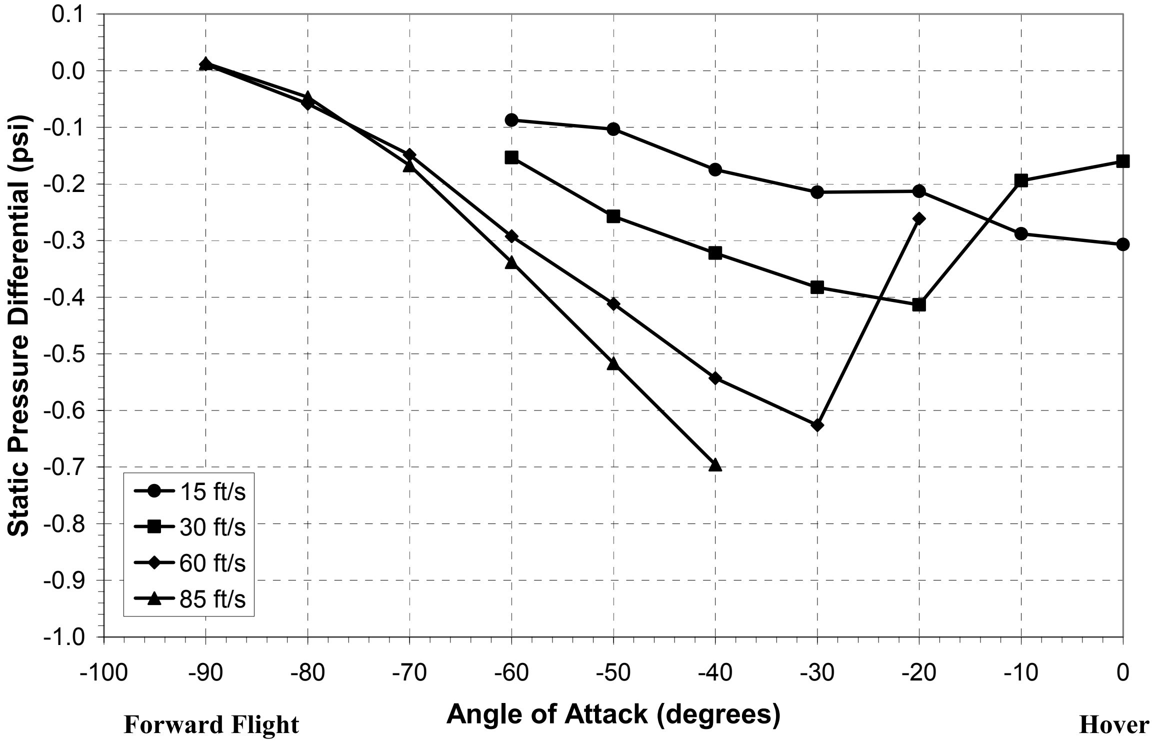

Figure 4-3: Static pressure differential between the windward and leeward lips as a function of angle of attack at various tunnel velocities and $n/n_{ref} = 1.00$.

asymmetric lift and resulting adverse pitching moment discussed previously. Although a change in angle of attack appears to have little effect on the pressure difference, the tunnel velocities shown in Figure 4-2 are relatively small, and larger wind speeds result in larger pressure differences, at least until stall occurs. Figure 4-3 shows the static pressure differential ($p_{0°} - p_{180°}$) between the windward (0 degrees azimuth) and leeward (180 degrees azimuth) lips as a function of angle of attack for various tunnel velocities ($p = \pm 0.0125$ psi). Note that at 30 ft/s and 60 ft/s stall occurs at angles of attack of -20 degrees and -30 degrees, respectively, which match the force and moment data presented later. Stall is not shown for the 85-ft/s case, but it is believed it would occur between -40 degrees and -30 degrees angle of attack. In a 15-ft/s crosswind, there appears to be no significant flow separation on the lip. Additionally, Figure 4-3 reiterates the fact that, until stall occurs, the duct lift becomes more asymmetric as the crosswind velocity increases.

In addition to pressure data, tufts for flow visualization were utilized during static testing of the Baseline and Enlarged lips as shown in Figure 4-4 and Figure 4-5, respectively. The Enlarged lip exhibits attached flow on the lip surface, whereas the tufts on the Baseline lip reveal the flow separation present on the interior of the duct lip. The tendency for flow on the Baseline

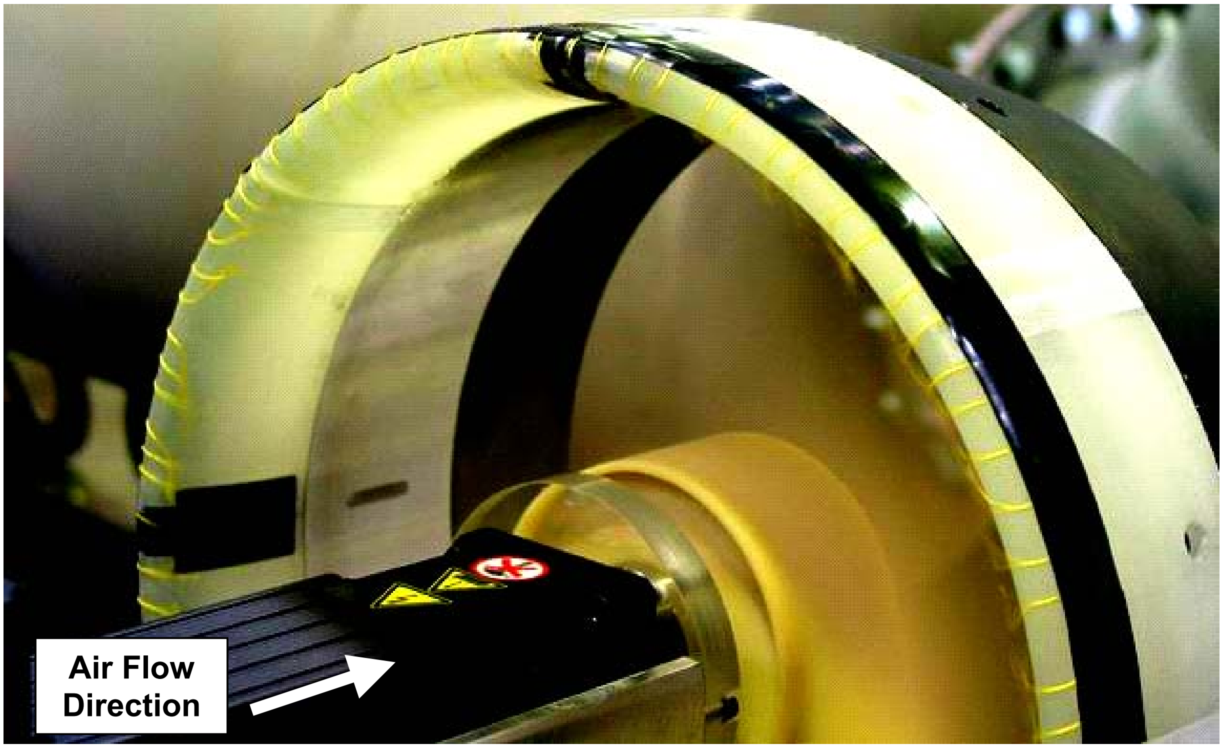

Figure 4-4: Tuft flow visualization of the Baseline lip, showing flow separation on the interior of the duct lip. The contrast was increased to improve tuft visibility.

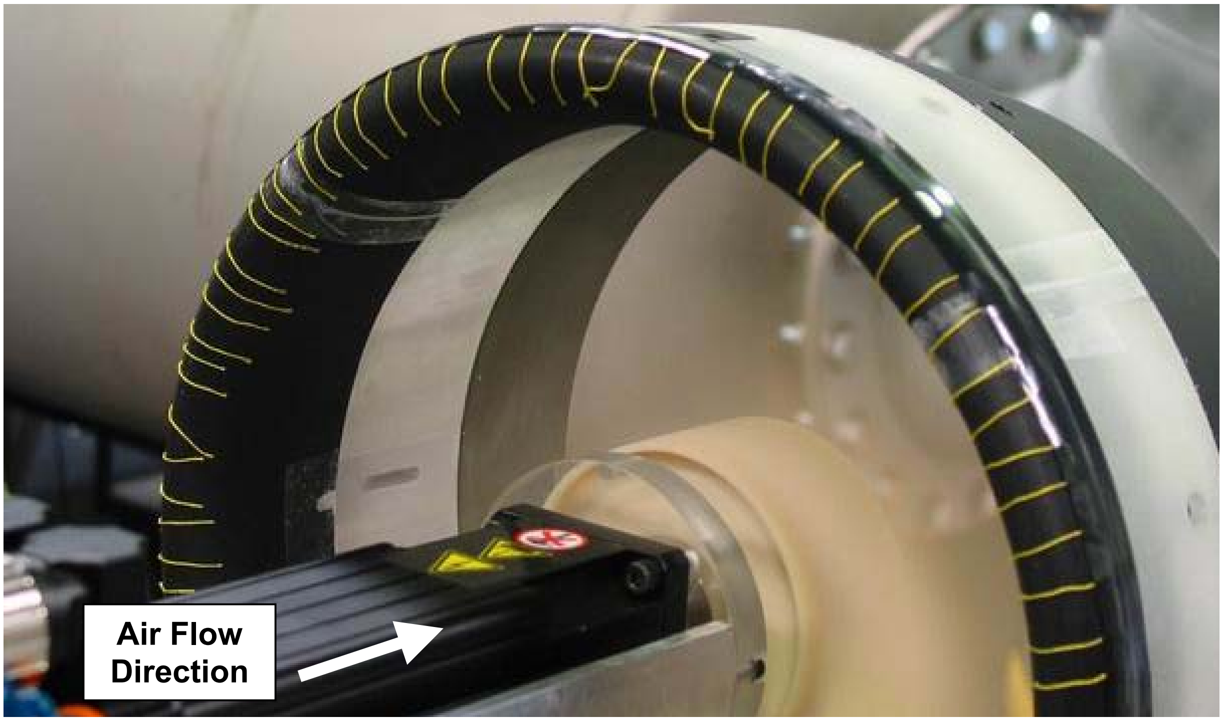

Figure 4-5: Tuft flow visualization of the Enlarged lip, showing attached flow on the interior of the duct lip.

lip to separate sooner than that on the Enlarged lip is due to its smaller leading edge radius and affects both its static and forward flight performance, as will be shown later.

4.1.2 Static Test Results

Static testing for the various lip geometries was completed at fan speeds ranging from $n/n_{ref} = 0.667$ to $n/n_{ref} = 1.17$, as shown in Figure 4-6 ($T/T_{ref} = \pm 0.08$). The results show the Elliptical and Circular Arc lips lagging behind the other three lips in static thrust performance. It is believed this is due to the excessive flow separation that occurs on the interior of the lips. For the Elliptical lip, the cause of the flow separation is the large rate of curvature that occurs at the leading edge, resulting in separation on a significant portion of the interior of the lip, while the separation on the Circular Arc lip occurs because the lip geometry is not thick enough to allow the adverse pressure gradient to change gradually.

The Baseline, Enlarged, and Revised lips have similar static thrust performance when viewed as a function of fan speed, but the differences in performance become more obvious when viewed as a function of power, Figure 4-7, non-dimensionalized using the reference power required for hover. In addition to reducing thrust, flow separation also increases the required

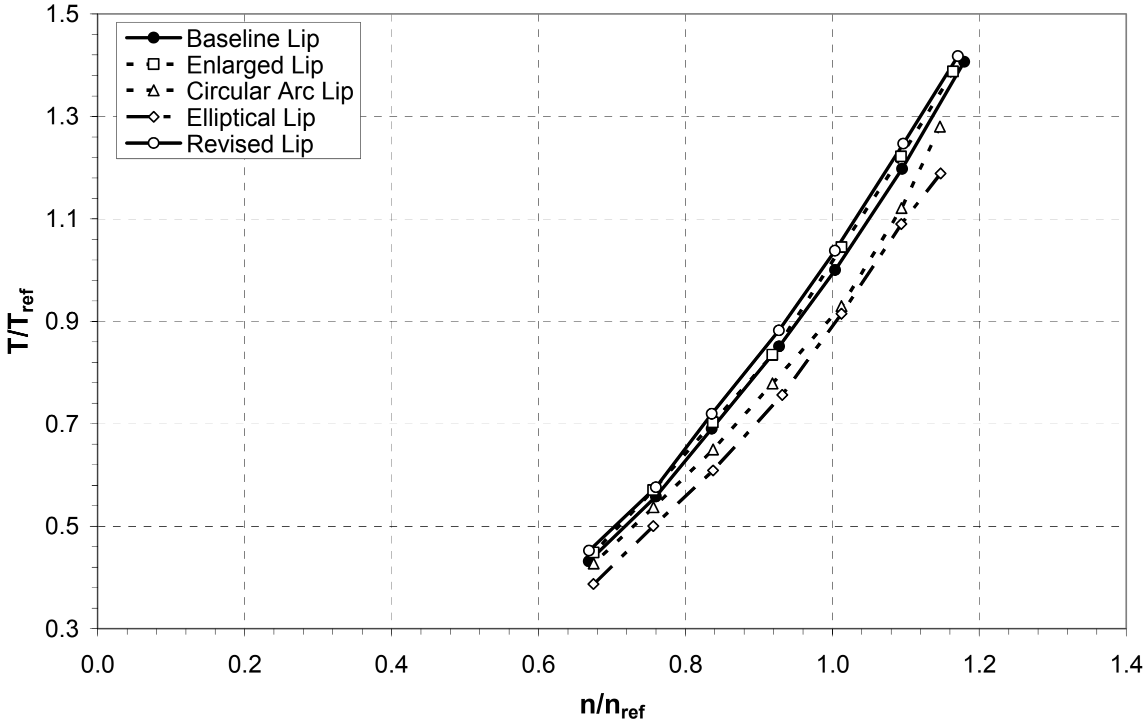

Figure 4-6: Comparison of static thrust results for the five duct lips at various motor speeds.

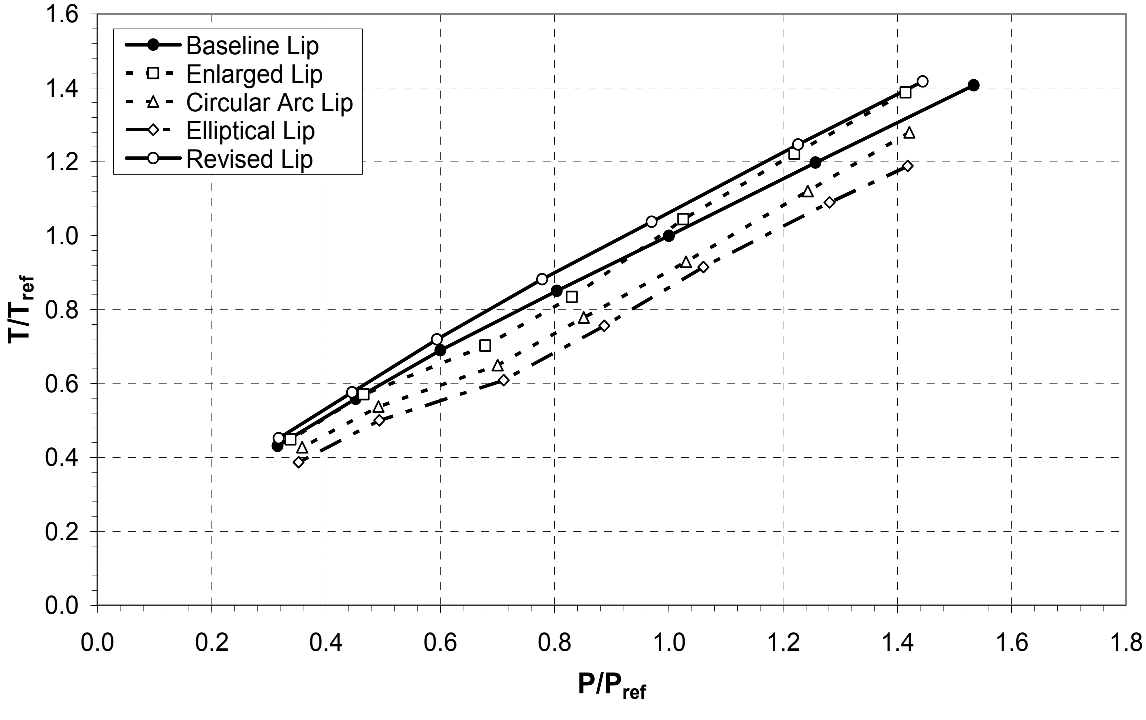

Figure 4-7: Comparison of thrust and power required for the various lip geometries in static conditions.

power from the motor because the turbulent flow causes the fan blades to be at a higher angle of incidence[23,24]. The Enlarged lip requires less power for a given thrust than the Elliptical and Circular Arc lips and is better than the Baseline lip above the thrust required for hover. However, the Revised lip outperforms all of the other lips at every fan speed, suggesting the lip leading edge radius has more influence than the duct wall thickness on the duct's contribution to the thrust. Again, the Elliptical and Circular Arc lips display lower performance in required power because of excessive flow separation.

The thrust stand was also utilized to determine the thrust load split between the duct and fan, and the results can be seen in detail in Appendix A. In short, the duct with the Revised lip provided slightly over half the total thrust, while the duct with the Baseline lip only contributed 35% of the total thrust. However, other factors besides the duct lip influence this load split value as explained in Appendix A.

4.1.3 Wind Tunnel Test Results

Static test results showed the Circular Arc and Elliptical lips lagging significantly behind the Baseline, Enlarged, and Revised lips. Therefore, to allow for more thorough wind tunnel testing, only the Baseline, Enlarged, and Revised lips were tested in the wind tunnel. The complete data set was acquired in two wind tunnel entries, the first of which tested the Baseline and Enlarged lips, while the second tested the Revised lip. Due to the importance of various independent variables, particularly crosswind velocity and angle of attack, on ducted fan flight characteristics, each tunnel entry had a different focus. The first entry, involving the testing of the Baseline and Enlarged lips, focused on how the vehicle performed at various wind speeds, and the second entry focused on the performance at various angles of attack. Ideally each lip geometry should be tested in similar conditions, but this was not possible due to budget constraints. To avoid displaying only one or two data points for a particular lip geometry on a plot with many data points for the other lip geometries, the data for the Revised lip is presented separately from the data for the other lips. However, a comparison between the data will be discussed for clarification. Additionally, it is beneficial for the reader to see the force and moment trends as functions of both tunnel velocity and angle of attack.

One particular test, used for data verification, involved orienting the vehicle at $\alpha = -90°$ (thrust vector point into the wind) and taking data at multiple wind tunnel velocities. From this data, a plot showing the dependence of the thrust coefficient on the advance ratio for each lip was created (Figure 4-8). The thrust coefficient is defined by

$$C_T = \frac{T}{\rho A \Omega^2 R^2}, \tag{4-1}$$

and the advance ratio is defined by

$$J = \frac{V_z}{\Omega D}, \tag{4-2}$$

according to Leishman[25]. Note that the thrust coefficient is non-dimensionalized using C_{Tref}, which is calculated using the T_{ref} mentioned previously. Figure 4-8 shows the thrust coefficient and the advance ratio correlate well because each curve follows a linear trend, and the difference in slopes corresponds to the difference in performance of each lip. This trend can also be seen in data presented by Kruger[11], Abrego, et. al.[17], and Mort, et. al.[26,27,28]. The reason none of the data points in Figure 4-8 lie above $C_T/C_{Tref} = 1$ is because, with the model oriented at α = -90°, the drag works directly against the thrust, preventing the vehicle from generating as much net thrust.

Lift, drag, and pitching moment were analyzed as functions of the crosswind velocity for the Baseline and Enlarged lips and angle of attack for the Revised lip. Lift and drag are the wind

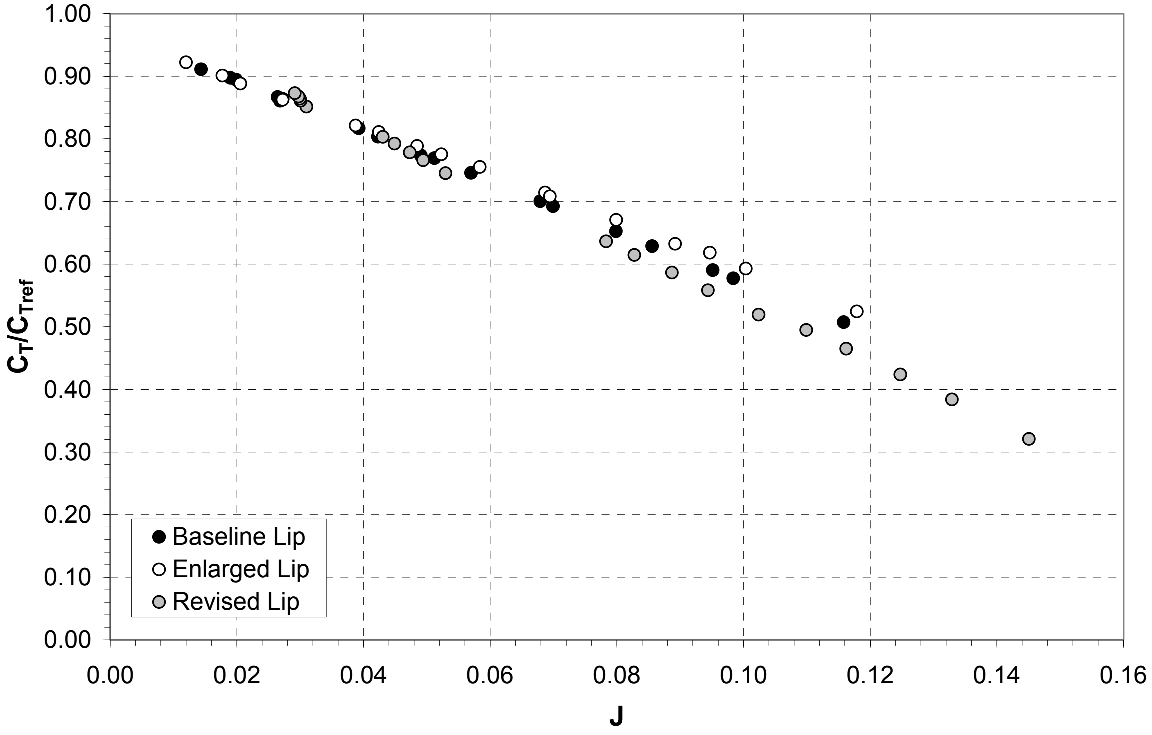

Figure 4-8: Thrust coefficient as a function of the advance ratio for the Baseline, Enlarged, and Revised lips at an angle of attack of -90 degrees.

coordinate system z- and x-forces, respectively (see Figure 2-2), which correspond to the body coordinate system forces when the vehicle is in hover ($\alpha = 0$). However, as the angle of attack changes, the difference between the wind coordinate system and body coordinate system forces increases. Since a change in angle of attack causes a rotation about the coordinate systems' y-axes, the pitching moment is the same in both the wind and body coordinate systems.

A detailed lift and drag analysis can be seen in Appendix A, but it is summarized here. The Enlarged lip generates slightly more lift than the Baseline lip, and the Revised lip shows a small improvement over the Enlarged lip, reflecting the trend seen in the static thrust results. As with the static results the differences between the performances of each lip geometry can be attributed to separated flow on the interior of the lip and the different lip leading edge radii. Since the Enlarged and Revised lips maintain attached flow longer than the Baseline lip, they can generate more lift. A look at the drag analysis reveals the differences between the three lips are small, particularly between the Baseline and Enlarged lips. However, the Revised lip displays slightly more drag than the other two lips, which, as will be shown later, influences its pitch characteristics.

As mentioned previously, momentum drag makes up a significant portion of the total drag. This can be seen in Figure 4-9, where the momentum drag has been estimated from Eq. (2-3) and compared to the measured drag for the Baseline lip at 0 degrees angle of attack. Figure 4-10 shows that approximately 80% of the total drag is caused by changing the momentum of the air flow. The scatter in the data near 10 ft/s is due to higher uncertainties at lower wind tunnel velocities. Note the slightly negative slope, which illustrates the increasing importance of pressure drag and friction drag on the vehicle body as the crosswind velocity increases. Although not shown, the momentum drag ratio for the Revised lip matches that of the Baseline and Enlarged lips, illustrating the lack of influence from the lip geometry on the momentum drag ratio.

Separated flow on the duct lip has the largest impact on pitching moment because it tends to create a more symmetric pressure distribution around the duct lip, and Figure 4-11 indicates this[26,27,28,29]. The pitching moment is non-dimensionalized with both T_{ref} and the duct diameter. As the crosswind velocity increases, the pitching moment ($M_y/T_{ref}d = \pm 0.0075$) also increases due to the larger drag force acting at the center of pressure. However, the pitching moment

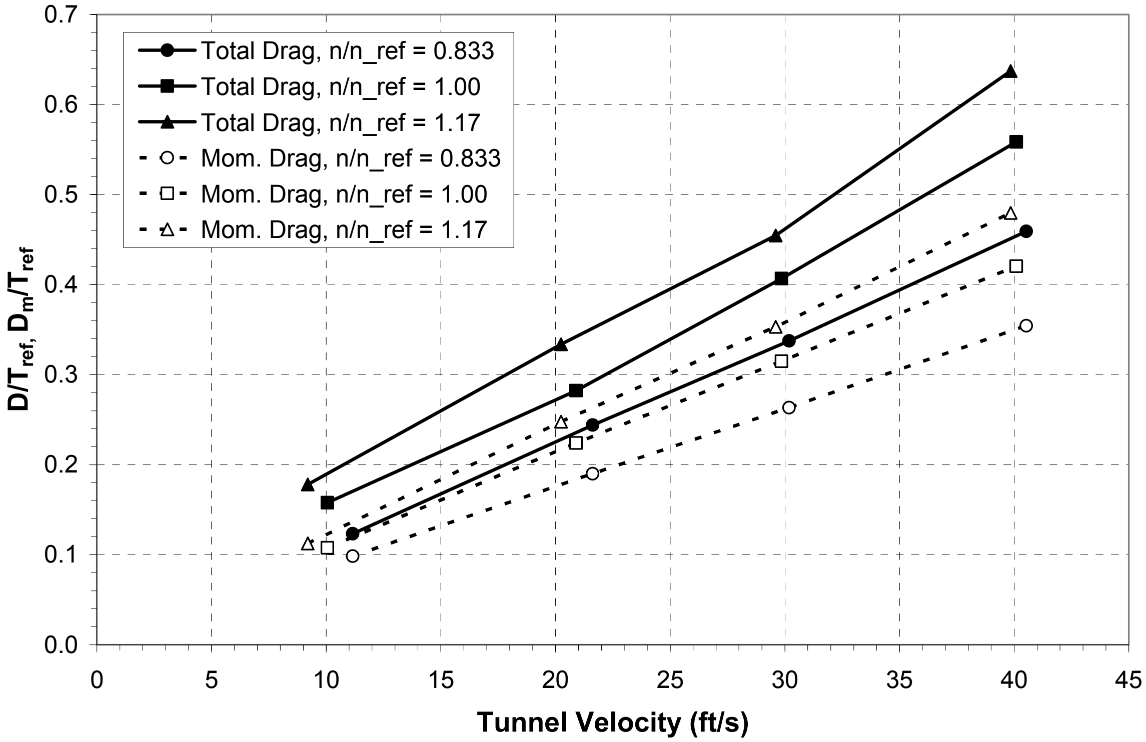

Figure 4-9: Comparison between total drag and momentum drag for the Baseline lip at various fan speeds and an angle of attack of 0 degrees.

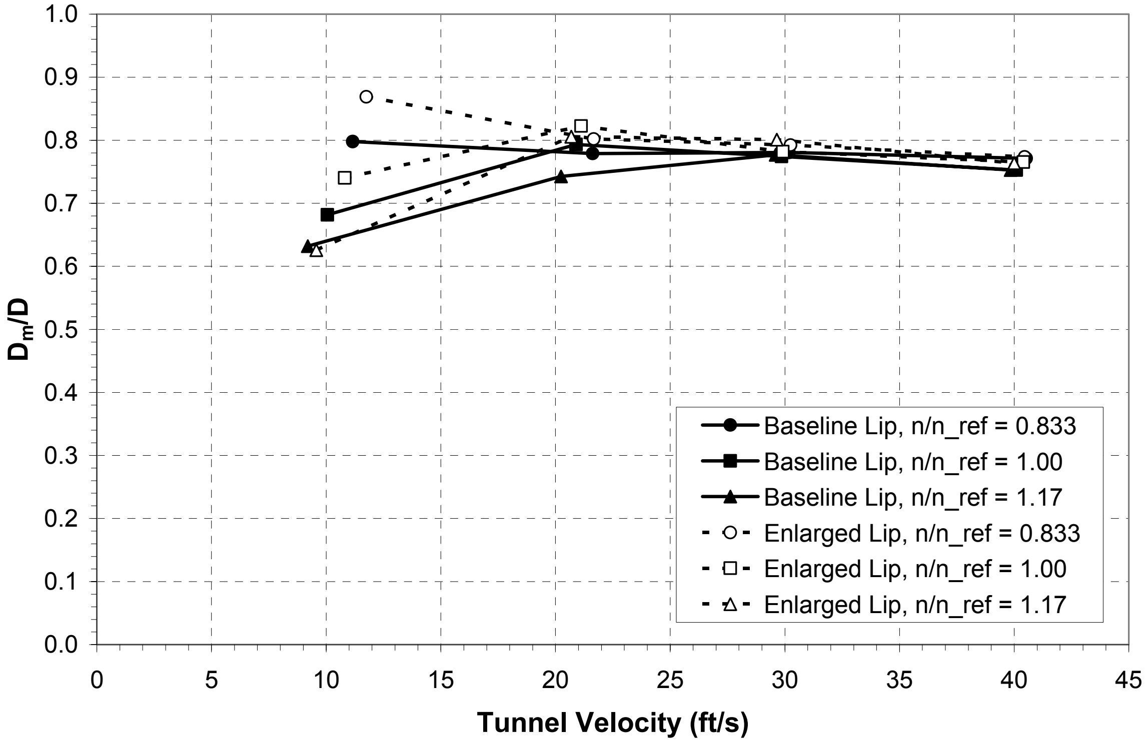

Figure 4-10: Ratio of momentum drag to total drag for both the Baseline and Enlarged lips at various fan speeds and an angle of attack of 0 degrees.

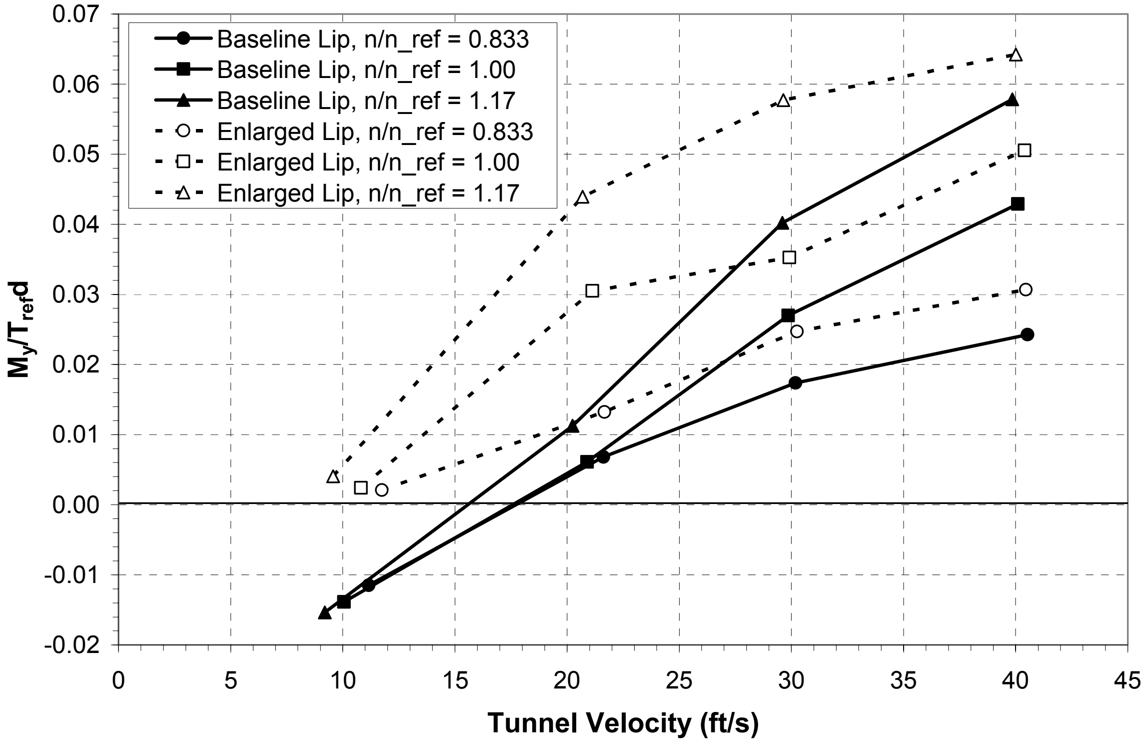

Figure 4-11: Pitching moment trends for various lip shapes and fan speeds at 0 degrees angle of attack.

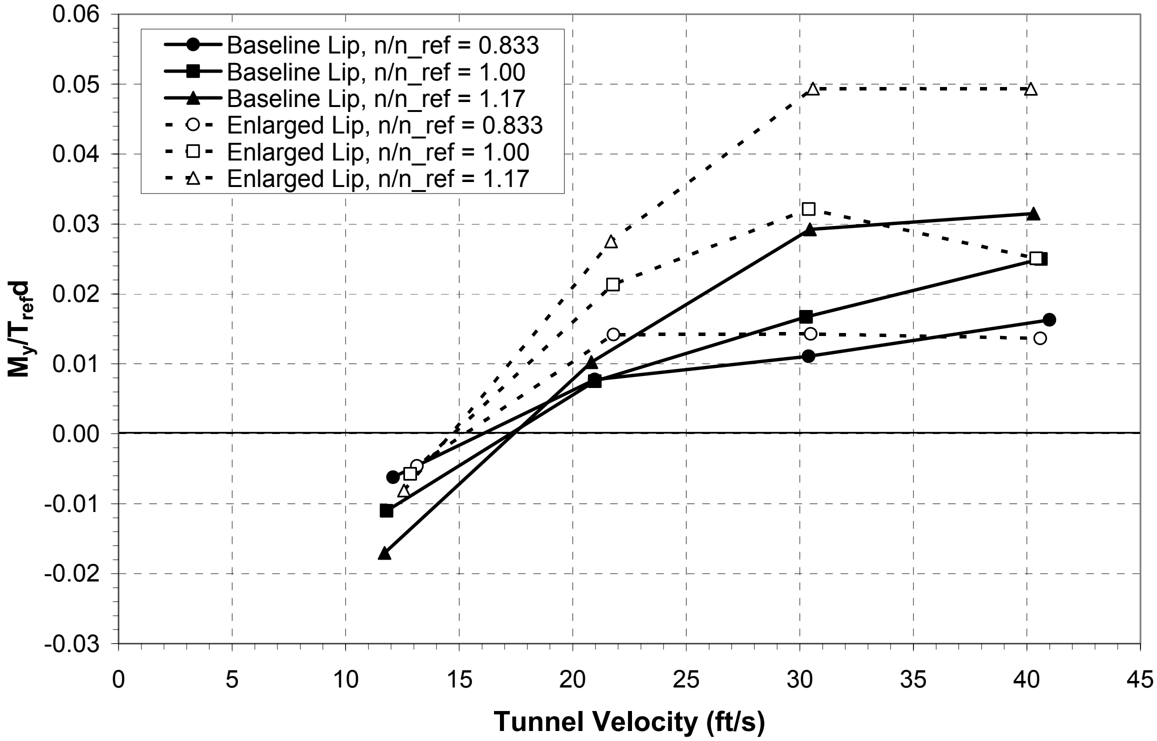

Figure 4-12: Pitching moment trends for various lip shapes and fan speeds at -15 degrees angle of attack.

begins to flatten out (shown more clearly in Figure 4-12 for $\alpha = -15°$) at high wind speeds in part because the profile drag on the vehicle body counteracts the moment generated by the momentum drag and the asymmetric lift. At $\alpha = -15°$ the pitching moments are lower than at $\alpha = 0°$ due to the reduction in the vertical distance between the center of pressure and the center of gravity as the vehicle tilts in to the wind, reducing the effect of the momentum drag on the pitching moment. Because of flow separation, the Baseline lip displays a smaller pitching moment, particularly at higher fan speeds, than the Enlarged lip.

The pitching moment trends ($M_y/T_{ref}d = \pm 0.009$) as a function of angle of attack are shown in Figure 4-13 though Figure 4-15 for the Revised lip at tunnel velocities of 30, 60, and 85 ft/s. The general trend is for the pitching moment to increase as the angle of attack becomes less negative because the lift and drag both increase with increase in angle of attack, and the asymmetric lift and momentum drag acting at the center of pressure are the root causes of the pitching moment. In following with the angle of maximum lift shown in Figure A-4, Figure 4-13 shows a peak in the pitching moment at an angle of attack of -20 degrees. As the vehicle continues to rotate towards $\alpha = 0°$, the lift begins to decrease, reducing the effect of the asymmetric lift on the pitching moment. However, at $\alpha = -20°$ the drag becomes positive because it overcomes the component of thrust in the wind coordinate system x-direction, thus increasing the effect of the momentum drag on the pitching moment. This accounts for the dip in the pitching moment curve above -20 degrees angle of attack in Figure 4-13. Figure 4-14 also shows a peak at the same angle of attack as the maximum lift (Figure A-5), but there is another hump at $\alpha = -60°$, which does not correspond with any lift peaks or drag sign changes. It is possible that a small separation bubble developed on the duct lip, reducing the load on the duct and increasing the load on the fan. Because most of the pitching moment is carried by the duct, as mentioned previously, the loss in duct lift decreased the pitching moment, but the increase in fan loading prevented a decrease in vehicle total lift and did not influence the pitching moment. At 85 ft/s, Figure 4-15, the profile drag has a larger influence on the pitching moment of the vehicle, but at angles of attack near zero (not shown in the plot) the momentum drag would probably generate a net positive pitching moment because of the high crosswind velocity.

Comparing the three lip geometries, the pitching moment for the Revised lip is about twice that of the Baseline lip, and the pitching moment for the Enlarged lip lies approximately halfway between values for the other two lips. The asymmetric lift distribution has a large influence on

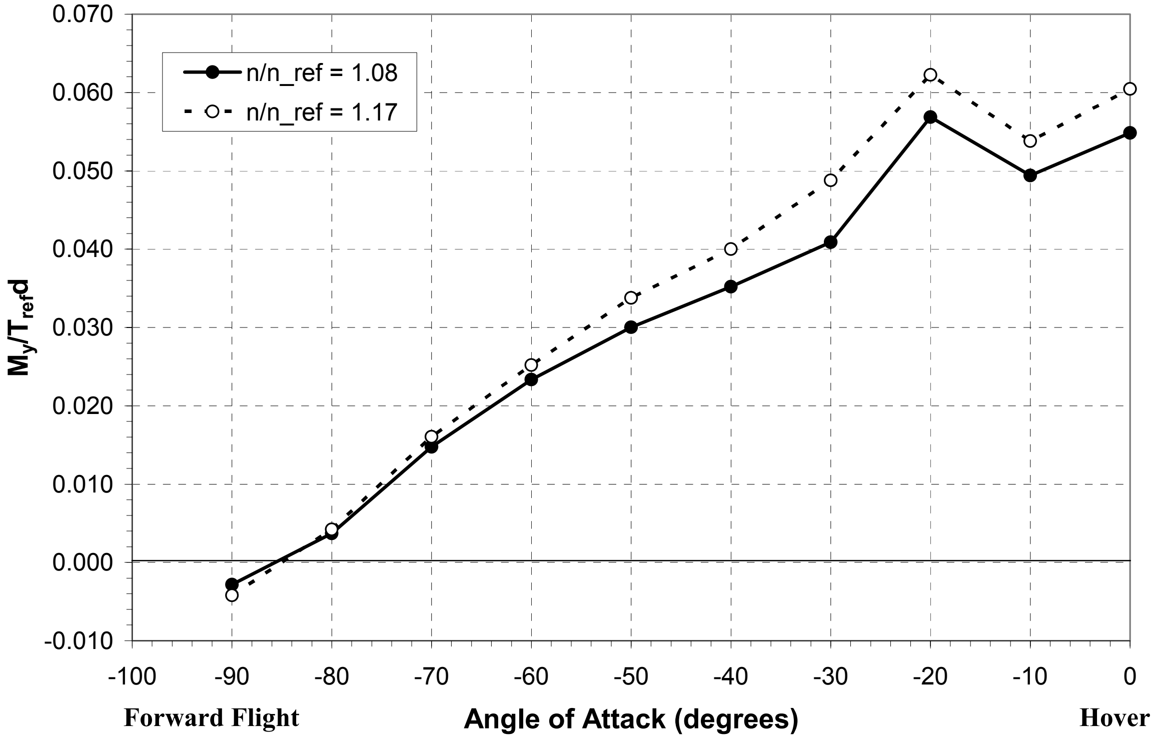

Figure 4-13: Pitching moment trends for the Revised lip as a function of angle of attack at various fan speeds and a tunnel velocity of 30 ft/s.

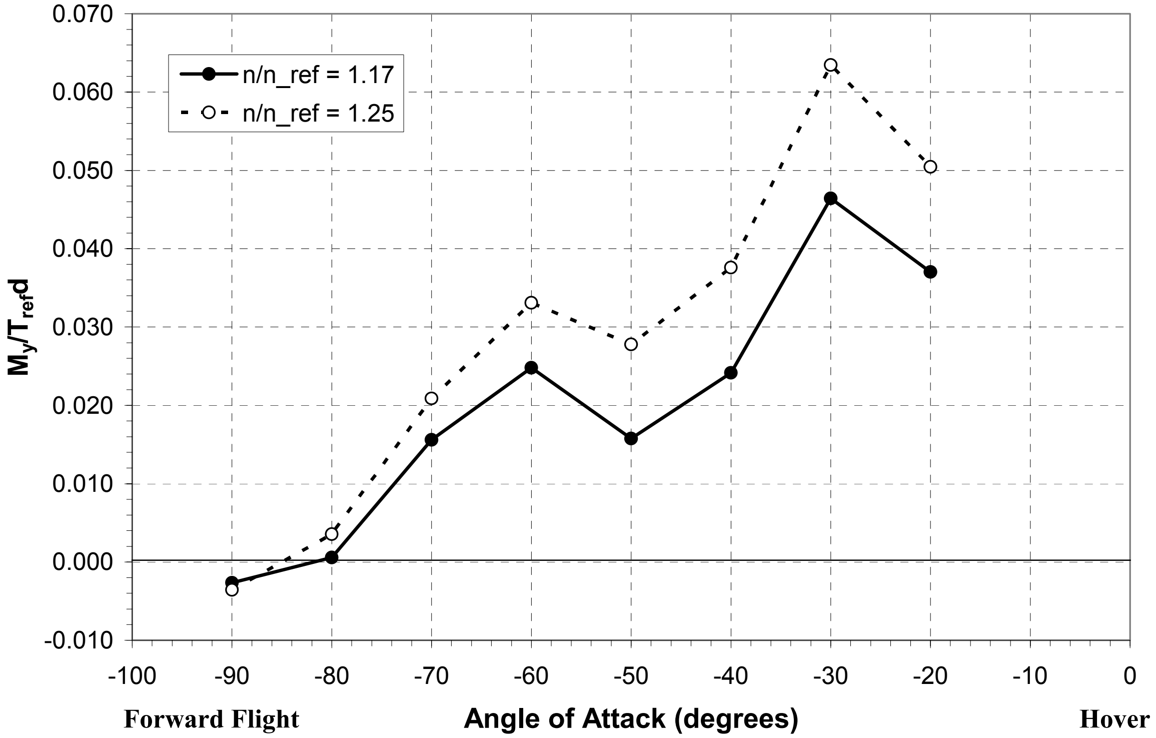

Figure 4-14: Pitching moment trends for the Revised lip as a function of angle of attack at various fan speeds and a tunnel velocity of 60 ft/s.

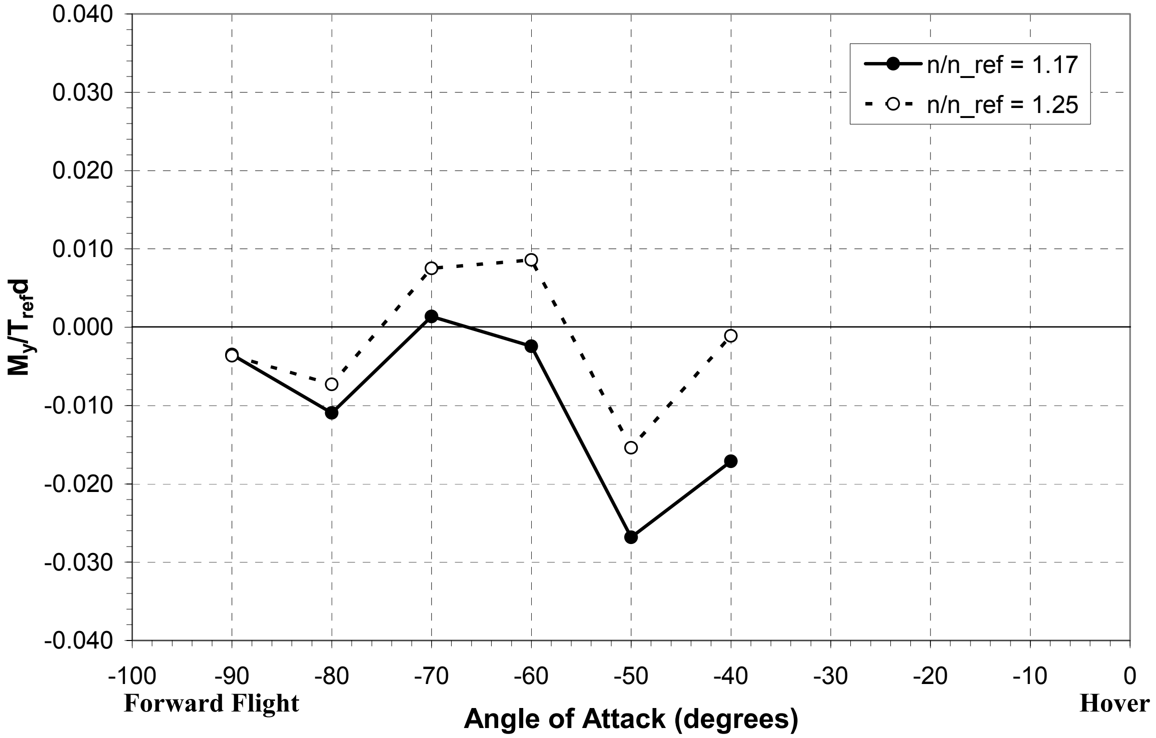

Figure 4-15: Pitching moment trends for the Revised lip as a function of angle of attack at various fan speeds and a tunnel velocity of 85 ft/s.

the difference between the pitching moments for the various lip geometries, but, as will be discussed next, the location of the center of pressure also has a hand in the pitch characteristics for each lip.

Momentum drag affects the pitching moment because it acts at the center of pressure as opposed to the center of gravity of the vehicle. The distance from the center of pressure to the center of gravity (approximately at the duct lip, typically) is the moment arm by which the drag is multiplied by to generate the pitching moment. Knowledge of the dependence of the center of pressure location, z_{cp}, on the crosswind velocity and angle of attack of the vehicle is beneficial in predicting pitching moment characteristics. The center of pressure location is calculated by dividing the pitching moment by the F_x force, taking into account all drag effects, not just those due to the momentum drag. For the Baseline and Enlarged lips Figure 4-16 shows the movement of the center of pressure ($z_{cp}/d = \pm0.024$) as the crosswind velocity increases with the duct at 0 degrees angle of attack, and Figure 4-17 shows the same but for an angle of attack of -15 degrees. The higher z_{cp} for the Enlarged lip reflects the larger pitching moment described

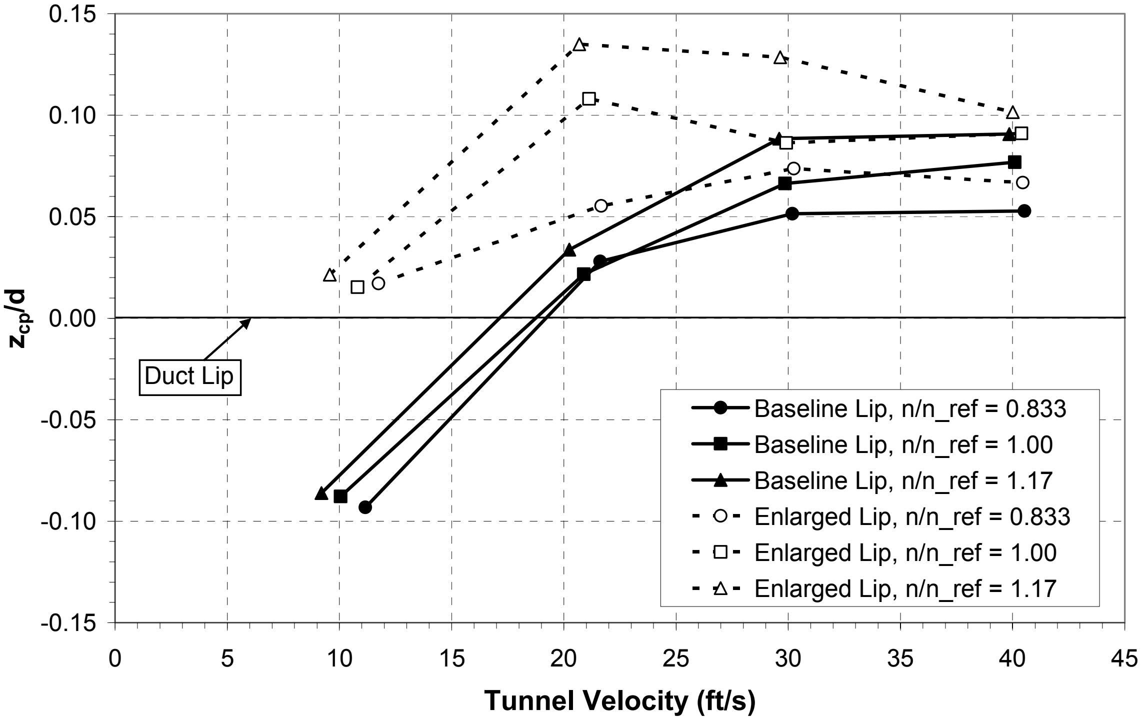

Figure 4-16: Comparison of the location of the center of pressure for the Baseline and Enlarged lips at various fan speeds and an angle of attack of 0 degrees.

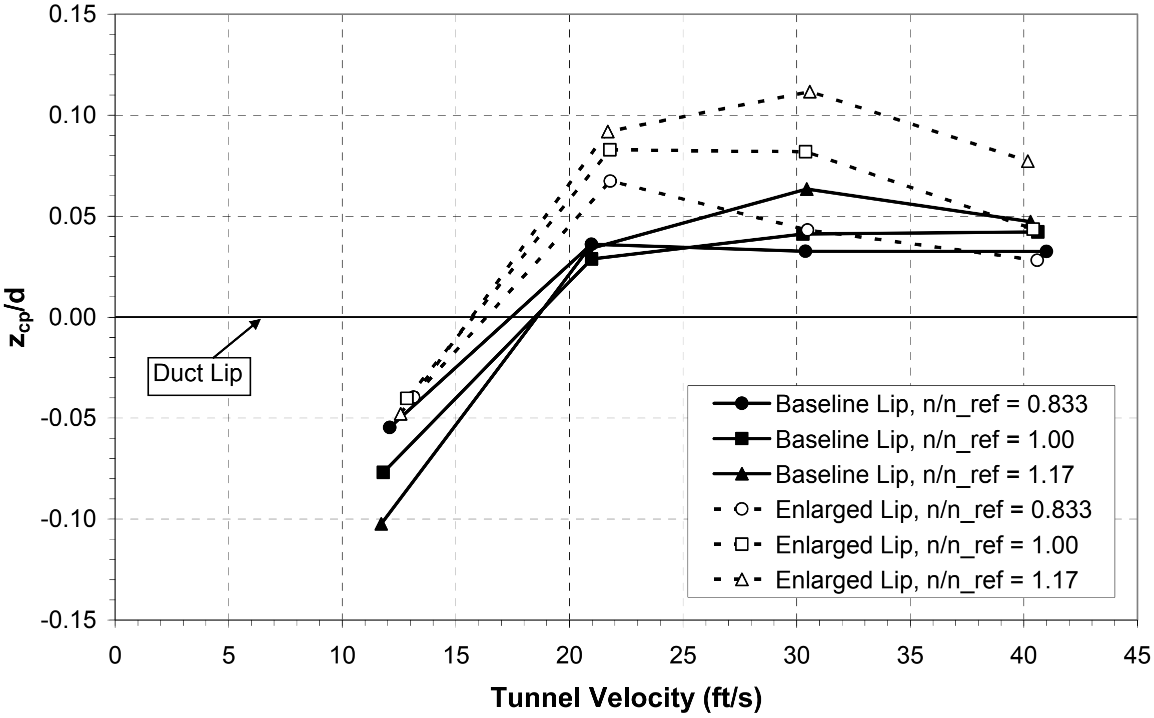

Figure 4-17: Comparison of the location of the center of pressure for the Baseline and Enlarged lips at various fan speeds and an angle of attack of -15 degrees.

previously. Also, above 20 ft/s z_{cp} begins to level off and even decreases slightly at higher tunnel velocities.

This can be seen further for the Revised lip in Figure 4-18 through Figure 4-20 where the center of pressure ($z_{cp} = \pm 0.020$) begins at a distance around 12% of the duct diameter above the duct lip at 30 ft/s and decreases to a location at or slightly below the duct lip at 85 ft/s. This explains why the pitching moment in Figure 4-15 (at 85 ft/s) is negative throughout most of the angle of attack range. The decrease in z_{cp} can be attributed to the smaller capture area of the freestream air that is ingested by the duct as the wind velocity increases and the larger influence of profile drag. Data at negative 90 degrees angle of attack is not plotted because z_{cp} tends to become large due to its inverse proportionality with F_x, which practically disappears at that angle. The most important information that these plots offer is that, although there is some small affect of angle of attack, the center of pressure location remains relatively constant over most of the angle of attack range presented, which corresponds to data presented by Fletcher[30]. Therefore, it can be assumed that z_{cp} is not a function of angle of attack, particularly at angles between -70 degrees and 0 degrees. Comparing the lip geometries, the center of pressure location for the Enlarged and Revised lips is relatively close, while the center of pressure for the

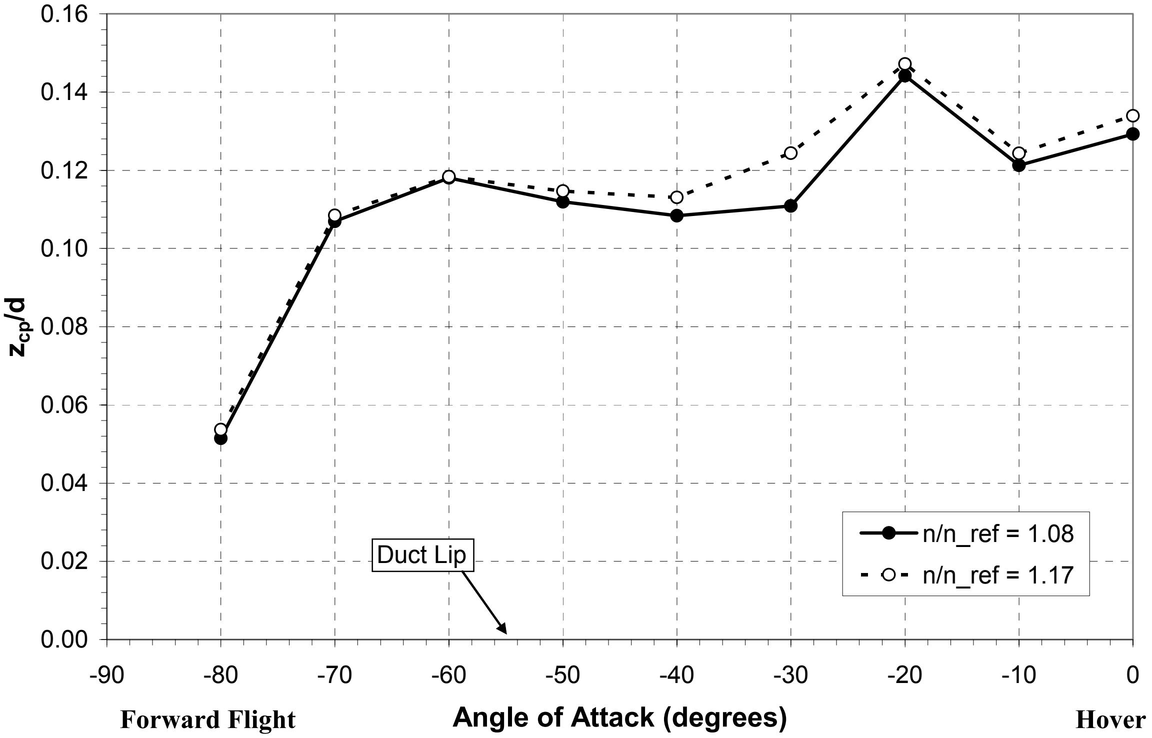

Figure 4-18: Center of pressure location as a function of angle of attack for the Revised lip at various fan speeds and a tunnel velocity of 30 ft/s.

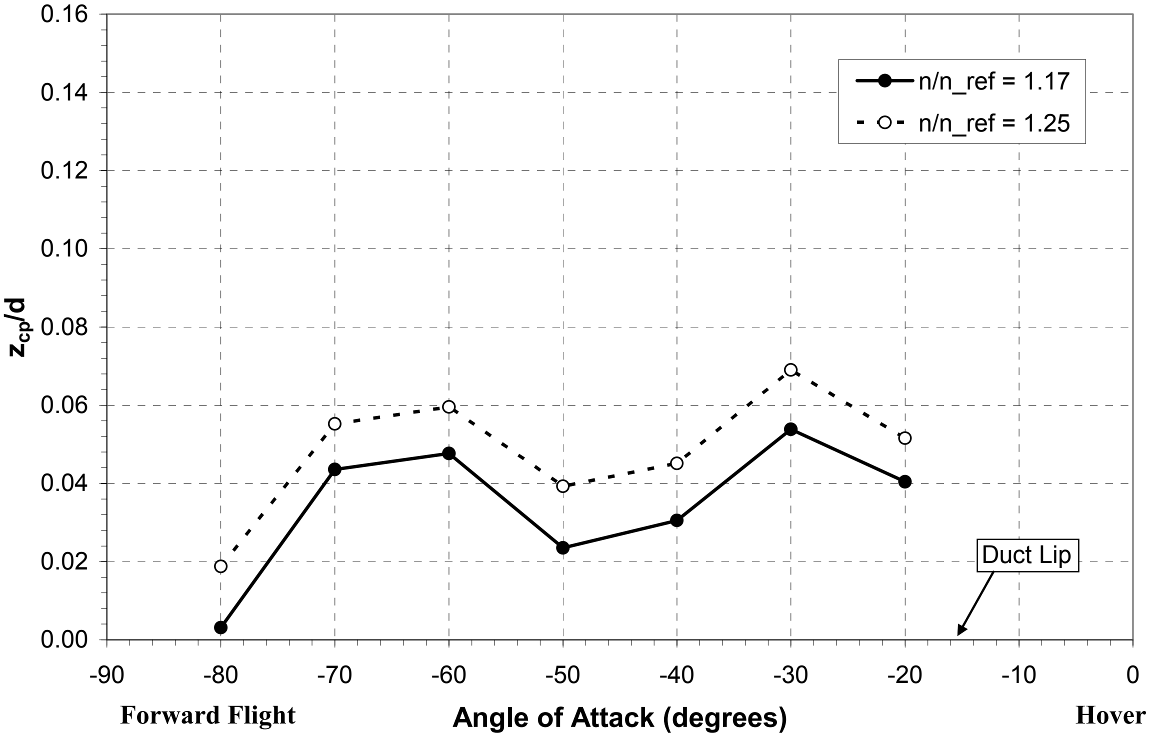

Figure 4-19: Center of pressure location as a function of angle of attack for the Revised lip at various fan speeds and a tunnel velocity of 60 ft/s.

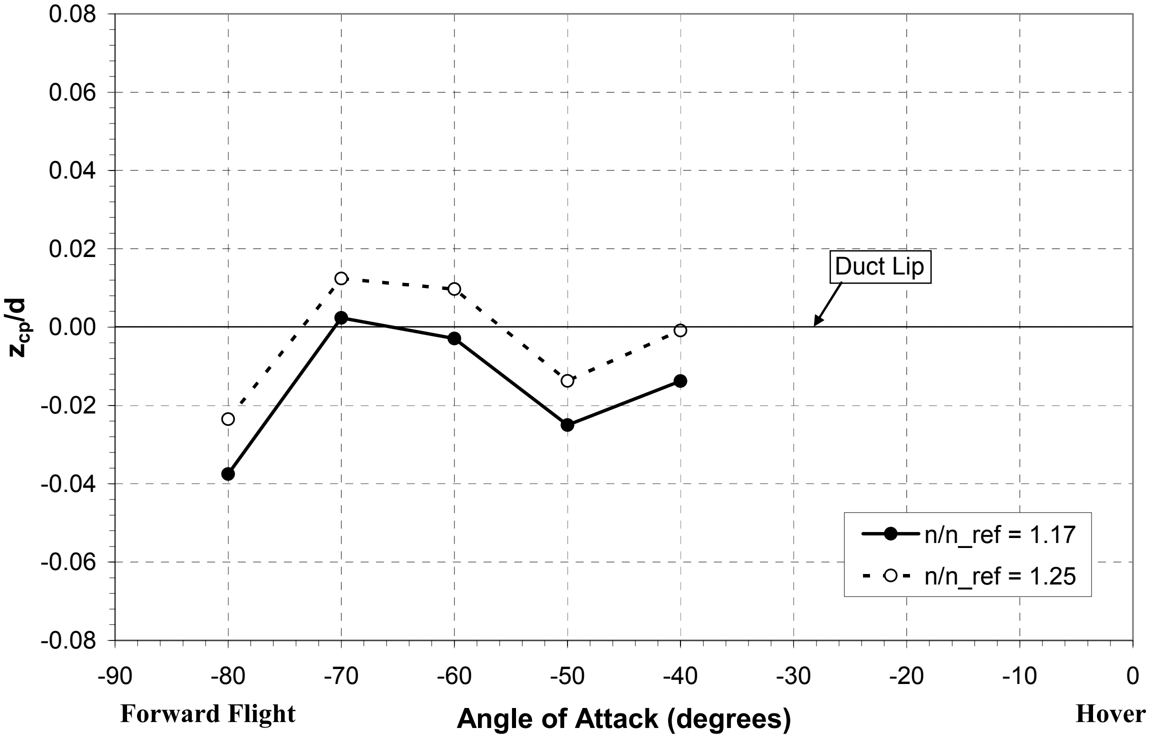

Figure 4-20: Center of pressure location as a function of angle of attack for the Revised lip at various fan speeds and a tunnel velocity of 85 ft/s.

Baseline lip falls to approximately 75% of z_{cp} for the other lips.

To summarize the duct lip testing, the Revised lip has the best static performance, while the Baseline lip performs best in crosswinds and forward flight. The primary reason for this, as shown in the diagnostic testing results, is flow separation on the interior of the duct lip. The Enlarged and Revised lips are less susceptible to flow separation due to their larger lip radii and lack of regions described by a high rate of curvature. Because of this, the Enlarged and Revised lips generate more thrust, and thus lift, in both static and forward flight conditions. However, the additional lift exacerbates the already asymmetric lift distribution, resulting in an increase in the adverse pitching moment. Additionally, the center of pressure location is affected by the lip geometry, causing the momentum drag to have a larger effect on the pitching moment as the center of pressure moves higher above the duct lip. Unfortunately, even the Baseline lip fails to improve the pitch characteristics to an acceptable level, enforcing the need for control vanes positioned aft of the duct for attitude control and vehicle trim.

4.2 Control Vane Results

Control vane effectiveness was determined by varying the control vane deflection from -30 degrees to +30 degrees in 5 degree increments and analyzing the resulting moments generated. The duct utilized the Revised lip shape because of its better static performance. Figure 4-21 shows control vane effectiveness, particularly pitch vane effectiveness ($M_y/T_{ref}d = \pm 0.003$), in static conditions as a function of the fan speed. This particular static testing was not performed on the thrust stand due to the difficulty in measuring the pitching moment with that setup. Instead, the wind tunnel setup, using the sting-mount balance, was utilized with the support strut mounted to a portable cart, and the testing was performed in an open area to create static conditions. Even with stators included in the model configuration to reduce fan swirl, the control vanes show limited effectiveness at large deflection angles due to flow separation. Particularly, deflection angles outside of the range from 20 degrees to -25 degrees display little improvement in pitching moment control. This can be seen more clearly in Figure 4-22, which shows the change in pitching moment as a function of vane deflection angle. At large deflection angles the slopes of the vane effectiveness curves begin to decrease and, in some cases, flatten out.

Flow tufts were utilized during static testing to confirm that flow separation was the cause of the loss of control authority, and the qualitative results can be seen in Figure 4-23 and

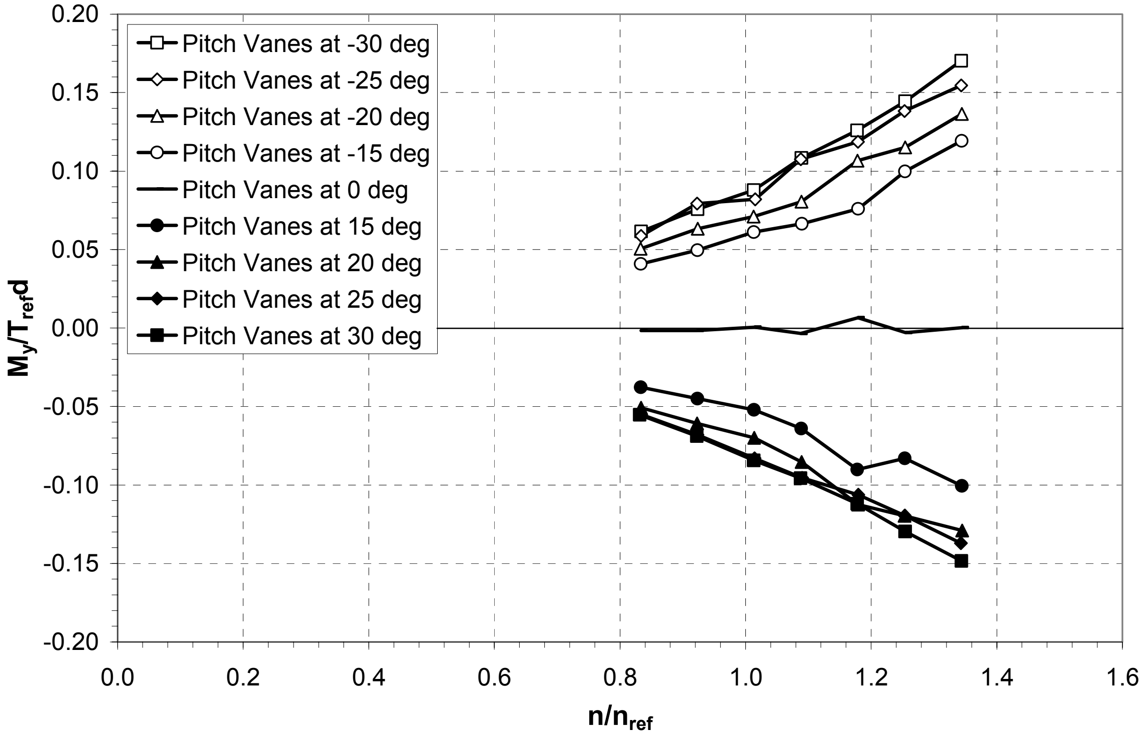

Figure 4-21: Control vane effectiveness (pitch vanes only) in static conditions as a function of the fan speed.

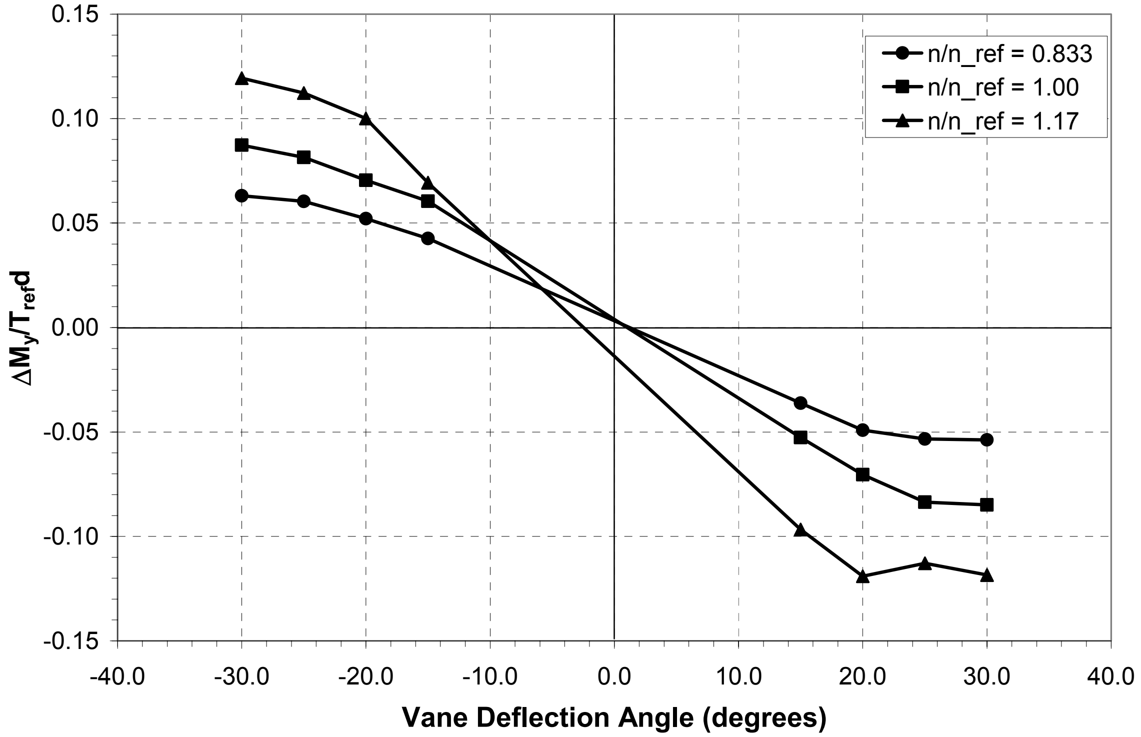

Figure 4-22: Control vane effectiveness (pitch vanes only) in static conditions as a function of vane deflection angle at various fan speeds.

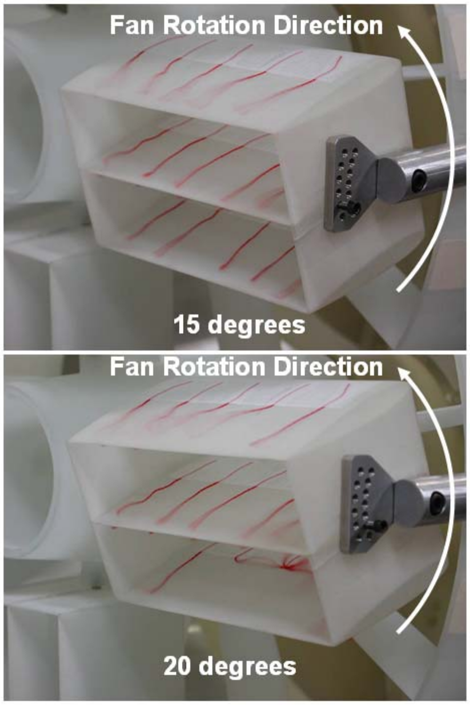

Figure 4-23: Tuft flow visualization on a control vane in static conditions and $n/n_{ref} = 1.00$ showing flow separation occurring between 15 degrees and 20 degrees vane deflection.

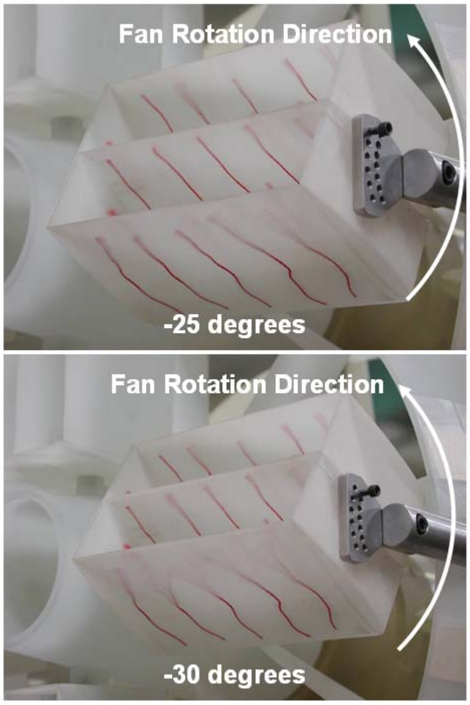

Figure 4-24: Tuft flow visualization on a control vane in static conditions and $n/n_{ref} = 1.00$ showing flow separation occurring between -25 degrees and -30 degrees vane deflection.

Figure 4-24. Figure 4-23 shows the control vane at 15 degrees, where a majority of the flow is attached to the three blades of the vane, and at 20 degrees, where separation is more noticeable on the top blade and the bottom blade is almost completely stalled. In Figure 4-24, the flow remains mostly attached even at -30 degrees vane deflection, although some separation is noticeable on the bottom blade at that deflection angle. Because of the fan rotation direction, when the vane is at a positive deflection it sees a larger angle of attack than when at a negative deflection, even with stators removing most of the swirl in the duct jet. This is the reason for the separation occurring at smaller deflection angles in the positive direction than in the negative direction. Overall, the information gathered from the tuft flow visualization corresponds with the data in Figure 4-21.

In addition to static testing, the control vane effectiveness was tested in the wind tunnel at various tunnel velocities and angles of attack. Figure 4-25, Figure 4-26, and Figure 4-27 show the pitching moment ($M_y/T_{ref}d$ = ±0.013) generated by pitch vane deflections as a function of angle of attack at 30 ft/s, 60 ft/s, and 85 ft/s, respectively. It is necessary to mention that the model configuration corresponding to this data included additional components, such as avionics

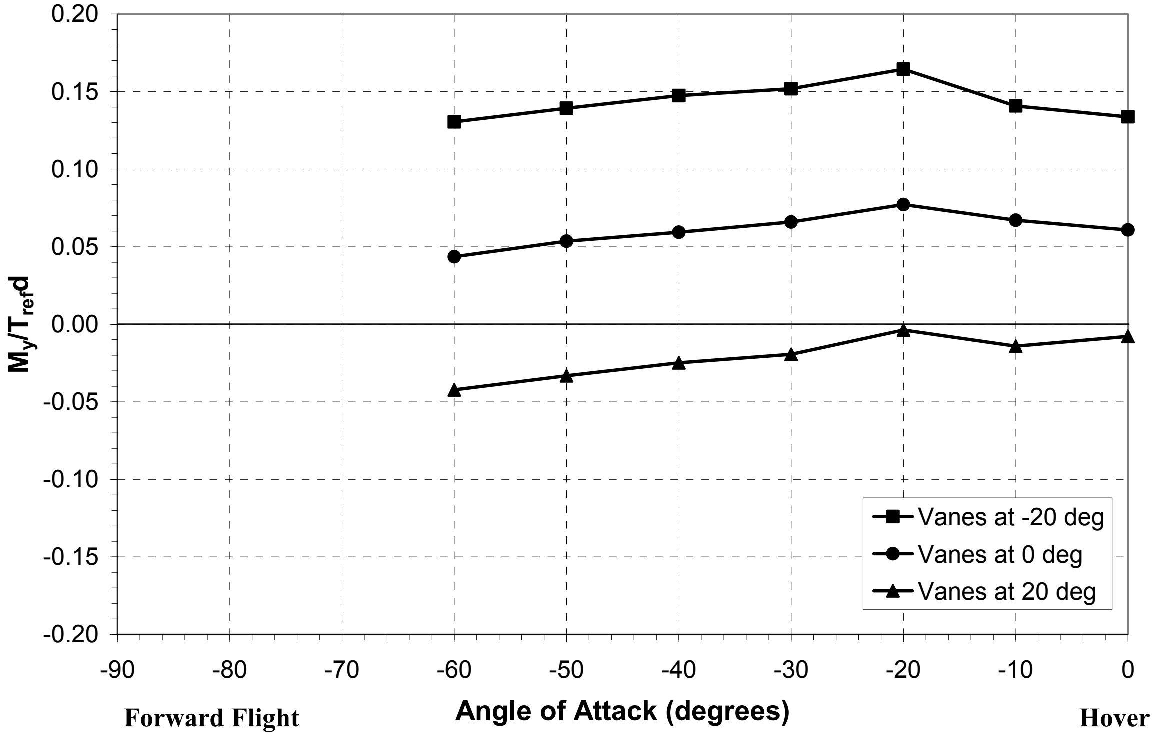

Figure 4-25: Control vane effectiveness (pitch vanes only) in crosswind conditions as a function of angle of attack at a tunnel velocity of 30 ft/s and n/n_{ref} = 1.08.

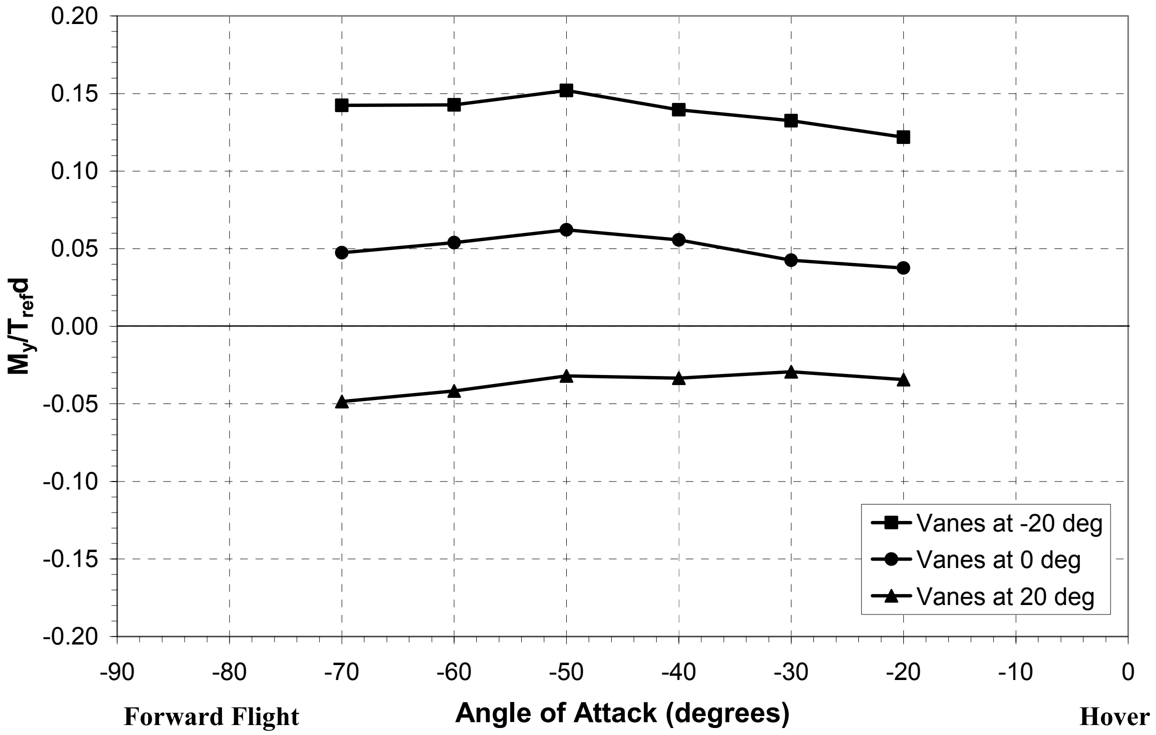

Figure 4-26: Control vane effectiveness (pitch vanes only) in crosswind conditions as a function of angle of attack at a tunnel velocity of 60 ft/s and $n/n_{ref} = 1.08$.

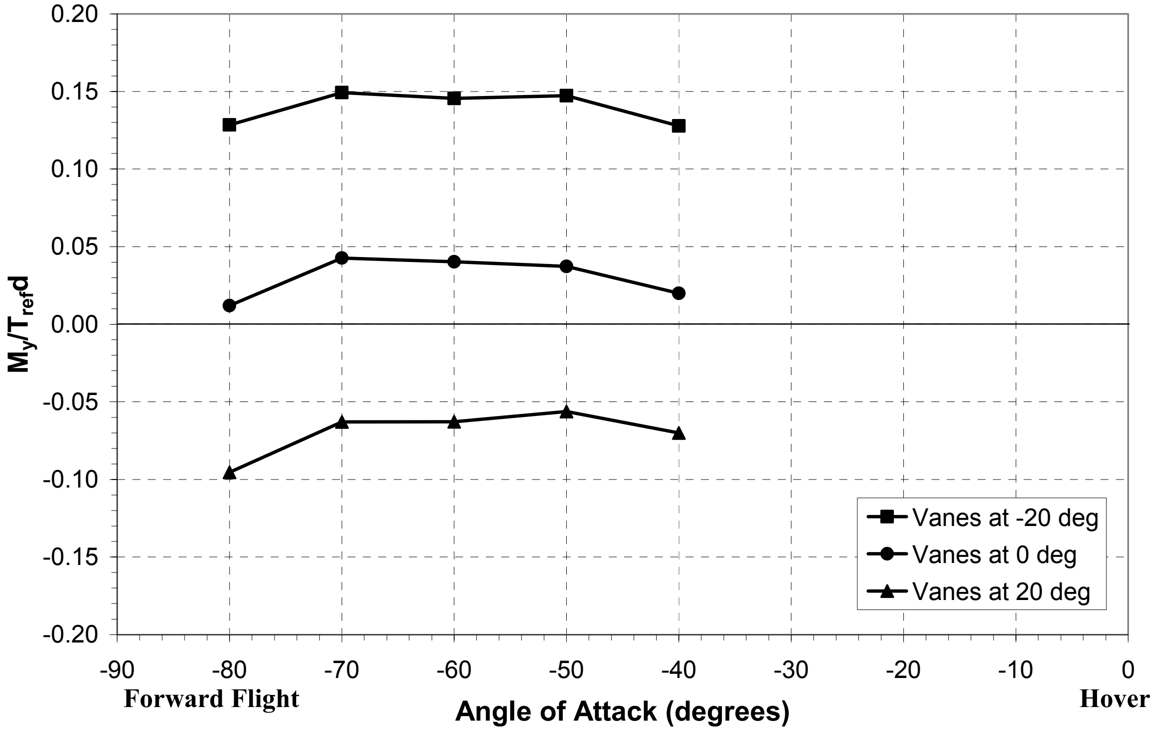

Figure 4-27: Control vane effectiveness (pitch vanes only) in crosswind conditions as a function of angle of attack at a tunnel velocity of 85 ft/s and $n/n_{ref} = 1.08$.

pods and replications of a small, two-cylinder piston engine and muffler, as shown in Figure 3-12, which would result in slightly different pitching moments, and thus vane effectiveness data, than if the clean duct configuration was tested. Nevertheless, this data still represents the trends associated with control vane effectiveness in a crosswind. The plots show that the control vane effectiveness curves shift down as the tunnel velocity increases due to the smaller pitching moments experienced by the vehicle at larger velocities and angles of attack closer to -90 degrees. Also, at each tunnel speed the vanes provide enough control authority to trim the vehicle ($M_y/T_{ref}d$ = 0). However, particularly at 30 ft/s, the trimmed control vane deflection is relatively large, preventing the vehicle from using additional deflection to further adjust its attitude.

An empirical trimmed control vane model was developed to determine the control vane deflections necessary to reduce the pitching moment to zero for various configurations. The model is based on the static control vane data shown in Figure 4-22, from which the slopes and intercepts for each fan speed curve can be obtained and applied to pitching moment data for a particular vehicle configuration. In order to verify the results from this model, it was applied to the wind tunnel control vane data shown in Figure 4-25 through Figure 4-27. The results, as

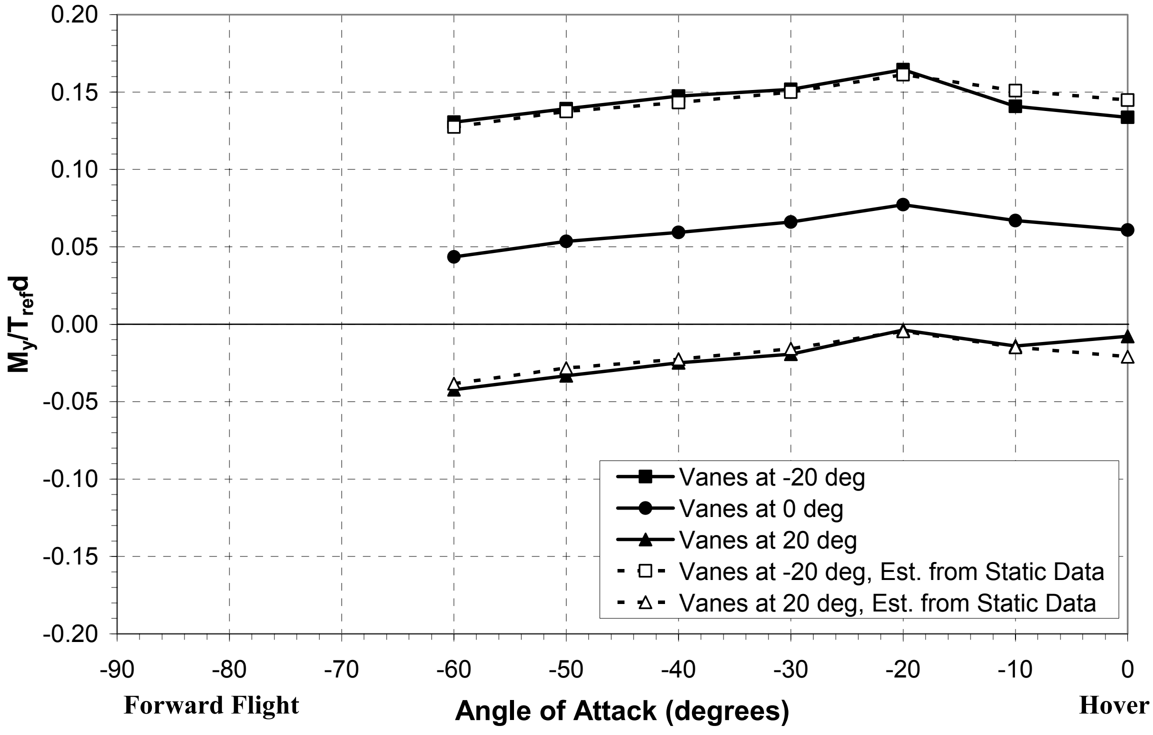

Figure 4-28: Verification of the trimmed control vane model applied to the wind tunnel control vane data at a tunnel velocity of 30 ft/s.

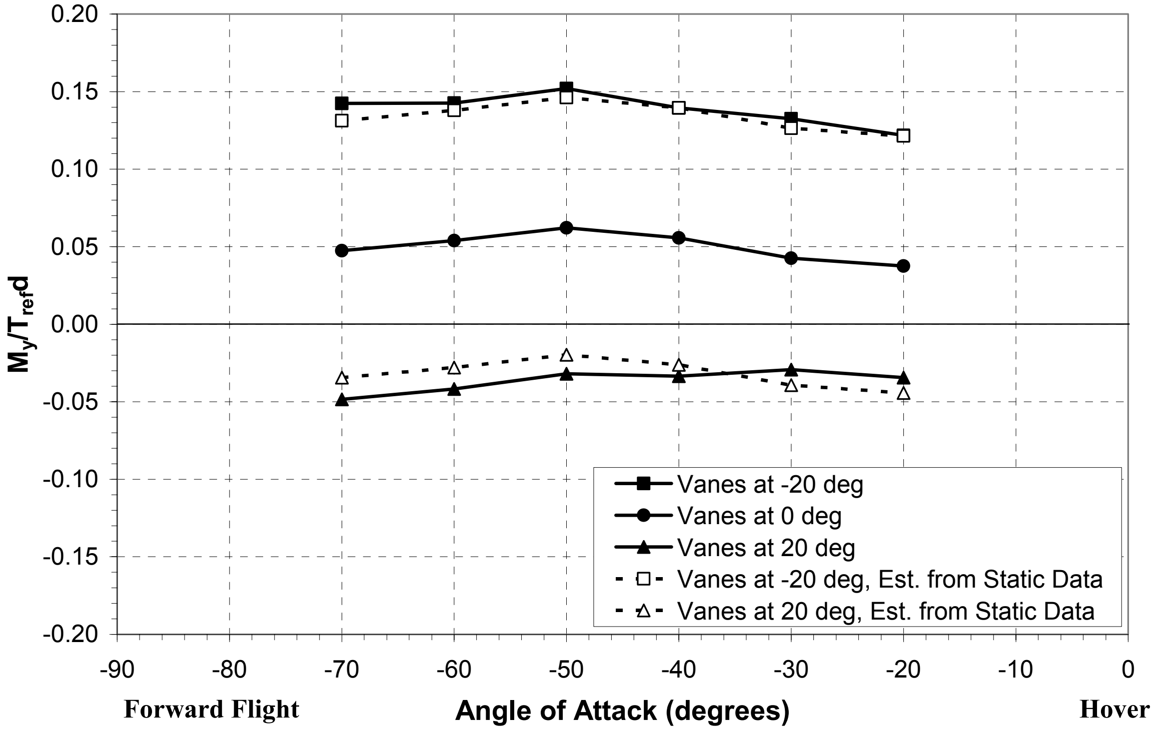

Figure 4-29: Verification of the trimmed control vane model applied to the wind tunnel control vane data at a tunnel velocity of 60 ft/s.

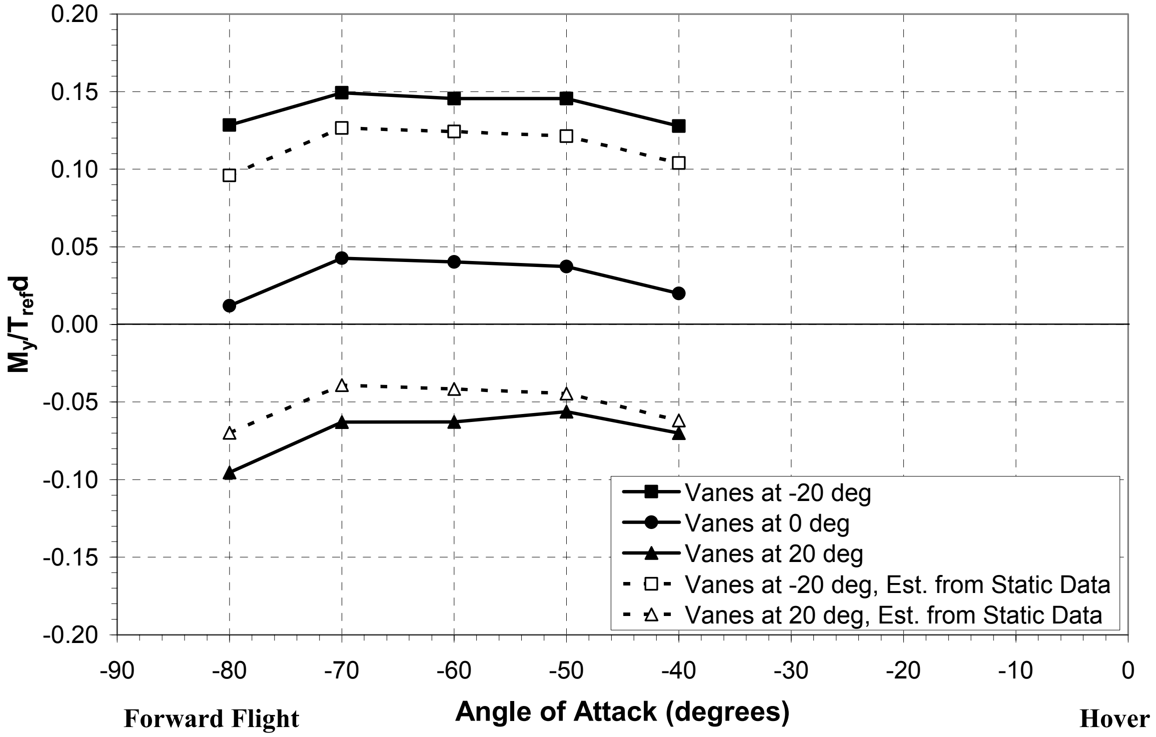

Figure 4-30: Verification of the trimmed control vane model applied to the wind tunnel control vane data at a tunnel velocity of 85 ft/s.

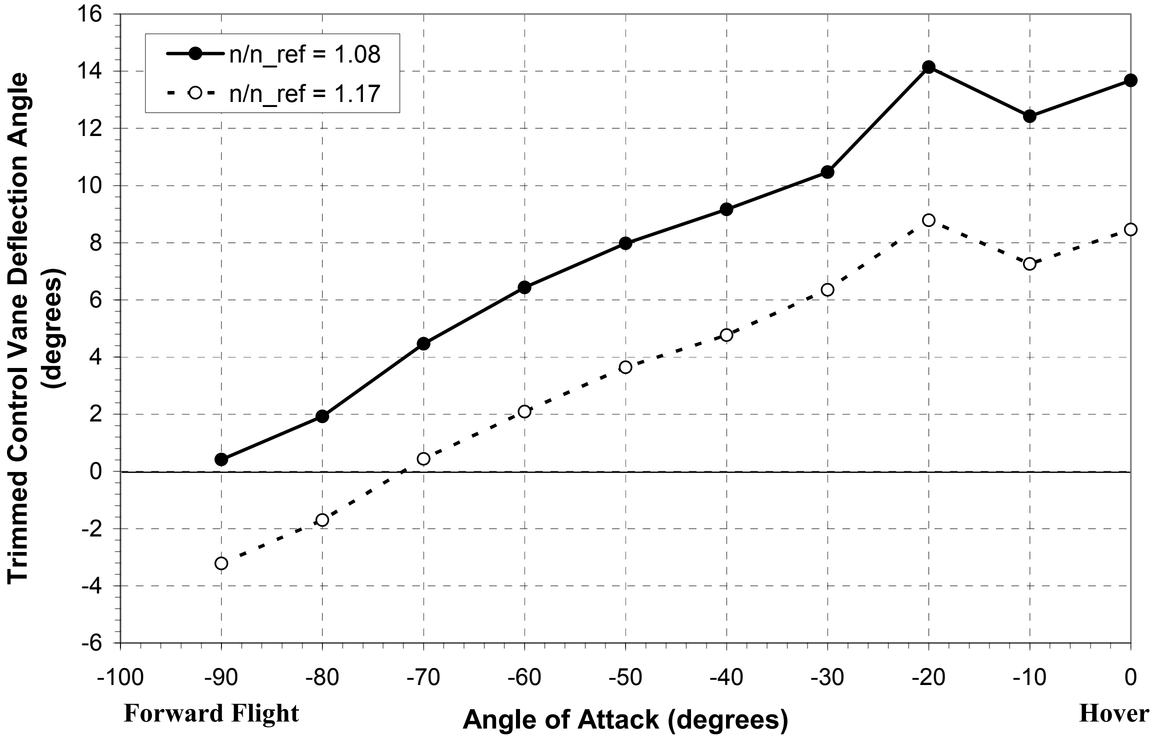

Figure 4-31: Trimmed control vane deflection angles as a function of the angle of attack for the Revised lip at a tunnel velocity of 30 ft/s and two fan speeds.

shown in Figure 4-28, Figure 4-29, and Figure 4-30, match best at lower tunnel velocities, as expected, since the model is based on static data. The model was also applied to the pitching moment results at 30 ft/s for the Revised lip to determine the control vane deflections necessary to trim the clean duct, and the results can be seen in Figure 4-31. Note that larger vane deflections are necessary for the lower fan speeds because the vane effectiveness is dependent on the amount of air moving through the duct since they lie within the duct jet. At angles of attack near hover, approximately 14 degrees of vane deflection is required to cancel the pitching moment generated by the duct. When the vanes stall at around 20 degrees deflection, there is little room left to make larger deflections for attitude control if necessary. This is the primary reason for research into other methods of reducing the adverse pitching moment associated with ducted fan UAVs, some of which are presented in the following sections.

4.3 Auxiliary Control Effector Results

The importance of the duct in the flight characteristics of ducted fan UAVs led to research into devices that could be applied to the duct to influence the aerodynamics. Particularly, auxiliary control effectors placed at the lip impact the flow around the lip, resulting in changes in the lift distribution and pitching moment on the vehicle. As with the control vane testing, the Revised lip shape was used in conjunction with the auxiliary control effectors because of its better performance in static conditions. Three control effectors were tested: lip spoiler, leading edge slat, and duct deflector. Each effector was tested in more than one configuration to determine its effectiveness both as an actuated device and as a permanently fixed device. For instance, the lip spoiler and duct deflector were applied to both the windward and leeward sides of the duct (non-actuated configuration), as well as only the windward side (actuated configuration). The leading edge slat was present on both sides of the duct throughout its entire testing, with the leeward side always featuring the base configuration while the windward side varied between the base, open, and closed configurations.

Their effects on the pitching moment ($M_y/T_{ref}d = \pm 0.006$) of the vehicle compared to the case with no control effectors can be seen in Figure 4-32. Both duct deflector configurations outperform the other control effectors. It is believed the windward only duct deflector performs better at more negative angles of attack because of the additional drag generated by the oncoming wind, and the configuration with the duct deflector on both sides of the duct performs better at angles of attack near zero because it is able to create a more symmetric lift distribution between the leeward and windward lips. The lip spoiler on the windward side also displays better performance than the clean duct case because of the separation induced on the duct lip, while the lip spoiler on both sides of the duct shows no significant improvement. The leading edge slat effects are somewhat surprising at first. While the base configuration on both sides of the duct show little improvement, as expected, the configurations with the open and closed leading edge slats actually display larger pitching moments. The initial assumption was that they were producing more lift instead of reducing the lift, as planned. However, an analysis of the lift ($L/T_{ref} = \pm 0.005$), as shown in Figure 4-33, shows this is not the case. Instead, the closed and open configurations produce slightly less lift than the case without control effectors, showing they performed as designed, although not as well as was hoped. This does not explain the larger pitching moment, though. For that, an analysis of the center of pressure location ($z_{cp}/d = \pm 0.018$)

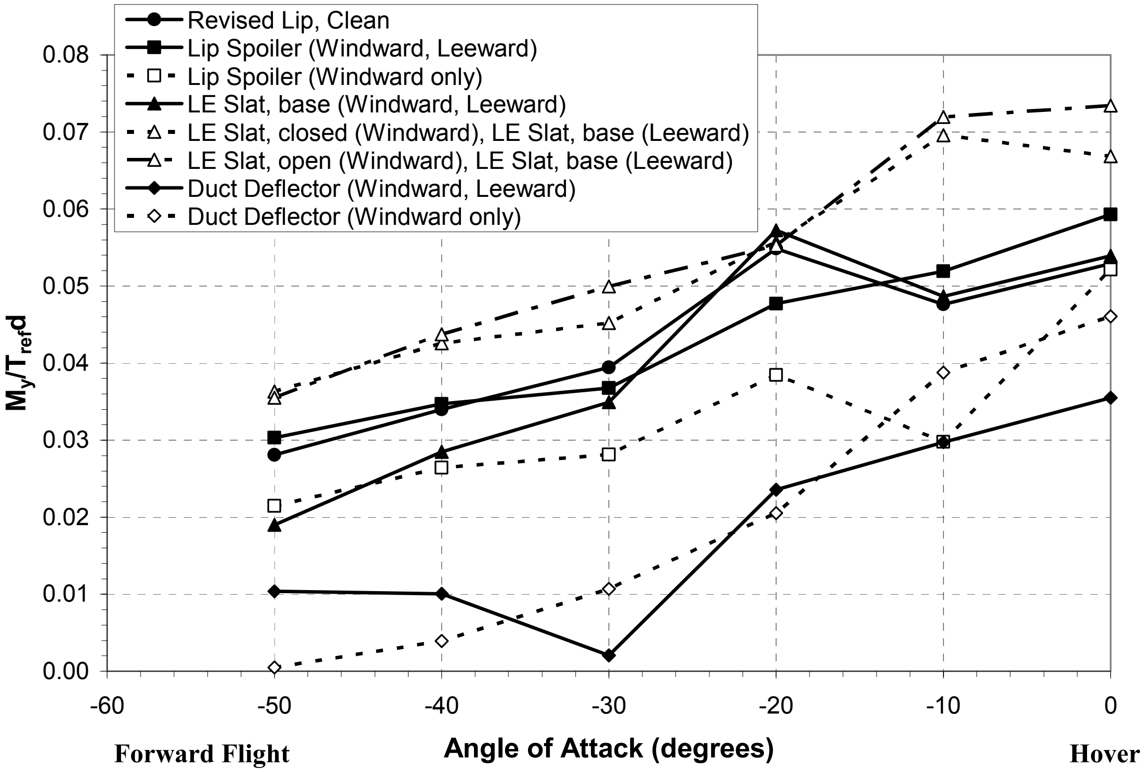

Figure 4-32: Effects of the auxiliary control effectors on the pitching moment as a function of angle of attack at a tunnel velocity of 30 ft/s and $n/n_{ref} = 1.08$.

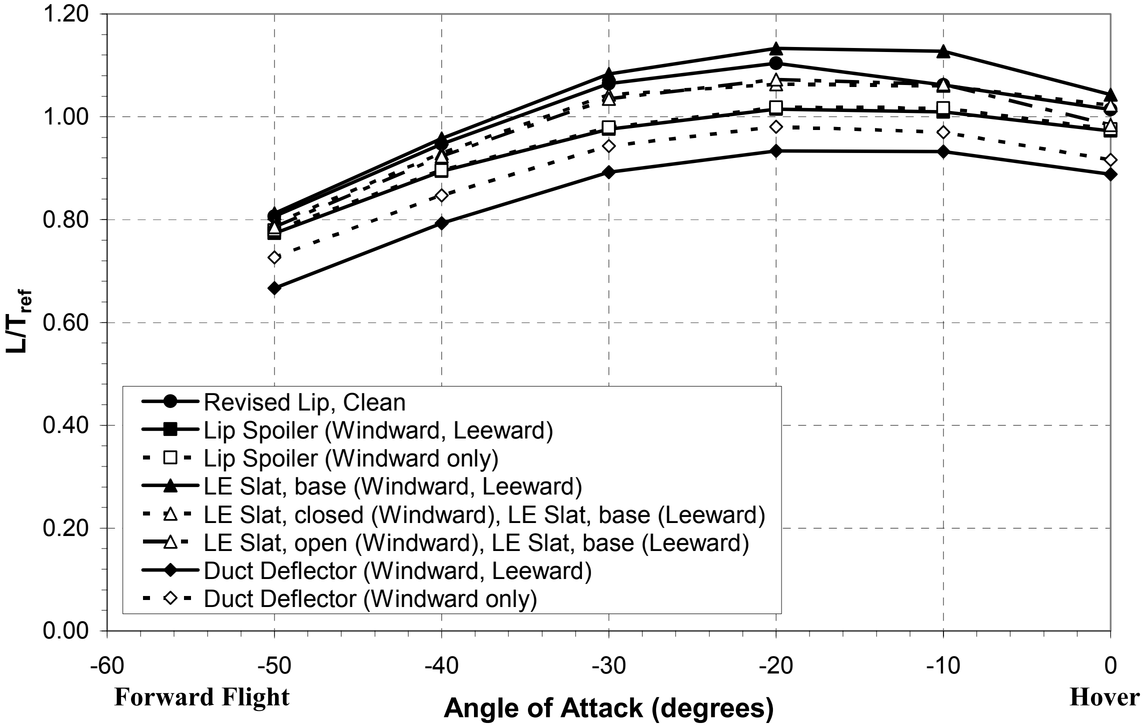

Figure 4-33: Effects of the auxiliary control effectors on the lift force as a function of angle of attack at a tunnel velocity of 30 ft/s and $n/n_{ref} = 1.08$.

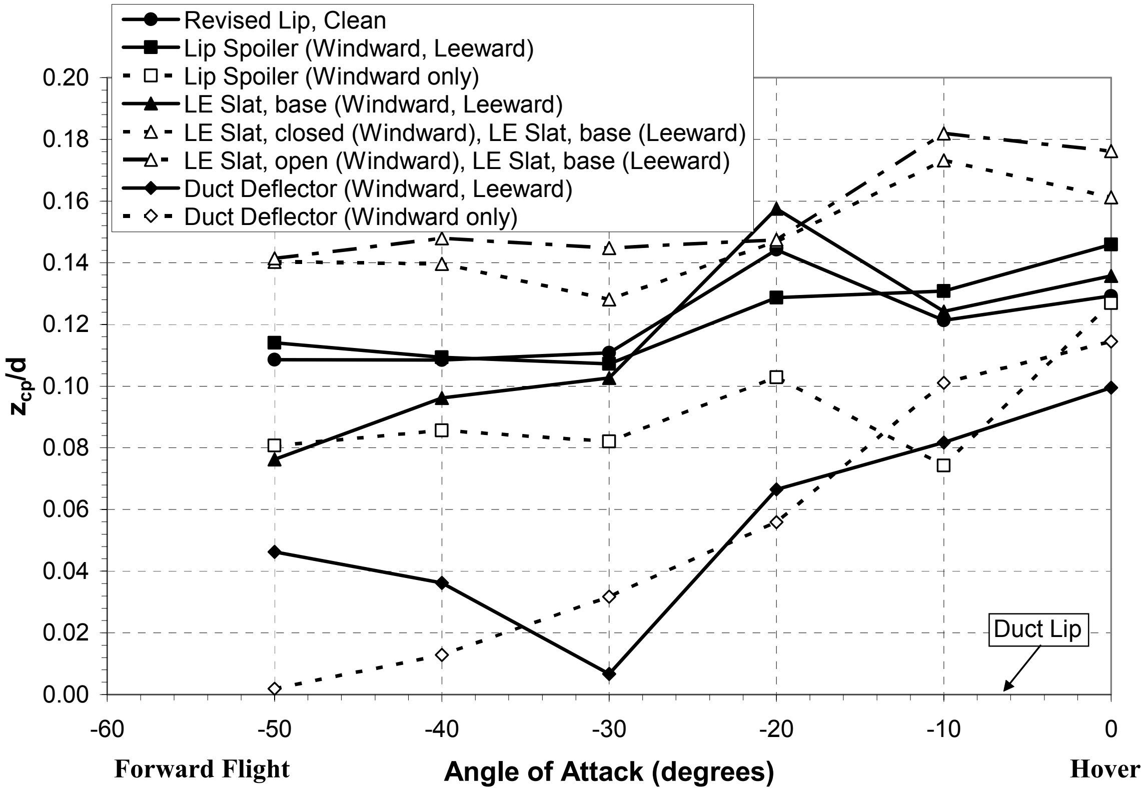

Figure 4-34: Effects of the auxiliary control effectors on the center of pressure location as a function of angle of attack at a tunnel velocity of 30 ft/s and $n/n_{ref} = 1.08$.

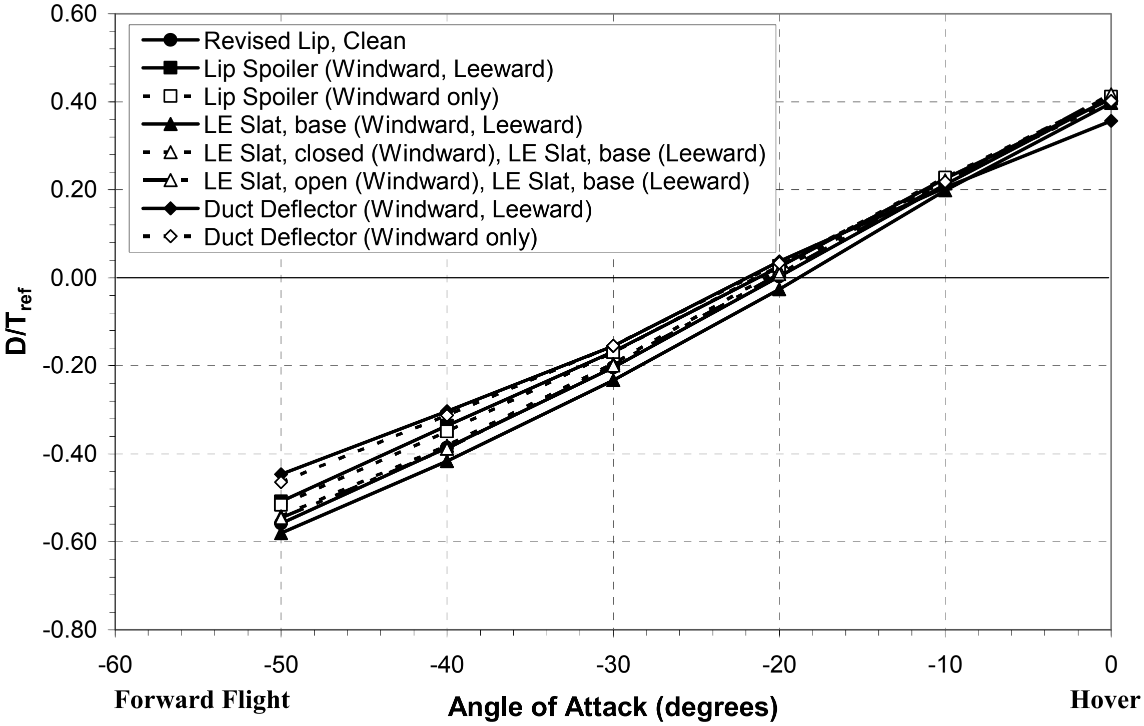

Figure 4-35: Effects of the auxiliary control effectors on the drag force as a function of angle of attack at a tunnel velocity of 30 ft/s and $n/n_{ref} = 1.08$.

was conducted, as shown in Figure 4-34, and it was found that the open and closed leading edge slats increase the height of the center of pressure above the duct lip, thus increasing the moment arm and pitching moment on the vehicle. The open configuration effectively increases the chord of the duct, while the closed configuration effectively increases the thickness of the duct, both of which push the center of pressure higher above the center of gravity of the vehicle. The duct deflector configurations and the windward lip spoiler lower the center of pressure location, which, in addition to the reduction in lift achieved by those designs, as shown in Figure 4-33, contribute to their better pitching moment performance.

The drag ($D/T_{ref} = \pm 0.017$) for each control effector configuration was plotted as a function of angle of attack to determine if any of the designs had additional adverse effects on the aerodynamics. Figure 4-35 shows very little difference between the designs, although as the angle of attack becomes more negative, the differences grow larger, with the duct deflector control effector displaying more drag than the other designs.

Lastly, the trimmed control vane model was applied to the pitching moment data for the auxiliary control effectors to determine the effect each has on the required control vane deflections for trim. Figure 4-36 shows the duct deflector configurations reduce the vane deflection angles by 15% to 30% in hover ($\alpha = 0°$), providing the control vanes with an additional 4 degrees of deflection for vehicle attitude control. The lip spoiler on the windward side also improves the trimmed control vane deflections over the clean duct case, but the difference is not as significant as that provided by the duct deflector configurations. The leading edge slat configurations require larger trimmed control vane deflections because of the larger pitching moment they generate.

In summary, the lip spoiler and the duct deflector show the most promise in reducing the adverse pitching moment and providing the control vanes with additional deflection range. Of the lip spoiler configurations, only the one with the lip spoiler on the windward side showed marked improvement over the clean duct case, while both duct deflector configurations showed significant improvement. In the future, more experimentation should be performed on these and alternative duct deflector designs to determine if perhaps one configuration has an advantage over the other. The current configurations for the leading edge slat actually produce adverse effects on the flight characteristics of the vehicle, but by switching the closed/open leading edge slat to the leeward side and applying the base leading edge slat to the windward side, the results

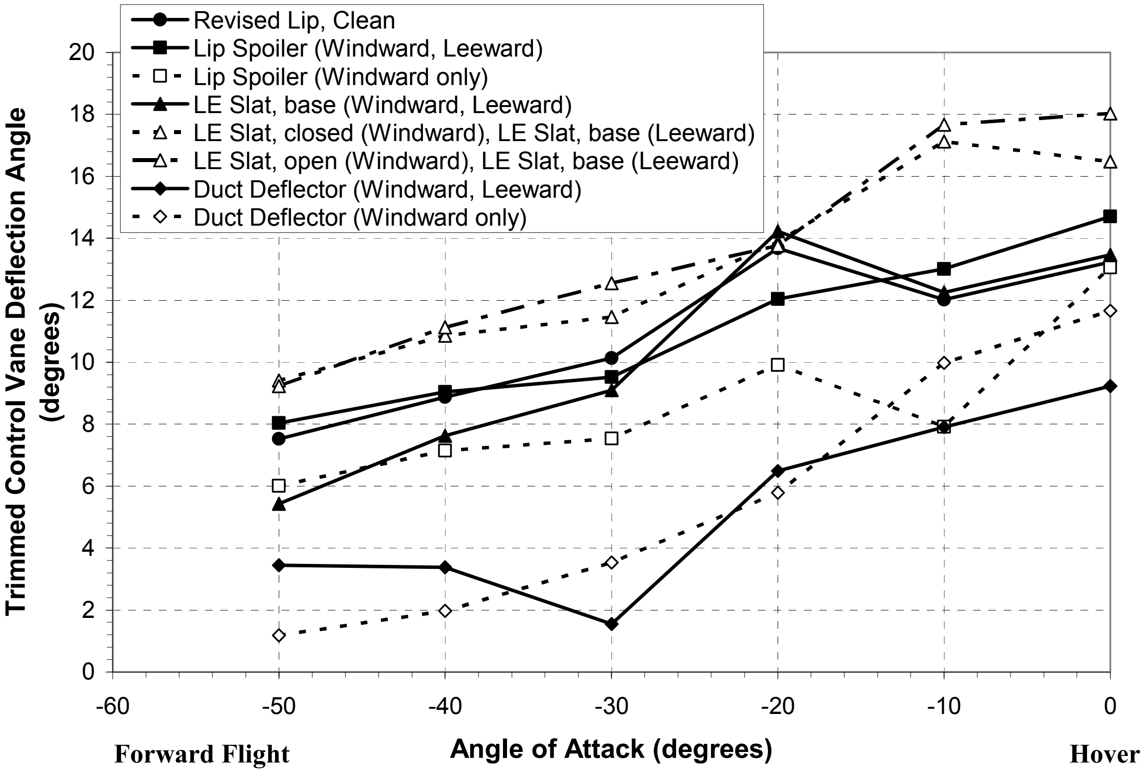

Figure 4-36: Trimmed control vane deflections as a function of angle of attack for the various auxiliary control effectors at a tunnel velocity of 30 ft/s and $n/n_{ref} = 1.08$

could potentially be reversed. In other words, there is room for improvement in the leading edge slat design.

4.4 Stabilizer Vane Testing

Due to the complexity and added weight of actuated control devices, two stabilizer vane configurations were tested to determine their effectiveness in reducing the adverse pitching moment. The passive (non-actuated) stabilizer vanes were designed to take advantage of the bending duct jet in a crosswind. The freestream flow in forward flight or in a crosswind turns the fan jet exiting the duct, allowing the stabilizer vanes to see an angle of attack and generate a force to counter the adverse pitching moment. While the stabilizer vane geometry remained constant, two configurations were tested: one with the leading edge of the stabilizer vanes 6 inches aft of the trailing edge of the duct, and the other 8 inches aft of the duct. Because of its improved static performance, the Revised lip was the chosen lip geometry throughout this testing. As with the wind tunnel control vane testing, the stabilizer vane testing was conducted with additional components attached to the model. To adjust for this, the change in pitching moment caused by each stabilizer vane configuration was added to the data for the clean duct case to show the effects the stabilizer vanes would have on a clean duct.

Figure 4-37, Figure 4-38, and Figure 4-39 show the stabilizer vane effects on the pitching moment ($M_y/T_{ref}d$ = ±0.011) at various angles of attack for 30 ft/s, 60 ft/s, and 85 ft/s, respectively. At 30 ft/s the 6-inch stabilizer vane only provides a small improvement in pitching moment because the crosswind does not bend the duct jet enough to produce a significant force on the vanes at that distance from the duct. Also, the duct jet protects the stabilizer vanes from the crosswind through most of the angles of attack, preventing a drag force from being generated on the vanes. However, at an angle of attack of -10 degrees, the 8-inch stabilizer vane configuration extends aft enough to see a larger angle of attack from the turned duct jet. Although the change in angle of attack may only generate a small change in force on the vanes, the large moment arm from the vanes to the center of gravity at the duct lip amplifies the effect the force has on the pitching moment, resulting in a sudden decrease in pitching moment from the additional force on the vanes. At 60 ft/s, the stabilizer vanes have a much larger effect because the duct jet has been turned more, and the vanes produce larger forces. Unfortunately,

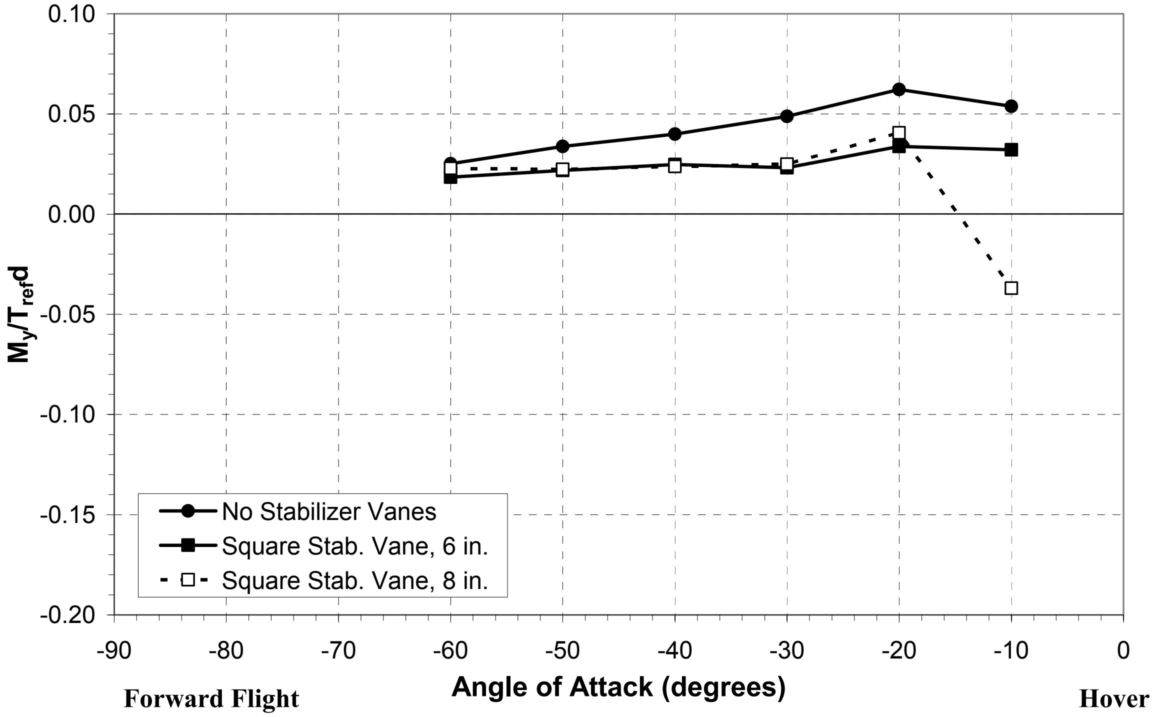

Figure 4-37: Effects of stabilizer vanes on the pitching moment as a function of angle of attack at a tunnel velocity of 30 ft/s and n/n_{ref} = 1.17.

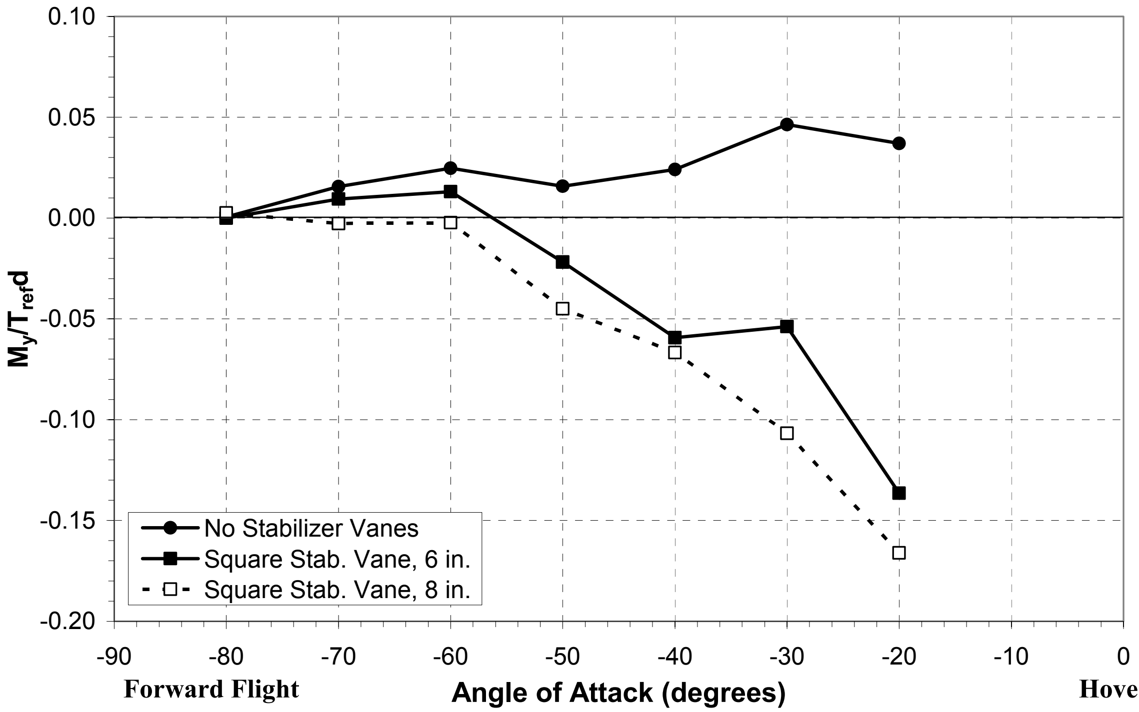

Figure 4-38: Effects of stabilizer vanes on the pitching moment as a function of angle of attack at a tunnel velocity of 60 ft/s and $n/n_{ref} = 1.17$.

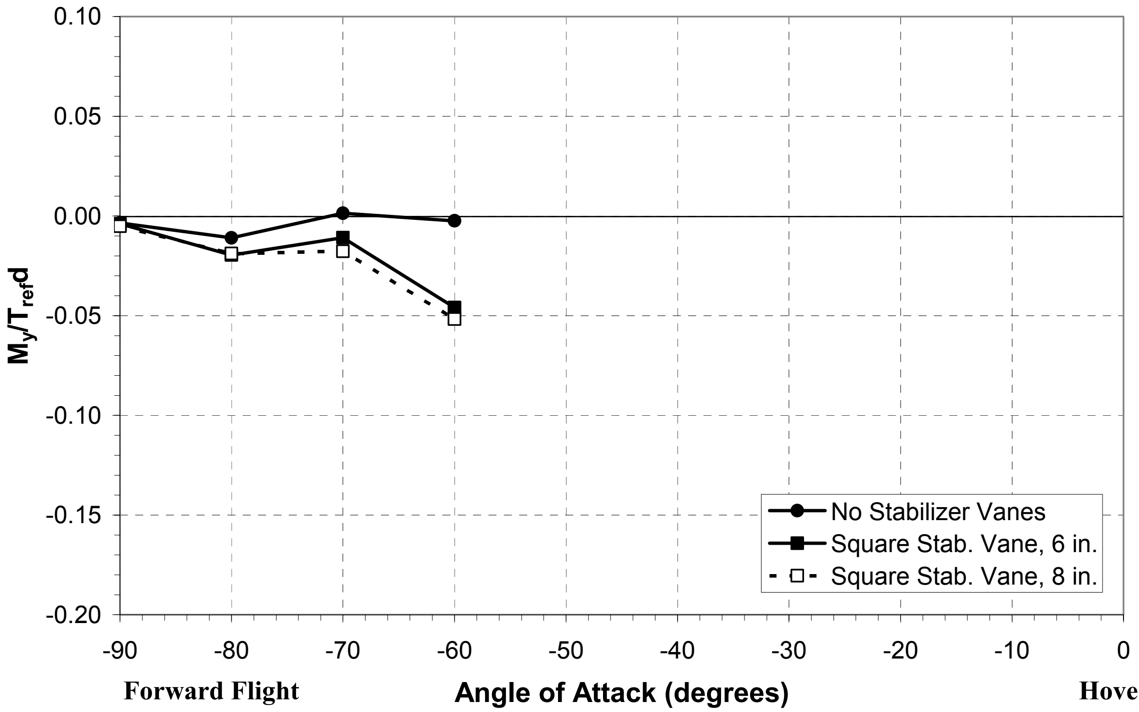

Figure 4-39: Effects of stabilizer vanes on the pitching moment as a function of angle of attack at a tunnel velocity of 85 ft/s and $n/n_{ref} = 1.17$.

though, the pitching moment is quite large in the negative direction, which would require additional input from the control vanes to trim the vehicle since the stabilizer vanes are not actuated in any way. At 85 ft/s, the vehicle does not necessarily need the stabilizer vanes, especially at angles of attack close to -90, but if installed without actuation, the stabilizer vanes would cause a net negative pitching moment that would need to be trimmed by the control vanes. In general, the center of pressure location for the stabilizer vane configurations at each tunnel velocity remains below the duct lip, further contributing to the negative pitching moments.

Figure 4-40 shows the drag ($D/T_{ref} = \pm 0.018$) on the vehicle as a function of angle of attack. There is very little difference in the drag between the stabilizer vane configurations and the configuration without stabilizer vanes until the angle of attack begins to approach zero because the crosswind has more influence in turning the duct jet at those angles of attack, allowing the vanes to be exposed to the crosswind. Even at angles of attack near 0 degrees, the drag difference is small, but those small differences can have a considerable impact on the drag due to the large moment arm between the stabilizer vanes and the center of gravity of the vehicle (duct lip). Figure 4-41, which displays the lift ($L/T_{ref} = \pm 0.007$) as a function of angle of attack, shows practically no difference across the angle of attack range. As the angle of attack moves from

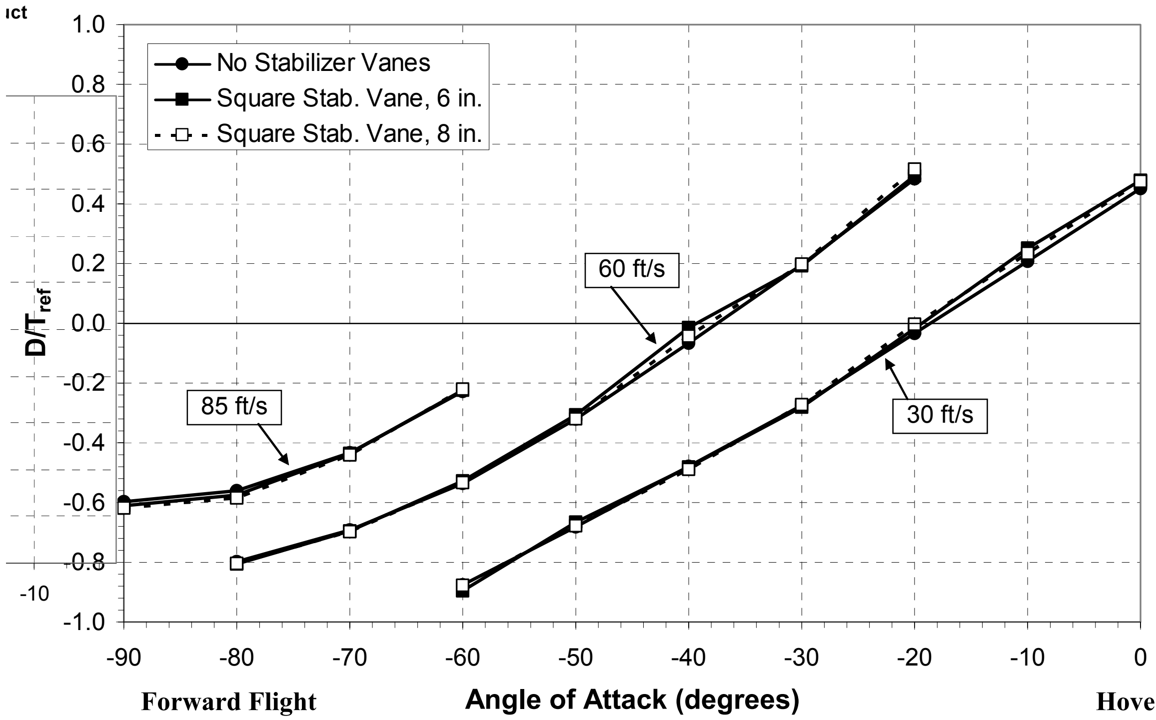

Figure 4-40: Effects of stabilizer vanes on the drag force as a function of angle of attack at 30, 60, and 85 ft/s and $n/n_{ref} = 1.17$.

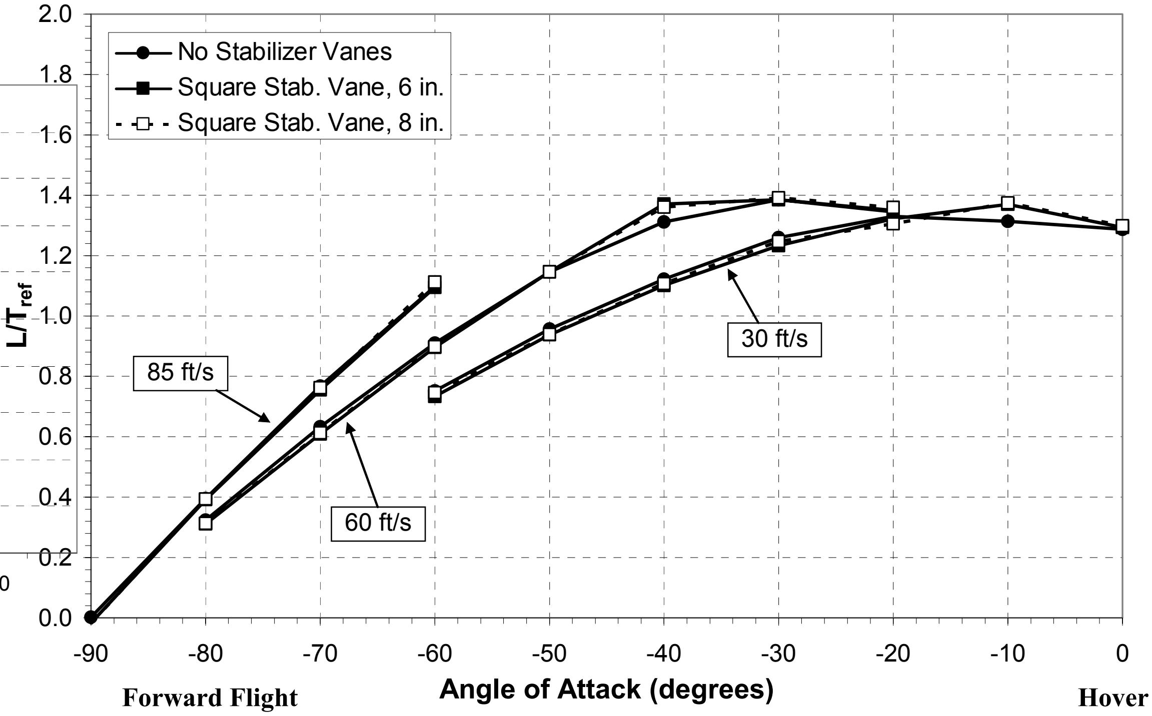

Figure 4-41: Effects of stabilizer vanes on the lift force as a function of angle of attack at 30, 60, and 85 ft/s and $n/n_{ref} = 1.17$.

-90° to 0°, the lift component of the force produced by the vanes due to the turning duct jet flow decreases, and at the angles of attack where the lift component would be largest, near -90°, the duct jet flow is not influenced by the crosswind enough to cause any significant turning of the flow. At angles of attack near 0°, the force on the vanes is primarily read as a drag force.

The trimmed control vane model, applied to the pitching moment data for the stabilizer vanes, reveals a reduction in required control vane deflection for the 6-inch stabilizer vane configuration at a tunnel velocity of 30 ft/s, as shown in Figure 4-42. The 8-inch configuration also reduces the required control vane deflection for most of the angle of attack range, but at an angle of attack of -10 degrees, when the pitching moment suddenly becomes negative, a large negative control vane deflection is necessary to trim the vehicle. This problem becomes even worse at a tunnel velocity of 60 ft/s as shown in Figure 4-43. In fact, at -20 degrees angle of attack the required control vane deflections for both stabilizer vane configurations are larger than the vanes are capable of. At 85 ft/s, Figure 4-44, because of the effects of the stabilizer vanes, the vehicle requires larger control vane deflections than the case without stabilizer vanes, but the effects are not as severe as at 60 ft/s, at least for the range of angles of attack shown.

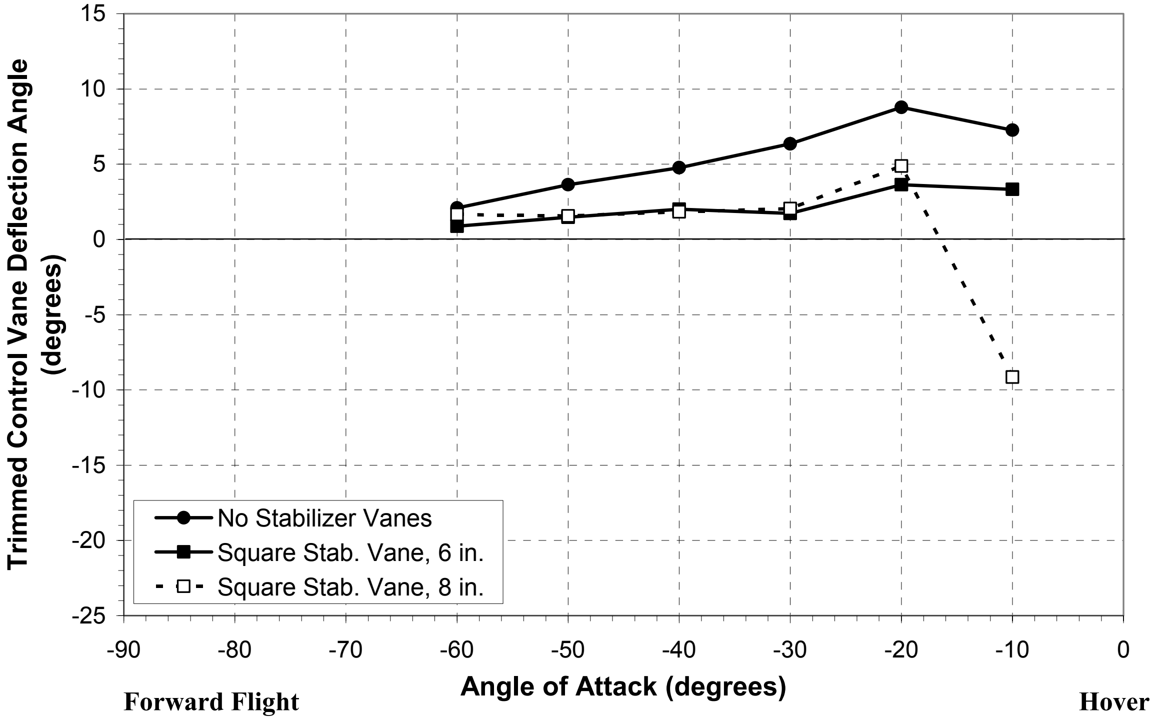

Figure 4-42: Trimmed control vane deflection angle as a function of angle of attack for the stabilizer vane configurations at a tunnel velocity of 30 ft/s and n/n_{ref} = 1.17.

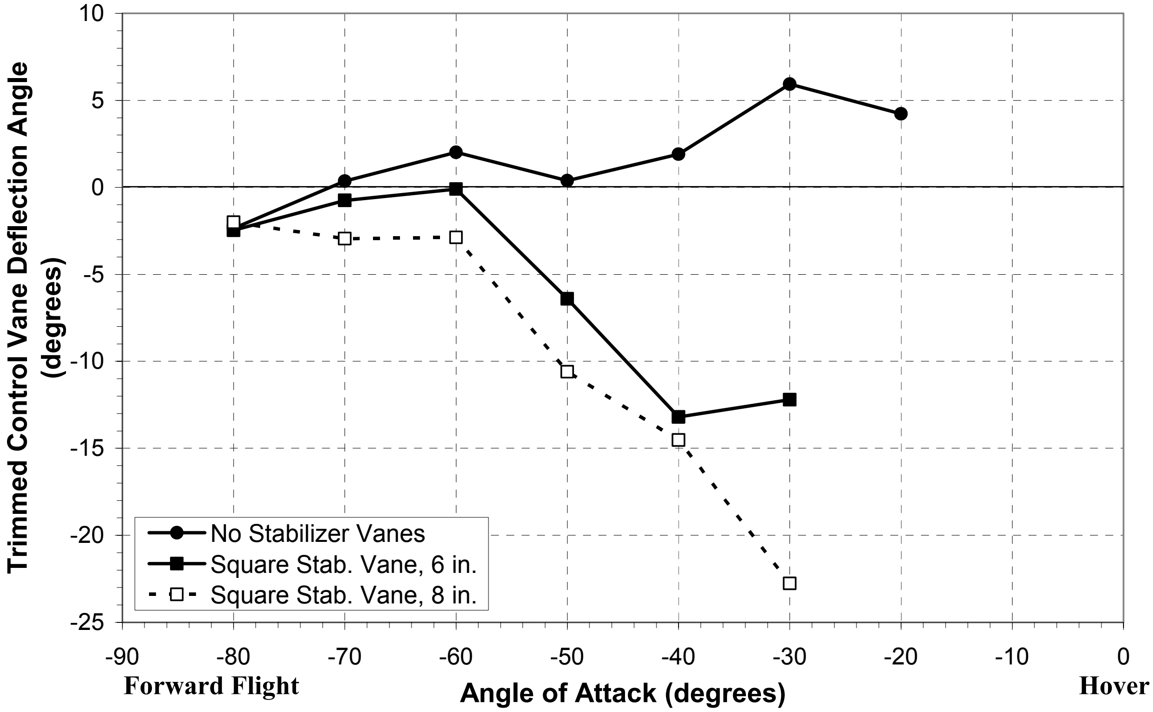

Figure 4-43: Trimmed control vane deflection angle as a function of angle of attack for the stabilizer vane configurations at a tunnel velocity of 60 ft/s and n/n_{ref} = 1.17.

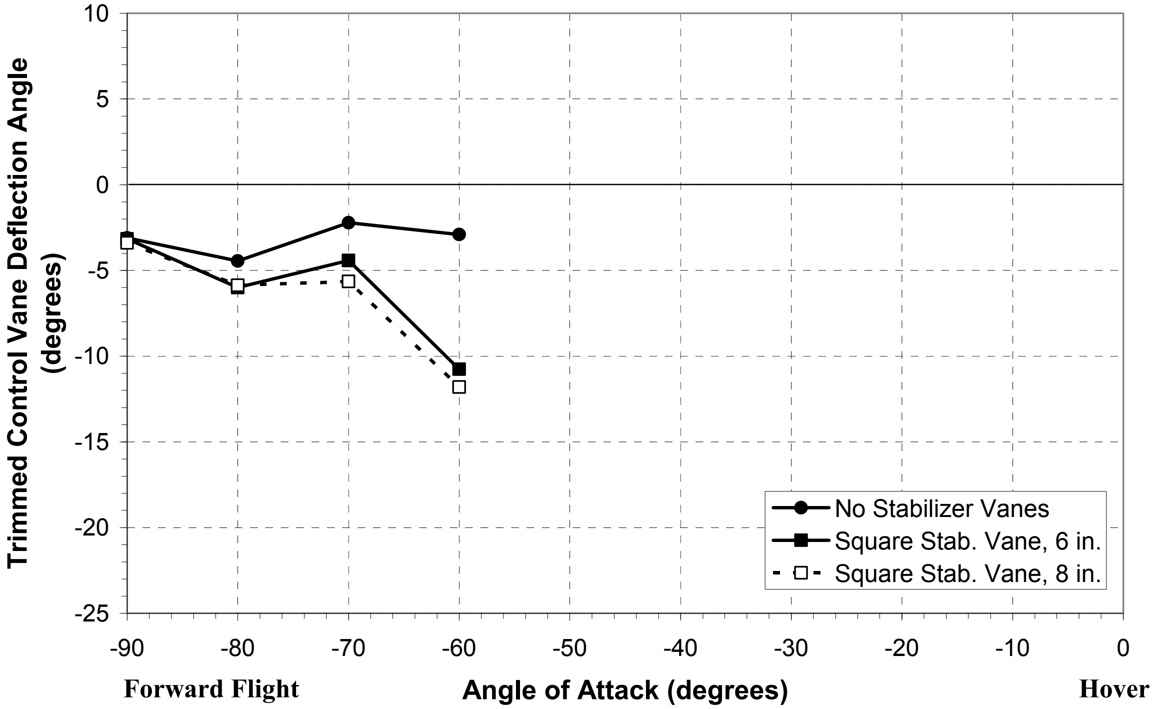

Figure 4-44: Trimmed control vane deflection angle as a function of angle of attack for the stabilizer vane configurations at a tunnel velocity of 85 ft/s and $n/n_{ref} = 1.17$.

Overall, the stabilizer vanes proved their capability in reducing the adverse pitching moment generated by the ducted fan, but they lack the ability to control the amount of influence they have over the controllability of the vehicle because they are not actuated. At small crosswind velocities, the stabilizer vanes provide an improvement in vehicle controllability over the configuration without stabilizer vanes, but at large crosswind velocities, the stabilizer vanes produce a net negative moment, which still requires large control vane deflections to achieve vehicle trim. Between the two configurations tested here, the 6-inch configuration showed better overall performance because it did not produce as severe negative moments as the 8-inch configuration at high tunnel velocities due to the smaller distance from the stabilizer vanes to the center of gravity at the duct lip.

Chapter 5: Conclusions

The importance of UAVs in modern warfare requires extensive research into improvements and modifications for better performance. Ducted fan VTOL UAVs are particularly subject to additional analysis because of their atypical aerodynamic qualities. While numerous factors influence how significantly these adverse aerodynamic attributes affect the performance of the UAV, it has been determined that it is the duct, not the fan, that affects the pitch characteristics the most. Particularly, duct lip shape has been determined to be one of the most influential factors in offsetting the effects of the adverse aerodynamic characteristics. While a particular lip shape may show promise in static conditions, its performance in windy conditions and forward flight could be inferior to other designs. In the same manner, lip shapes that perform well in crosswinds are not necessarily ideal for static hover.

Five lip geometries have been presented here, three of which were tested in both static and windy conditions. The remaining two lip shapes, Elliptical and Circular Arc, displayed inferior static performance compared to the Baseline, Enlarged, and Revised lips, and testing for those geometries was discontinued. The primary cause for the difference in performance between the Baseline lip and the Enlarged and Revised lips was the presence of separated flow on the interior surface of the Baseline lip caused by its smaller leading edge radius. Flow separation on the duct lip influences whether the duct will perform well in static or crosswind conditions. The presence of flow separation in static conditions reduces the static performance of the vehicle by decreasing the amount of lift the duct produces. Additionally, flow separation is undesirable because it increases the required power from the motor. However, in a crosswind the presence of flow separation reduces the lift asymmetry around the duct lip, which reduces the positive pitching moment, allowing the vehicle to tilt into the wind to maintain position or attain forward flight. In addition, lip shaping affects the center of pressure location, which ultimately affects the pitch characteristics of the vehicle and its forward flight performance. A design that reduces the height of the center of pressure above the center of gravity would theoretically have a reduced pitching moment and better handling qualities in crosswinds. The effects of duct wall thickness were determined to be small compared to the effects of lip leading edge radius, but more testing should be completed to decide this conclusively. Future work in this area should consist of a more detailed optimization of the duct lip geometry to find the best compromise between hover and forward flight performance. Also, a more extensive flowfield analysis should be conducted, involving tufts, pressure measurements, particle image velocimetry (PIV), and CFD, to gain a better understanding of the flow behavior in the vicinity of the duct lip.

Duct lip shaping alone cannot remove all of the adverse aerodynamic characteristics of ducted fan UAVs, which is why most vehicles of this type have some sort of primary attitude and trim control in the form of control vanes aft of the duct. The control vanes tested here displayed effectiveness in generating relatively large pitching moments, but at large deflections separation occurred on the surface of the vanes, reducing their effectiveness at those deflections. A trimmed control vane model was developed using static control vane data and verified using wind tunnel control vane data, and it was applied to the wind tunnel data for the Revised lip to determine the required control vane deflections to trim the vehicle (reduce the pitching moment to zero). Because of the large pitching moments generated by the duct, the required vane deflections were also large, reducing the range of control vane deflection angles available to further alter the vehicle's attitude.

As a result, auxiliary control effectors at the duct lip, designed to be actuated, were tested in the form of a lip spoiler, duct deflector, and a leading edge slat. The duct deflector reduced the adverse pitching moment the most by reducing the amount of airflow over the portion of the duct lip where it was positioned. This reduction in pitching moment also reduced the required control vane deflection for trim by over 15%. The lip spoiler on the windward side of the duct also improved the pitch characteristics of the vehicle, but to a lesser degree, by inducing flow separation on the interior of the duct. Optimization of the duct deflector and the lip spoiler should be conducted in the future to improve their performance and further reduce the required control vane deflections for trim. The leading edge slat configurations produced the opposite of what was expected, in that they generated an increase in the adverse pitching moment. In effect, they pushed the center of pressure location further above the duct lip, increasing the effects of the momentum drag on the pitching moment.

Unfortunately, auxiliary control effectors of the type tested require actuation, which increases the weight and complexity of the vehicle. An alternative method of control without excessively adding weight to the vehicle involves adding stabilizer vanes in the duct jet. These were tested in two configurations, 6 inches and 8 inches aft of the duct. At low crosswind velocities, the stabilizer vanes effectively reduced the pitching moment of the vehicle to more acceptable levels.

However, at higher wind velocities, the effects of the stabilizer vanes generated a net negative pitching moment even larger in magnitude than the pitching moment generated by the duct alone.

Based on this research, controlling the flow separation on the duct lip and the location of the center of pressure are the keys to improving the flight characteristics of ducted fan UAVs. Flow separation is necessary in crosswinds and forward flight to reduce the asymmetric lift, which contributes to the adverse pitching moment. However, attached flow is desired in static conditions to improve the duct's contribution to the vehicle thrust and allow a larger payload. Considering this, a compromise has to be made between the static and forward flight performance of the vehicle. Although static thrust is important, without acceptable forward flight characteristics, the vehicle could easily lose control.

The results presented here suggest the Baseline lip shows the most promise in both flight regimes. It outperformed the other lip geometries in forward flight performance, and the sacrifice in static thrust is not significant. In addition to the primary control vanes positioned aft of the duct, an actuated duct deflector-type auxiliary control effector should be used at the lip of the duct to further improve the aerodynamic characteristics of the vehicle. Additionally, advances in materials have allowed for the option of variable geometry to be incorporated in ducted fan UAV design. By utilizing a variable geometry duct lip, the vehicle could improve its performance in all flight conditions by varying the amount of duct lift azimuthally. In hover, the vehicle could optimize the duct lip to have a large leading edge radius to maintain attached flow and increase lift, while in forward flight and crosswinds, the vehicle could reduce the leading edge radius on the windward side of the duct, inducing separated flow on that side and reducing the adverse pitching moment.

In general this research has shown the importance of duct lip shaping and the effects of various shapes on the static and forward flight characteristics of the vehicle. Even though duct lip shaping alone cannot eliminate all of the adverse aerodynamics of the vehicle, various control devices, such as control vanes, auxiliary control effectors, and stabilizer vanes, have been shown to improve the performance of the vehicle in crosswinds and forward flight.

References

1. http://www.hiller.org/flying-platform.shtml

2. de Piolenc, F. Marc, Wright, George E., Jr. *Ducted Fan Design*. Vol. 1. West Covina, CA: Mass Flow, 2001.

3. Sacks, Alvin H. "The Flying Platform as a Research Vehicle for Ducted Propellers." 26th Annual Meeting of the Institute of the Aeronautical Sciences, New York, January 1958.

4. http://www.nosc.mil/robots/images/arod2.jpg

5. Arlowe, H. D. "Airborne Remote Operated Device." AUVS-88, The Fifteenth Annual Technical Symposium and Exhibition of the Association for Unmanned Vehicle Systems, San Diego, CA, June 1988.

6. White, John E., Phelan, John R. "Stability Augmentations and Control Decoupling for the Airborne Remotely Operated Device." AIAA 87-2453, AIAA Guidance, Navigation, and Control Conference, Monterey, CA, August 1987.

7. http://www.moller.com/aerobot/

8. U.S. Patent 4,795,111, January 3, 1989.

9. U.S. Patent 6,450,445, September 17, 2002.

10. Lipera, L., Colbourne, J. D., Tishler, M. B., Mansur, M. H., Rotkowitz, M. C., Patangui, P. "The Micro Craft iSTAR Micro Air Vehicle: Control System Design and Testing." AHS 57th Annual Forum, Washington, D.C., May 2001.

11. Kruger, W. "On Wind Tunnel Tests and Computations Concerning the Problem of Shrouded Propellers." NACA Technical Memorandum 1202, January 1944.

12. Grunwald, Kalman J., Goodson, Kenneth W. "Division of Aerodynamics Loads on a Semispan Tilting-Ducted-Propeller Model in Hovering and Transition Flight." NASA TN D-1257, NASA Langley, 1962.

13. Graf, Will, Fleming, Jonathan, Ng, Wing, Gelhausen, Paul. "Ducted Fan Aerodynamics in Forward Flight." AHS International Specialists' Meeting on Unmanned Rotorcraft, Chandler, AZ, January 2005.

14. Weir, Robert J. "Aerodynamic Design Considerations for a Free-Flying Ducted Propeller." AIAA 88-4377-CP, AIAA Atmospheric Flight Mechanics Conference, Washington, D.C., 1988.

15. McCormick, Barnes W., Jr. *Aerodynamics of V/STOL Flight*. Mineola, New York: Dover Publications, 1999.

16. Black, Donald M., Wainauski, Harry S., Rohrbach, Carl. "Shrouded Propellers – A Comprehensive Performance Study." AIAA 68-994, AIAA 5th Annual Meeting and Technical Display, Philadelphia, PA, October 1968.

17. Abrego, Anita I., Bulaga, Robert W. "Performance Study of a Ducted Fan System." American Helicopter Society Aerodynamics, Acoustics, and Test and Evaluation Technical Specialists Meeting, San Francisco, CA, January 2002.

18. Friend, Carl F. "VTOL Flight – Performance, Stability and Control." *VTOL Vehicles – Practice and Potential*. Ed. Dr. C. Ming Wong. Vol. 3. North Hollywood, California: Western Periodicals Co., 1966.

19. Fleming, Jonathan, Jones, Troy, Ng, Wing, Gelhausen, Paul, Enns, Dale. "Improving Control System Effectiveness for Ducted Fan VTOL UAVs Operating in Crosswinds." 2nd AIAA UAV Conference and Workshop & Exhibit, San Diego, CA, September 2003.

20. http://www.aoe.vt.edu/research/facilities/stab/tunnel_descrip.php

21. Fleming, Jon. "Developing an Effective Control System for VTOL UAVs in Adverse Winds: An Investigation of Techniques for Improving Ducted Fan Aerodynamic Performance in Crosswinds." Phase I Final Report, Army Contract #DAAH10-03-C-0019, Army Report # USAAMCOM TR 03-D-12, June 2003.

22. Fleming, Jon, Graf, Will. "Wind Tunnel Data Report – Army VTOL Phase II/Honeywell MAV Wind Tunnel Testing Data Release 2.00." Techsburg Internal Document, Blacksburg, VA, August 2004.

23. Parlett, Lysle P. "Experimental Investigation of Some of the Parameters Related to the Stability and Control of Aerial Vehicles Supported by Ducted Fans." NASA TN D-616, NASA Langley, November 1960.

24. Martin, P. B., Boxwell, D. A. "Design, Analysis, and Experiments on a 10-inch Ducted Rotor VTOL UAV." AHS International Specialists' Meeting on Unmanned Rotorcraft, Chandler, AZ, January 2005.

25. Leishman, J. Gordon. *Principles of Helicopter Aerodynamics*. Cambridge: Cambridge University Press, 2000.

26. Mort, Kenneth W., Gamse, Berl. "A Wind-Tunnel Investigation of a 7-Foot-Diameter Ducted Propeller." NASA TN D-4142, NASA Langley, 1967.

27. Mort, Kenneth W., Yaggy, Paul F. "Aerodynamic Characteristics of a 4-Foot-Diameter Ducted Fan Mounted on the Tip of a Semispan Wing." NASA TN D-1301, NASA Langley, 1962.

28. Mort, Kenneth W. "Performance Characteristics of a 4-Foot-Diameter Ducted Fan at Zero Angle of Attack for Several Fan Blade Angles." NASA TN D-3122, NASA Langley, 1965.

29. Martin, Preston, Tung, Chee. "Performance and Flowfield Measurements on a 10-inch Ducted Rotor VTOL UAV." AHS 2004-0264, American Helicopter Society 60th Annual Forum, Baltimore, MD, June 2004.

30. Fletcher, Herman S. "Experimental Investigation of Lift, Drag, and Pitching Moment of Five Annular Airfoils." NACA TN 4117, Langley Field, VA, October 1957.

31. Rabinowicz, Ernest. *An Introduction to Experimentation*. Reading, Massachusetts: Addison-Wesley Publishing Company, 1970.

Appendix A: Supplementary Results

Duct Lip Testing – Static Results

One of the key traits of the static thrust stand is that it can be used to determine the load split between the duct and fan by separating the duct from the thrust load cell. This analysis was completed for the Baseline, Enlarged, and Revised lips and can be seen in Figure A-1 as a percentage of the total thrust carried by the duct alone as a function of motor speed. The results show that, although all three lips have very similar static thrust values, the Revised and Enlarged lips provide a larger percentage of the thrust than the Baseline lip. However, in this testing, the duct lip is not the sole contributor to the duct thrust. Stators positioned just aft of the fan were used in the testing of the Baseline and Revised lips, which contribute to the duct's percentage of the total thrust. Due to its larger wall thickness, the Enlarged lip achieves practically the same duct load percentage as the Revised lip but without the aid of stators. Also, the stators tested with the Revised lip were a slightly improved design than those used with the Baseline lip, which could account for the larger load on the duct assembly.

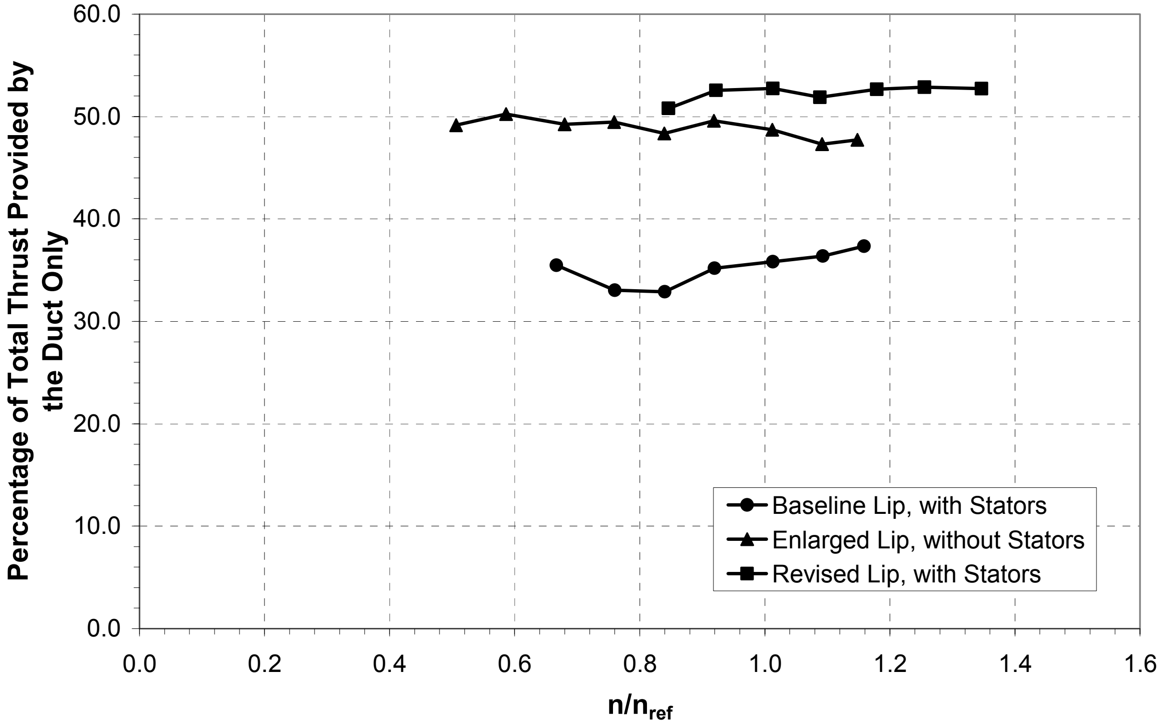

Figure A-1: Load split analysis between the duct and fan for the Baseline, Enlarged and Revised lips in static conditions.

Duct Lip Testing – Wind Tunnel Results

Figure A-2 and Figure A-3 show the lift (L/T_{ref} = ±0.005) versus the crosswind velocity at an angle of attack of 0 degrees and -15 degrees, respectively, for the Baseline and Enlarged lips. Again, lift is presented in non-dimensional form using the reference thrust and motor speed associated with the vehicle weight. Also, an angle of attack of 0 degrees corresponds to hover, and the angle of attack becomes negative as the vehicle tilts into the wind. Figure A-2 shows a slight decrease in lift as the crosswind velocity increases, and as the fan speed increases, this trend becomes more noticeable. The decrease in lift can be attributed to an increase in the amount of separated flow present on the interior of the lip. At higher wind speeds, the windward side of the duct sees a larger angle of attack, and thus begins to lose lift as the flow separates. Notice that the Enlarged lip attains more lift at higher fan speeds because of its ability to maintain attached flow longer. The primary difference between Figure A-2 and Figure A-3 is that the lift curve increases slightly with increase in crosswind velocity for the α = -15° case. The cause of this, again, lies with separated flow, or the lack thereof. When the vehicle is tilted into the wind, the windward lip sees a lower angle of attack than it would in hover. Therefore, less flow separation is present on the duct lip, allowing it to generate more lift as the crosswind

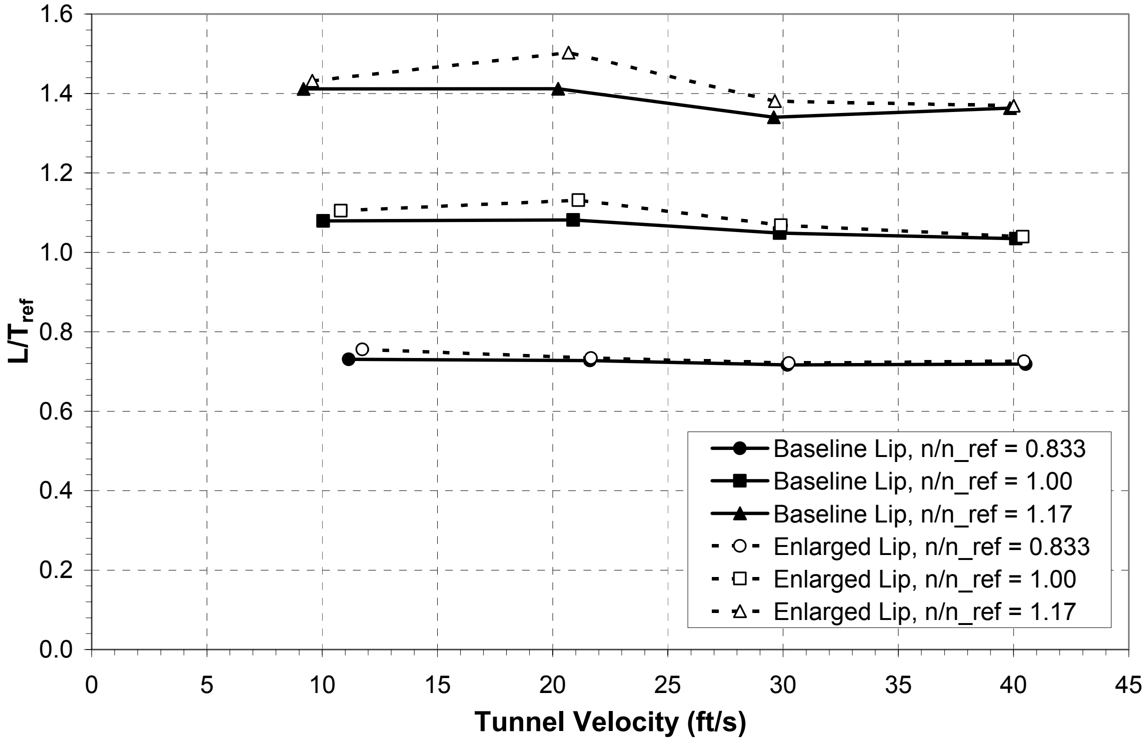

Figure A-2: Lift trends for various lip shapes and fan speeds at 0 degrees angle of attack.

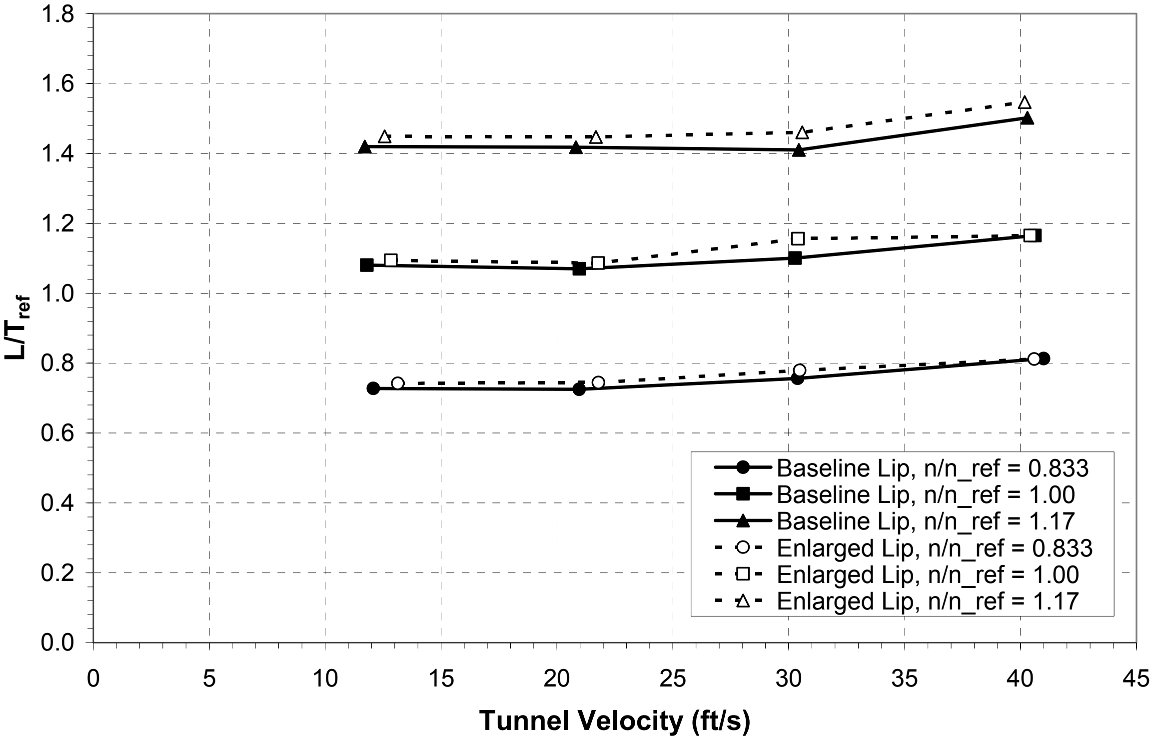

Figure A-3: Lift trends for various lip shapes and fan speeds at -15 degrees angle of attack.

velocity increases.

Figure A-4, Figure A-5, and Figure A-6 show the lift ($L/T_{ref} = \pm 0.009$) as a function of angle of attack for the Revised lip at 30, 60, and 85 ft/s. At the higher tunnel velocities, data was not taken at angles of attack near zero because the aerodynamic forces and resulting moments on the model would have exceeded the limits of the sting-mount balance. Also, according to the analysis performed by AVID LLC (Graf, et. al.[10]), those angles are well outside the vehicle trimmed flight envelope. It is interesting to note that the maximum lift does not occur when the vehicle's thrust vector is vertical ($\alpha = 0°$) but instead occurs at some negative angle of attack. For instance, in Figure A-4, which shows the lift at a tunnel velocity of 30 ft/s, the maximum lift occurs at an angle of attack of -20 degrees. At 60 ft/s, an angle of attack of -30 degrees is necessary to achieve maximum lift, as shown in Figure A-5. This can be attributed to the duct's contribution to the lift. Incidentally, the angles of maximum lift correspond to the stall angles from the diagnostic pressure data shown in Figure 4-3. The fact that there is not a sudden drop in the lift after the angle of maximum lift implies the duct lip stalls gradually. Comparing the lift performance of the Revised lip to that of the Baseline and Enlarged lip, the Revised lip generates slightly more lift, reflecting the static performance results. This analysis takes into account the

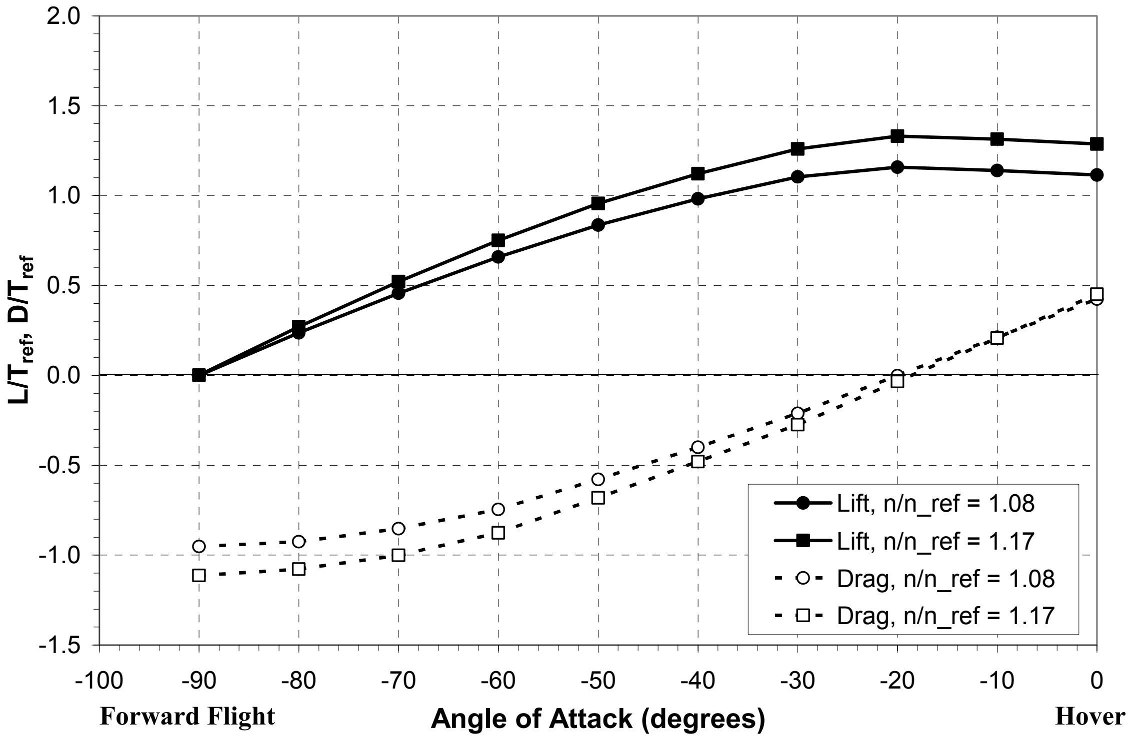

Figure A-4: Lift and drag trends for the Revised lip as a function of angle of attack at various fan speeds and a tunnel velocity of 30 ft/s.

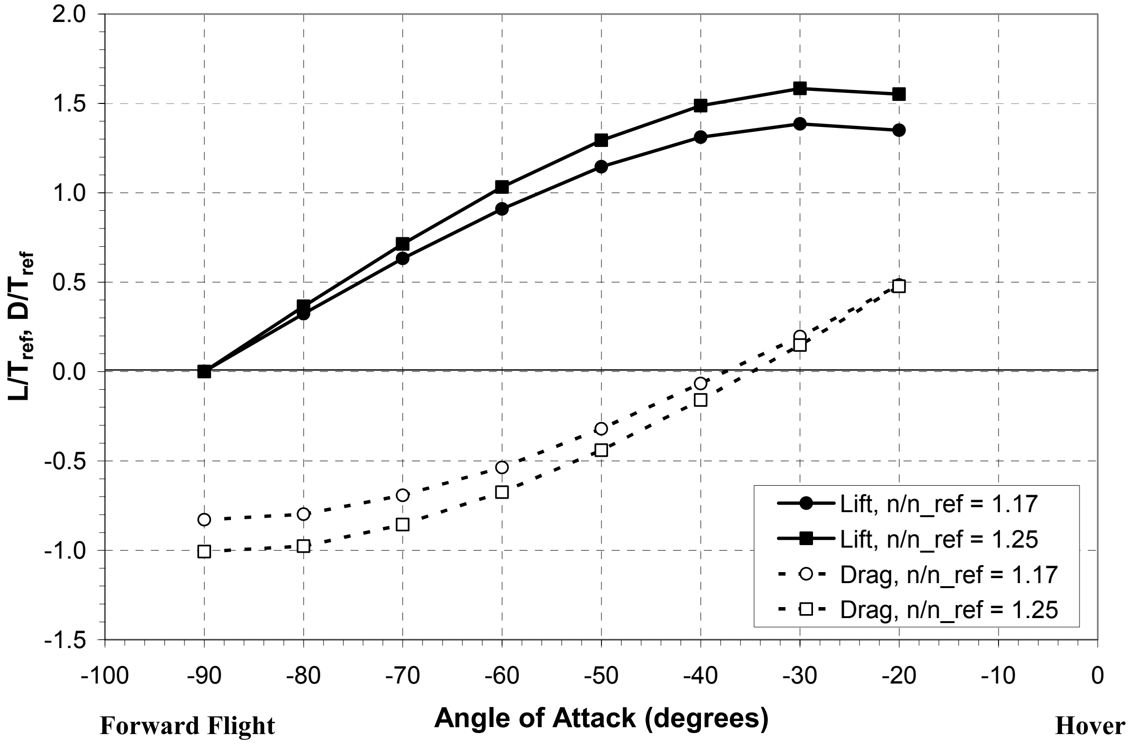

Figure A-5: Lift and drag trends for the Revised lip as a function of angle of attack at various fan speeds and a tunnel velocity of 60 ft/s.

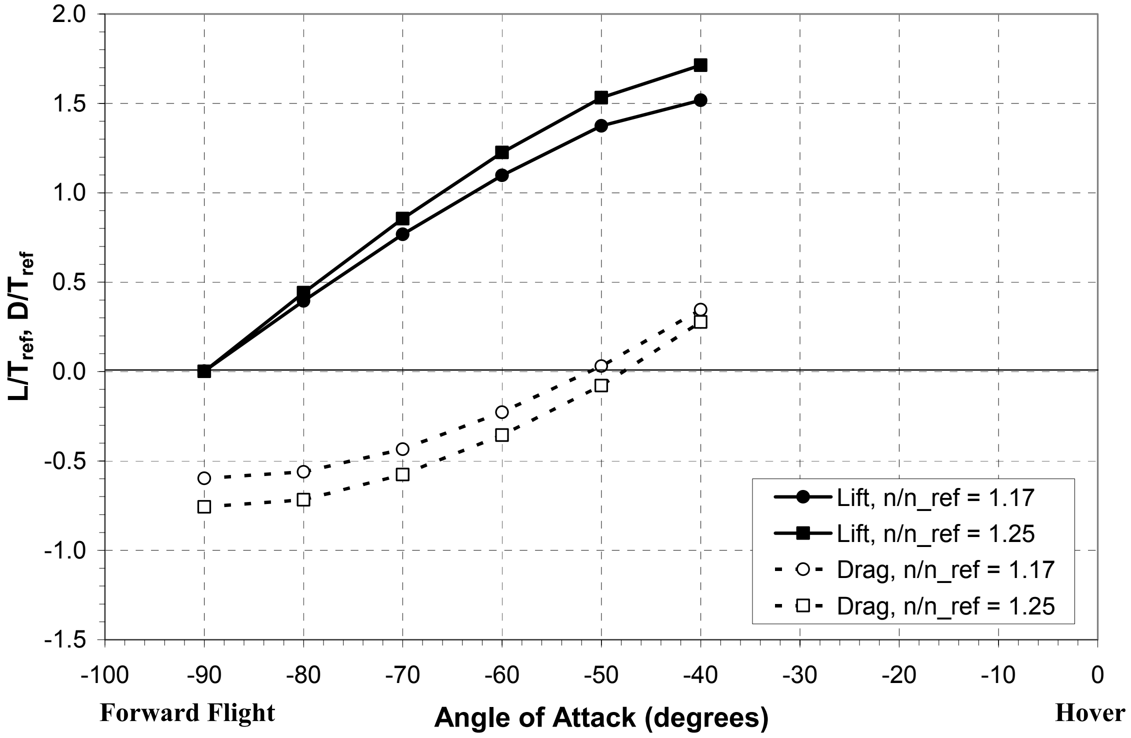

Figure A-6: Lift and drag trends for the Revised lip as a function of angle of attack at various fan speeds and a tunnel velocity of 85 ft/s.

difference in duct diameters between the two wind tunnel entries.

Figure A-4 through Figure A-6 also show the drag ($D/T_{ref} = \pm 0.016$) for the Revised lip as a function of the angle of attack for the three different tunnel velocities. By plotting the lift and drag together on the same plot, the reader can more efficiently determine the angle of attack necessary to maintain position (drag equal to zero). As one would expect, the vehicle must tilt more into the wind to maintain position as the crosswind velocity increases. As an example, in a 30-ft/s crosswind (Figure A-4), the vehicle would have to tilt into the wind approximately -20 degrees to maintain position. At 85 ft/s (Figure A-6), the necessary angle is approximately -50 degrees.

The drag ($D/T_{ref} = \pm 0.019$) for the Baseline and Enlarged lips is shown in Figure A-7 and Figure A-8 as a function of tunnel velocity at angles of attack of 0 and -15 degrees, respectively. Equation (2-3) states that momentum drag will increase linearly with an increase in V_x (crosswind velocity), assuming the lift force is not a function of the tunnel velocity, which was shown to be a reasonably good assumption in Figure A-2. However, lift is a function of the fan

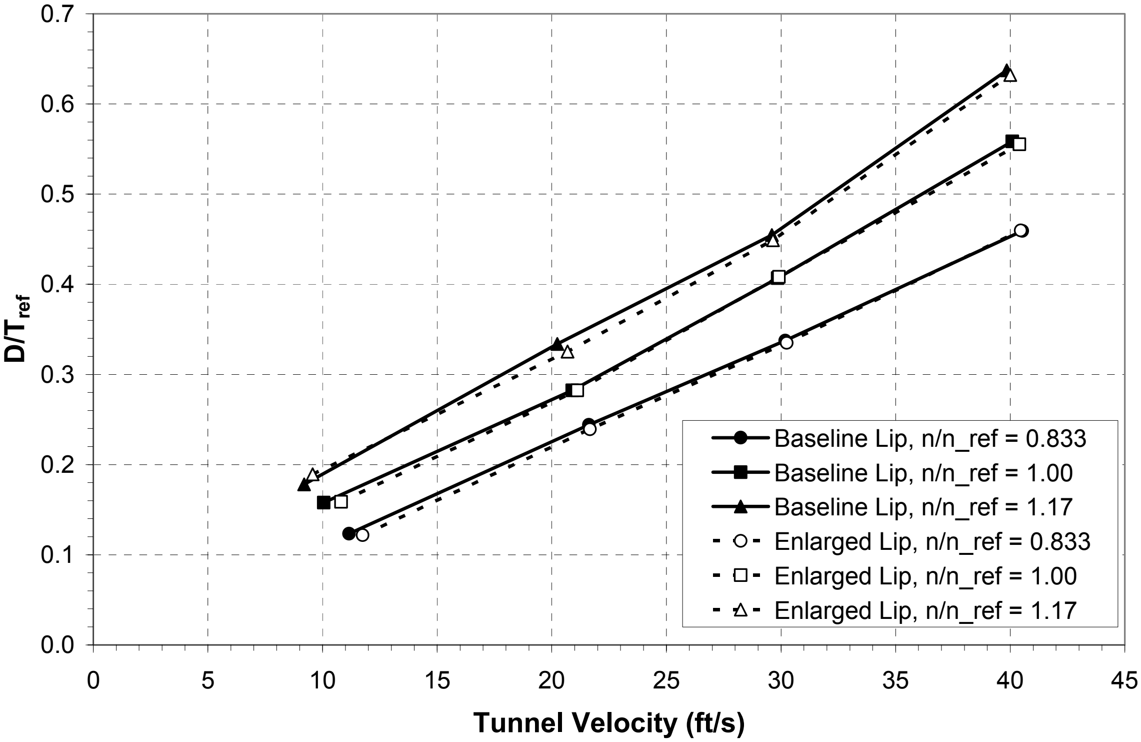

Figure A-7: Drag trends for various lip shapes and fan speeds at 0 degrees angle of attack.

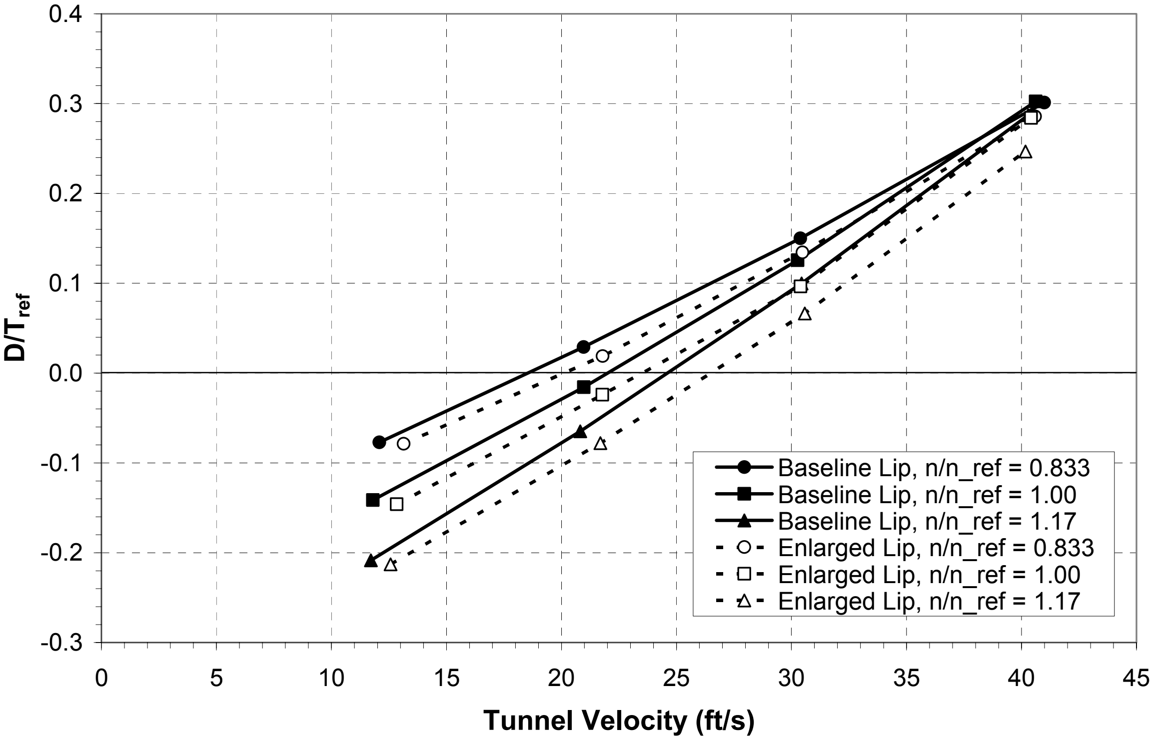

Figure A-8: Drag trends for various lip shapes and fan speeds at -15 degrees angle of attack.

speed, which causes the slope of the drag curve to increase with fan rpm. Figure A-7 and Figure A-8 reflect the results of Equation (2-3) in that the slopes of each curve are linear and increasing with fan speed, but at an angle of attack of -15 degrees, a component of the vehicle thrust acts against the drag force, thus reducing the total drag. In fact, the vehicle is producing negative drag, or a positive force into the wind, at the lower wind velocities, allowing it to tolerate wind gusts of up to around 20 ft/s at this angle of attack. The differences in drag between the various lip geometries are small, particularly between the Baseline and Enlarged lips. However, the Revised lip shows a slight increase in the drag force, which, as will be shown later, has an impact on the pitch characteristics of the vehicle.

Sting Balance Shroud and Support Strut Interference

The wind tunnel test configuration consisted of the shrouded sting balance mounted to the front of the model. This configuration was chosen for multiple reasons: it allowed the duct jet to be unobstructed, it allowed for smaller uncertainties in the small yawing moment results, and it improved the ease of the electric motor wiring. The primary disadvantages of this configuration are the interference effects caused by the sting balance shroud and the support strut when the model is at angles of attack near -90 degrees. At these angles of attacks, the wakes shedding off the shroud and strut are ingested by one side of the duct, as shown in Figure A-9, affecting the forces and moments that the vehicle experiences. At angles of attack above approximately -50 degrees, the wake effects are minimized. Even though the primary purpose of this research was to examine flight characteristics at lower speeds (i.e. angles of attack typically above -50 degrees), the interference effects at angles of attack near -90 degrees were still examined. In order to quantify the interference effects at large angles of attack, a false strut and false shroud were added to the test configuration, as shown in Figure A-10. The primary purpose of these devices was to generate additional wakes, which would be ingested by the opposite side of the duct. Data was taken at multiple tunnel velocities and angles of attack with each of the false components attached individually, and the results were compared to data without the false components.

The false strut analysis is shown first in Figure A-11 and Figure A-12, which show the effects on the thrust and rolling moment of the vehicle. As shown in Figure A-11, the thrust is only affected by the strut at angles of attack below -70 degrees, and the effect becomes more

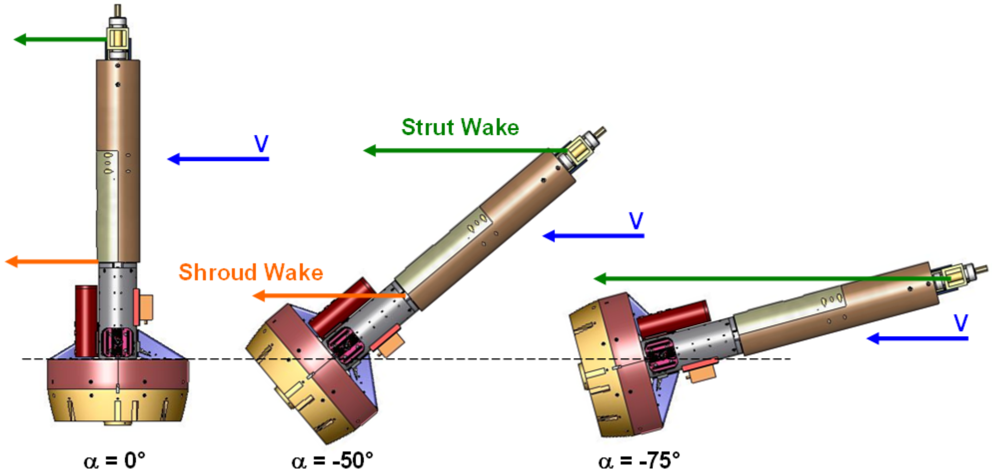

Figure A-9: Wind tunnel model setup viewed from the top, showing the sting balance shroud wake and the support strut wake at various angles of attack.

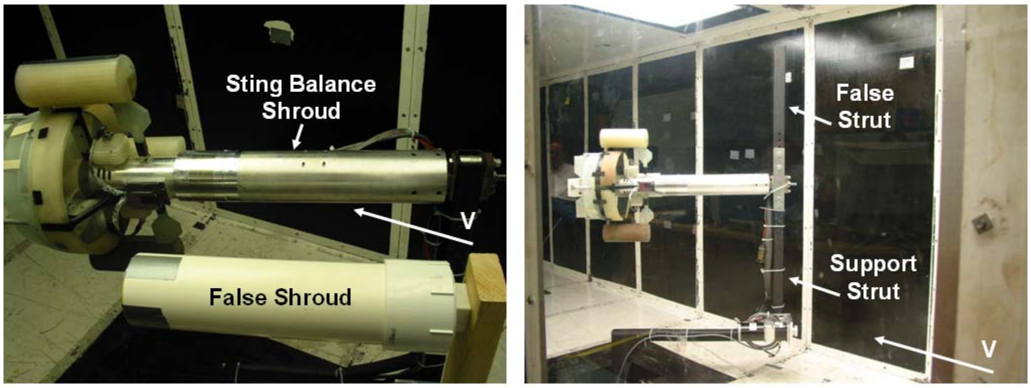

Figure A-10: Photographs of wind tunnel model setup incorporating the false shroud (left) and the false strut (right).

significant as the angle of attack approaches -90 degrees. The configuration with the false strut in addition to the support strut generates more thrust at -90 degrees angle of attack because the struts block some of the freestream flow and reduce the total drag on the vehicle. The effects on the rolling moment are shown in Figure A-12. The rolling moment is affected because the strut wake is ingested by the lower portion of the duct, which generates an asymmetry about the vehicle x-axis, causing a rolling moment. Again, the data shows large differences at -90 degrees caused by the false strut wake. Another noticeable difference appears at -65 degrees angle of attack, where the data for the configuration without the false strut shows a sharp drop in the rolling moment, while the data for the configuration with the false strut is much smoother. The sharp drop in the rolling moment is most likely due to the asymmetry in duct lift caused by the single strut wake and perhaps a localized region of separation on the interior of the duct.

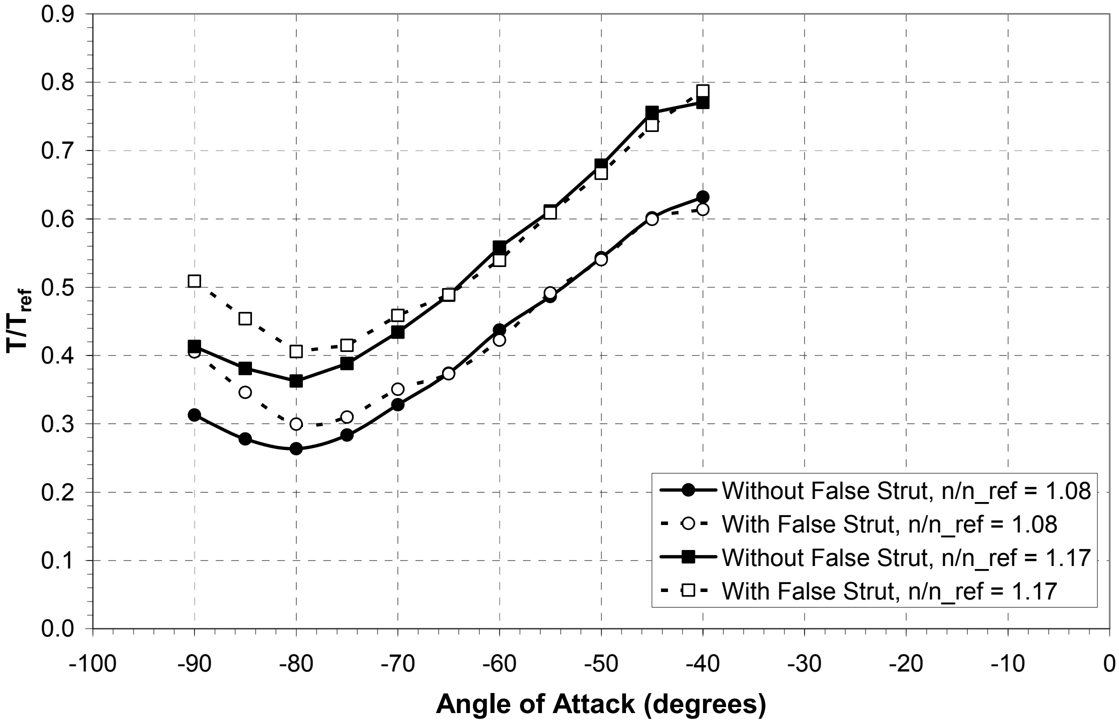

Figure A-11: Thrust as a function of angle of attack for configurations with and without the false strut at various fan speeds and a tunnel velocity of 85 ft/s.

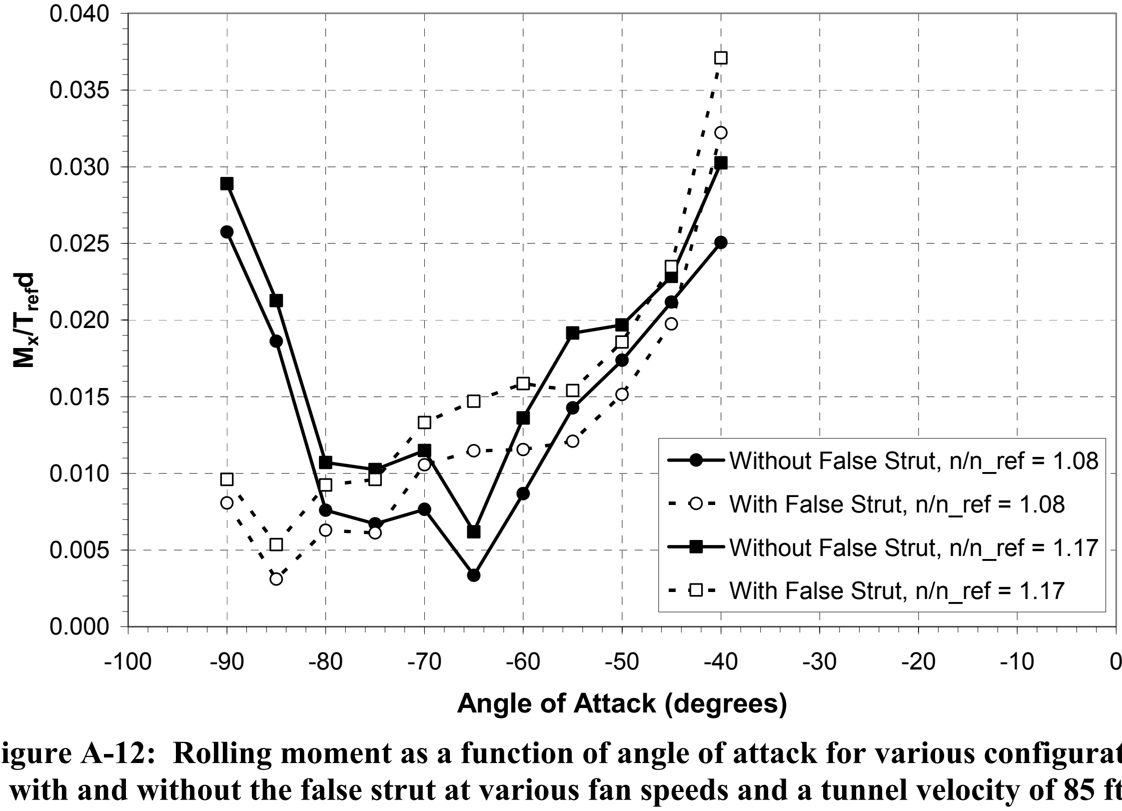

Figure A-12: Rolling moment as a function of angle of attack for various configurations with and without the false strut at various fan speeds and a tunnel velocity of 85 ft/s.

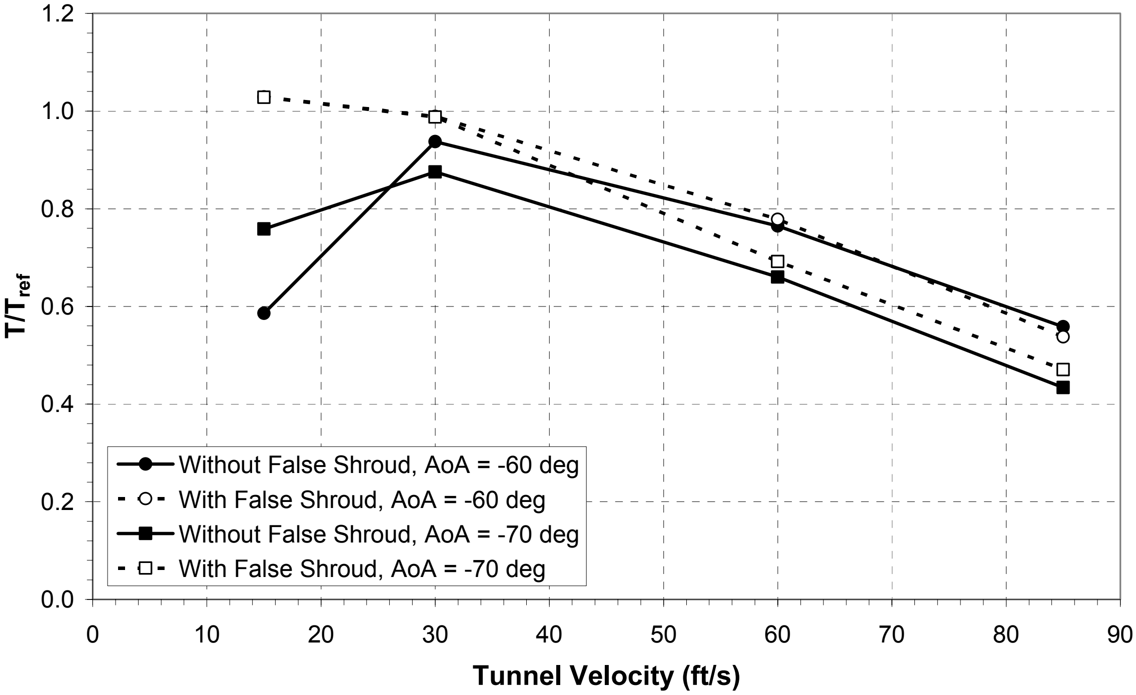

Figure A-13: Thrust as a function of tunnel velocity for configurations with and without the false shroud at various angles of attack and a fan speed of n/n_{ref} = 1.17.

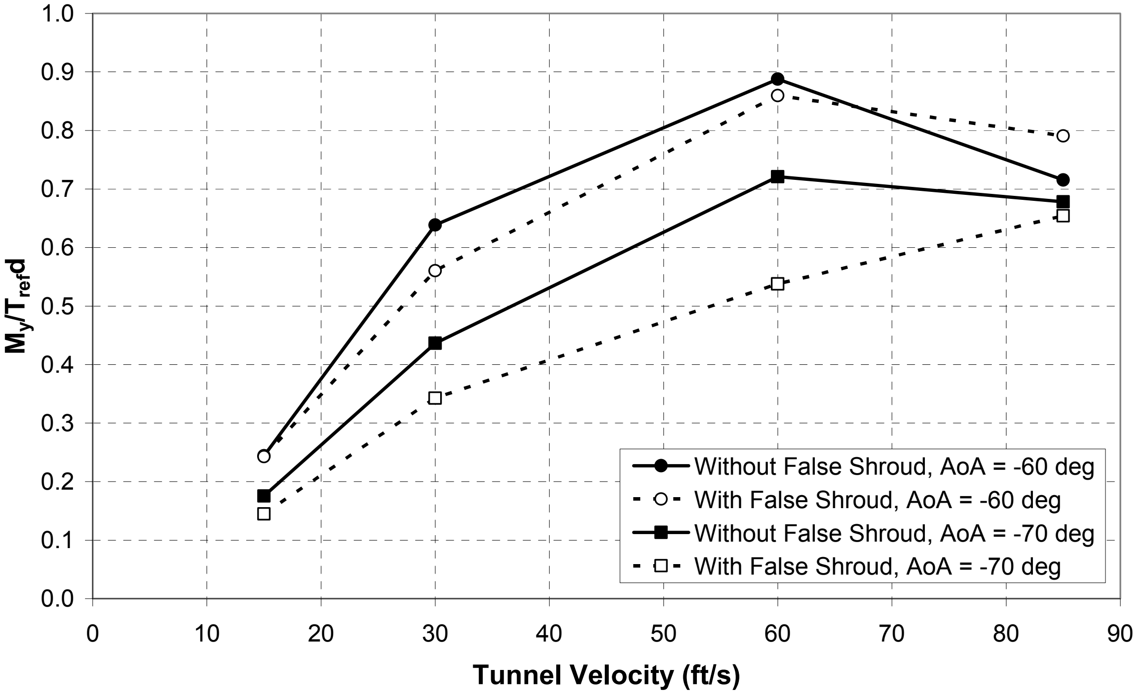

Figure A-14: Pitching moment as a function of tunnel velocity for configurations with and without the false shroud at various angles of attack and a fan speed of n/n_{ref} = 1.17.

The false shroud analysis is shown in Figure A-13 and Figure A-14. Figure A-13 displays the effects of the shroud wake on the thrust of the vehicle. Again, the configuration with the false shroud generates more thrust because it reduces the total drag on the vehicle. The difference in the configurations is more noticeable at low speeds because the fan ingests more of the wake. Figure A-14 examines the effects of the shroud wake on the pitching moment of the vehicle. The configuration with the false shroud reduces the pitching moment because it generates a more symmetric pressure distribution around the duct lip.

In summary, the wind tunnel test configuration resulted in interference effects at large angles of attack due to the model lying in the wakes of the sting balance shroud and support strut. These effects tend to grow larger as the angle of attack approaches -90 degrees. Since, the focus of the research was on relatively low vehicle speeds, high angles of attack are not necessary, negating most of the interference effects from the shroud and strut.

Appendix B: Uncertainty Calculations

The uncertainty analysis performed on the data presented here is based on the method provided by Rabinowicz[31], along with the help and support of Dr. Wing Ng, Jonathan Fleming, and Troy Jones. A selection of the figures presented previously in Chapter 4 is reproduced here with error bars to give the reader an idea of the amount of uncertainty in the data. While most of the uncertainty calculations are based on standard deviations calculated in the data collection process, uncertainties in physical measurements, such as model dimensions and the mass of the calibration weights, are also included.

According to Rabinowicz[31], if one assumes f is a function of a, b, c, and d,

$$f = F(a,b,c,d)\,, \tag{A-1}$$

then the uncertainty in f can be written as the square root of the sum of the squares of the derivative of the function with respect to each variable times the uncertainty in the variable, as shown in Equation (A-2)

$$\delta f = \sqrt{\left(\frac{\partial F}{\partial a}\delta a\right)^2 + \left(\frac{\partial F}{\partial b}\delta b\right)^2 + \left(\frac{\partial F}{\partial c}\delta c\right)^2 + \left(\frac{\partial F}{\partial d}\delta d\right)^2}\ . \tag{A-2}$$

From Equation (A-2), uncertainty equations can be derived for the necessary variables based on the equations used to solve for them. For instance, the first set of results presented (Figure 4-6) shows the vehicle thrust as a function of fan speed. The thrust, or F_z, is measured by the load cell (static testing) and the sting-mounted, strain gauge balance (wind tunnel testing) in the form of a change in voltage. In order to determine the correlation between the voltage and the applied force, a calibration was performed prior to the testing, which resulted in a set of calibration constants and a linear relationship. Therefore, the equation for F_z becomes

$$F_z = c_{Fz} V_{Fz}\,, \tag{A-3}$$

and its uncertainty equation becomes

$$\delta F_z = \left(\left(V_{Fz}\delta c_{Fz}\right)^2 + \left(c_{Fz}\delta V_{Fz}\right)^2\right)^{1/2}, \tag{A-4}$$

where c_{Fz} and V_{Fz} are the F_z calibration constant and measured voltage, respectively. The uncertainty in the calibration constant is determined from the equation used during the calibration process,

$$c_{Fz} = \frac{W_{Fz}}{V_{Fz}}, \tag{A-5}$$

resulting in an uncertainty equation equal to

$$\delta c_{Fz} = \left(\left(\frac{1}{V_{fz}} \delta W_{Fz} \right)^2 + \left(\frac{-W_{Fz}}{V_{Fz}^2} \delta V_{Fz} \right)^2 \right)^{1/2}, \tag{A-5}$$

where W_{Fz} is the applied weight in the F_z direction used during calibration. The uncertainty in the weight is ascertained from the error in the scale (0.001 lb), and the uncertainty in the balance voltage is determined using the standard deviation of the acquired data and assuming a normal distribution,

$$\delta V_{Fz} = \frac{\sigma_{Fz}}{(N-1)^{1/2}}, \tag{A-6}$$

where σ_{Fz} is the standard deviation of the F_z voltage data and N is the number of samples. Similarly, the uncertainties in the other calibration constants can be found, with the constants for the moment channels requiring an additional moment arm term in their equations. The values used in the remainder of the uncertainty analysis are as follows

$$\delta c_{Fz}(loadcell) = \pm 0.01 lb/V,\ \delta c_{Fz}(balance) = \pm 0.002 lb/V,$$

$$\delta c_{Fx} = \pm 0.005 lb/V,\ \delta c_{My} = \pm 0.07 ftlb/V.$$

The larger uncertainty in the pitching moment can be attributed to the effects of the uncertainty in the moment arm measurement (±1/16 inch).

Knowing the uncertainties in the calibration constants, the uncertainty in F_z can finally be found, and error bars can be applied to the appropriate plots. Figure B-1 replicates Figure 4-6 but additionally shows the error bars for each lip. The Enlarged and Circular Arc lips had the most uncertainty, while the Baseline and Revised lips had the least. This trend continues throughout the rest of the data. The uncertainty in the fan speed is calculated using the standard deviation,

$$\delta n = \frac{\sigma_n}{(N-1)^{1/2}}, \tag{A-7}$$

and its average uncertainty value was around $n/n_{ref} = \pm 1.2\text{x}10^{-4}$.

Next, plots of thrust as a function of power were presented. The equation to calculate power can be seen in Equation (A-8),

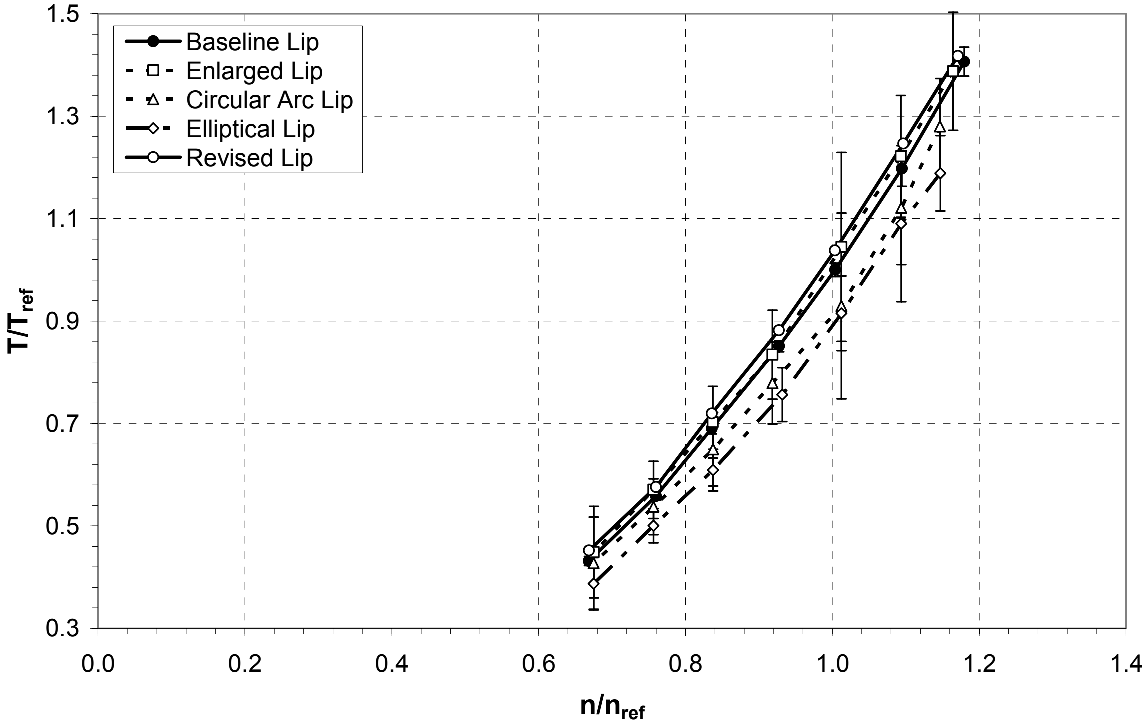

Figure B-1: Replica of Figure 4-6 (static thrust) with error bars added.

$$P = Qn\left(\frac{2\pi}{60}\right)\left(\frac{1}{550}\right), \tag{A-8}$$

where Q is the motor torque, n is the fan speed, and the constants convert the units to horsepower. Applying Equation (A-2) to Equation (A-8) yields

$$\delta P = \left(\left(\frac{2\pi}{60(550)} n\delta Q\right)^2 + \left(\frac{2\pi}{60(550)} Q\delta n\right)^2\right)^{1/2}, \tag{A-9}$$

in which everything is known except for the uncertainty in the motor torque, which can be found using the standard deviation of the motor torque data,

$$\delta Q = \frac{\sigma_Q}{(N-1)^{1/2}}. \tag{A-10}$$

Uncertainties in the power ranged from P/P_{ref} = ±4x10^{-4} for the Baseline and Revised lips to P/P_{ref} = ±5.5x10^{-4} for the Enlarged, Circular Arc, and Elliptical lips.

For the wind tunnel data, plots of lift, drag, pitching moment, and center of pressure location were presented as functions of crosswind velocity for the first wind tunnel entry and angle of attack for the second wind tunnel entry. Since only the body-axis coordinate system forces and moments were measured during testing, the lift and drag forces (wind-axis coordinate system) can be calculated using the following equations

$$L = -F_x \sin(-\alpha) - F_z \cos(-\alpha) \tag{A-11}$$

$$D = -F_x \cos(-\alpha) + F_z \sin(-\alpha), \tag{A-12}$$

where α is the angle of attack of the vehicle. Therefore the uncertainty equations for lift and drag are as follows

$$\delta L = \left((-\sin(-\alpha)\delta F_x)^2 + (-\cos(-\alpha)\delta F_z)^2 + ((F_x \cos(-\alpha) - F_z \sin(-\alpha))\delta\alpha)^2 \right)^{1/2} \tag{A-13}$$

$$\delta D = \left((-\cos(-\alpha)\delta Fx)^2 + (\sin(-\alpha)\delta F_z)^2 + ((-F_x \sin(-\alpha) - F_z \cos(-\alpha))\delta\alpha)^2 \right)^{1/2} \tag{A-14}$$

The uncertainty in F_x can be found in a similar fashion as the method used to solve for the uncertainty in F_z above. The uncertainty in the angle of attack was assumed to be ±1 degree based on the accuracy of the manual turntable control and the initial angle measurements.

The uncertainties in the lift forces for all the lips are too small to show up on the plots (about $L/T_{ref} = \pm 0.005$ for the Baseline and Enlarged lips and $L/T_{ref} = \pm 0.009$ for the Revised lip). This is also true for the drag forces for the Revised lip (approximately $D/T_{ref} = \pm 0.016$).

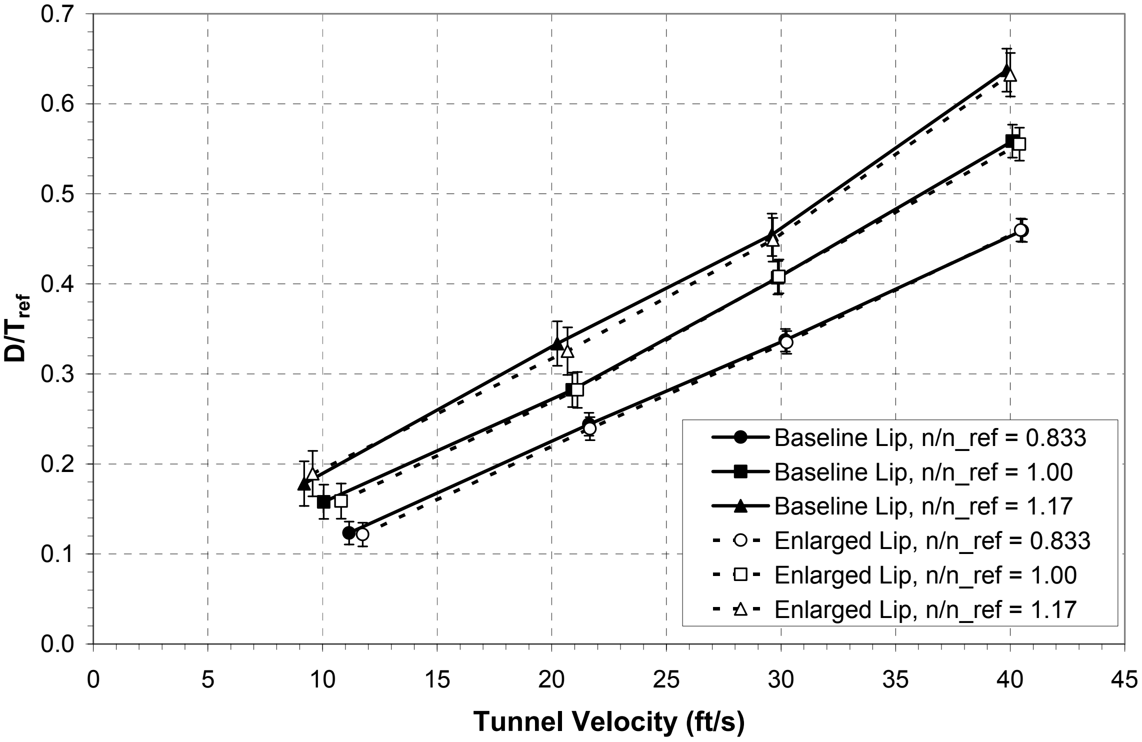

Figure B-2: Replica of Figure A-7 (0 degrees angle of attack) with error bars added.

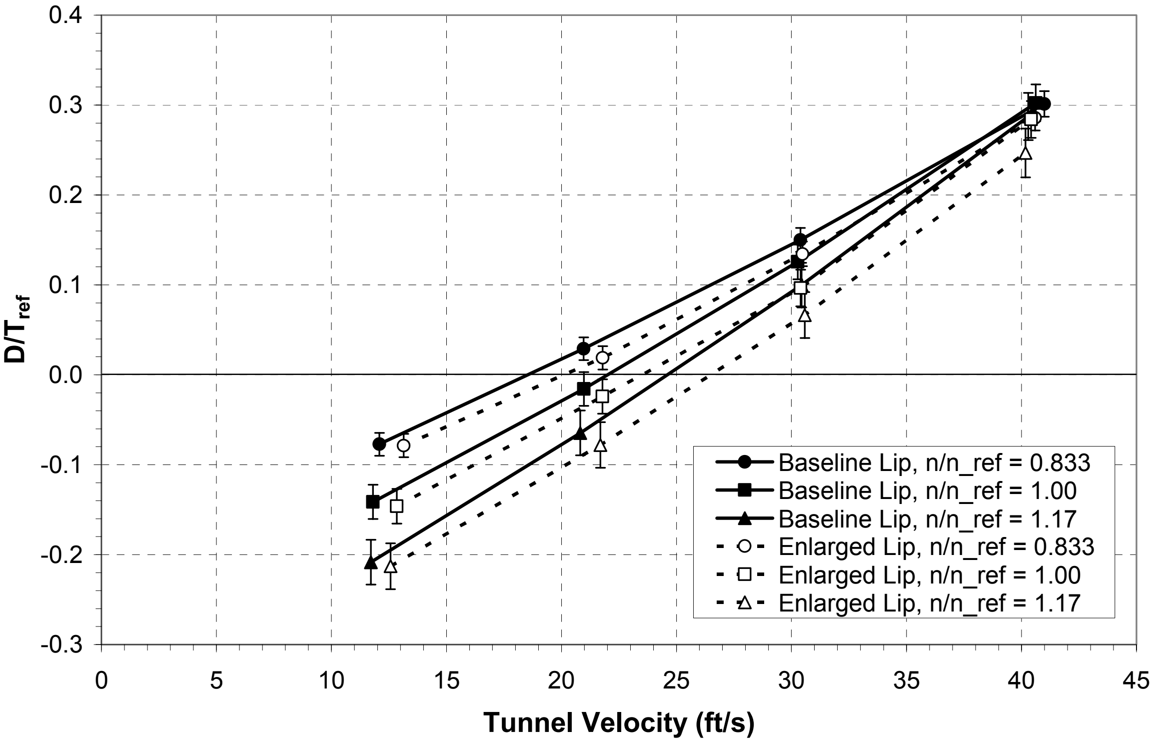

Figure B-3: Replica of Figure A-8 (-15 degrees angle of attack) with error bars added.

However, for the Baseline and Enlarged lips, the uncertainties in the drag forces, although small ($D/T_{ref} = \pm 0.019$), can be seen in Figure B-2 and Figure B-3 because the axes are scaled smaller.

For a change in angle of attack only, the pitching moment is the same in both the body-axis coordinate system and the wind-axis coordinate system. However, the F_x force contributes to the pitching moment measured by the balance. Therefore, the total pitching moment is made up of the pitching moment signal and the F_x signal times the moment arm from the balance center to the model center of gravity (duct lip), as shown in Equation (A-15).

$$M_y = c_{My} V_{My} - F_x d \tag{A-15}$$

The uncertainty equation for the pitching moment can be seen in Equation (A-16).

$$\delta M_y = \left(\left(V_{My} \delta c_{My} \right)^2 + \left(c_{My} \delta V_{My} \right)^2 + \left(-d \delta F_x \right)^2 + \left(-F_x \delta d \right)^2 \right)^{1/2} \tag{A-16}$$

The standard deviation in the pitching moment voltage is used to determine the uncertainty in the pitching moment voltage,

$$\delta V_{My} = \frac{\sigma_{My}}{\left(N - 1 \right)^{1/2}} . \tag{A-17}$$

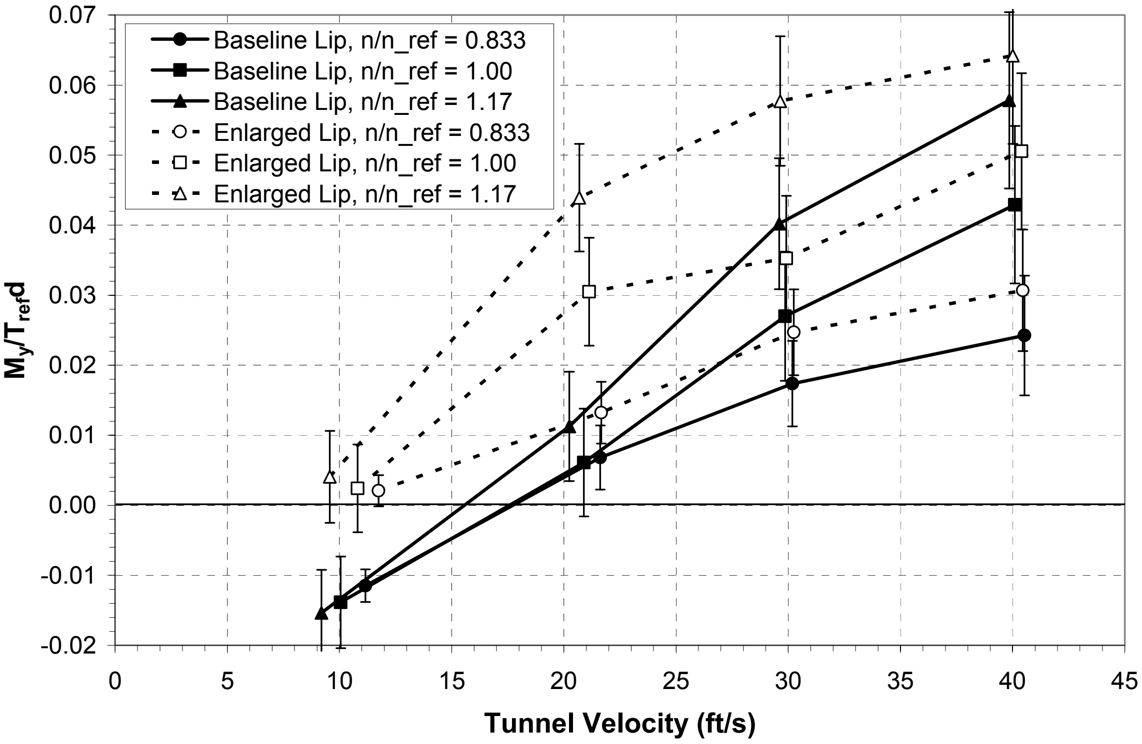

Figure B-4: Replica of Figure 4-11 (0 degrees angle of attack) with error bars added.

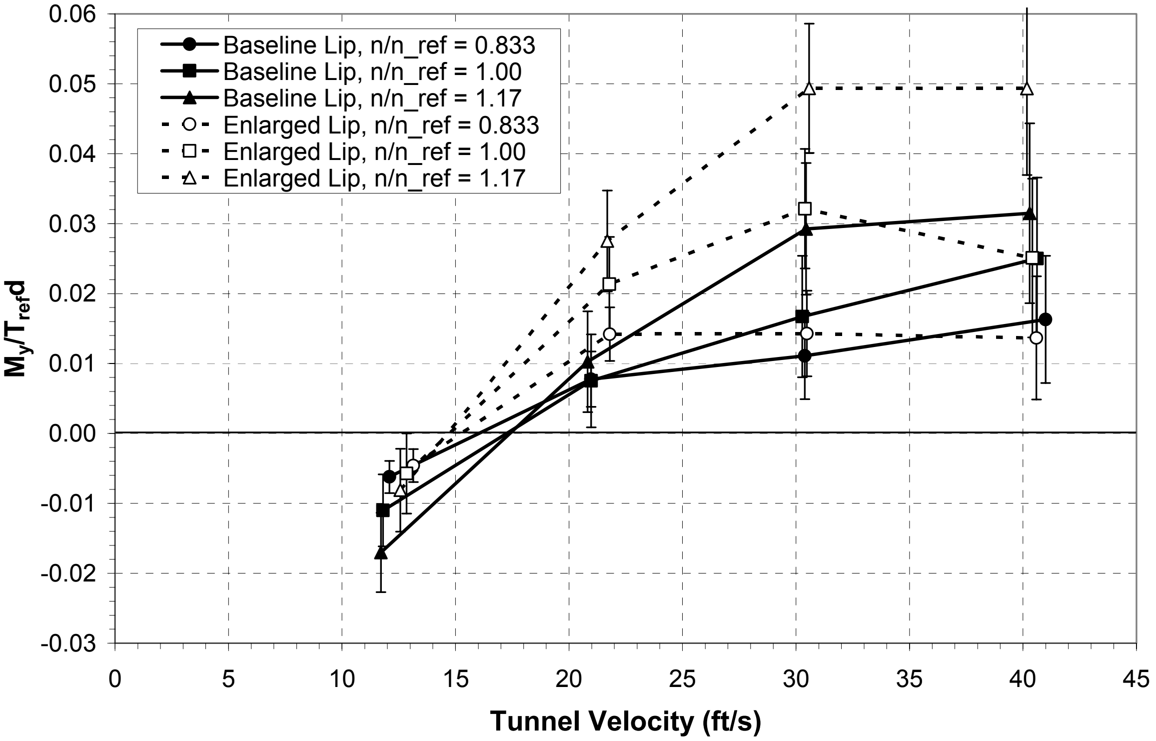

Figure B-5: Replica of Figure 4-12 (-15 degrees angle of attack) with error bars added.

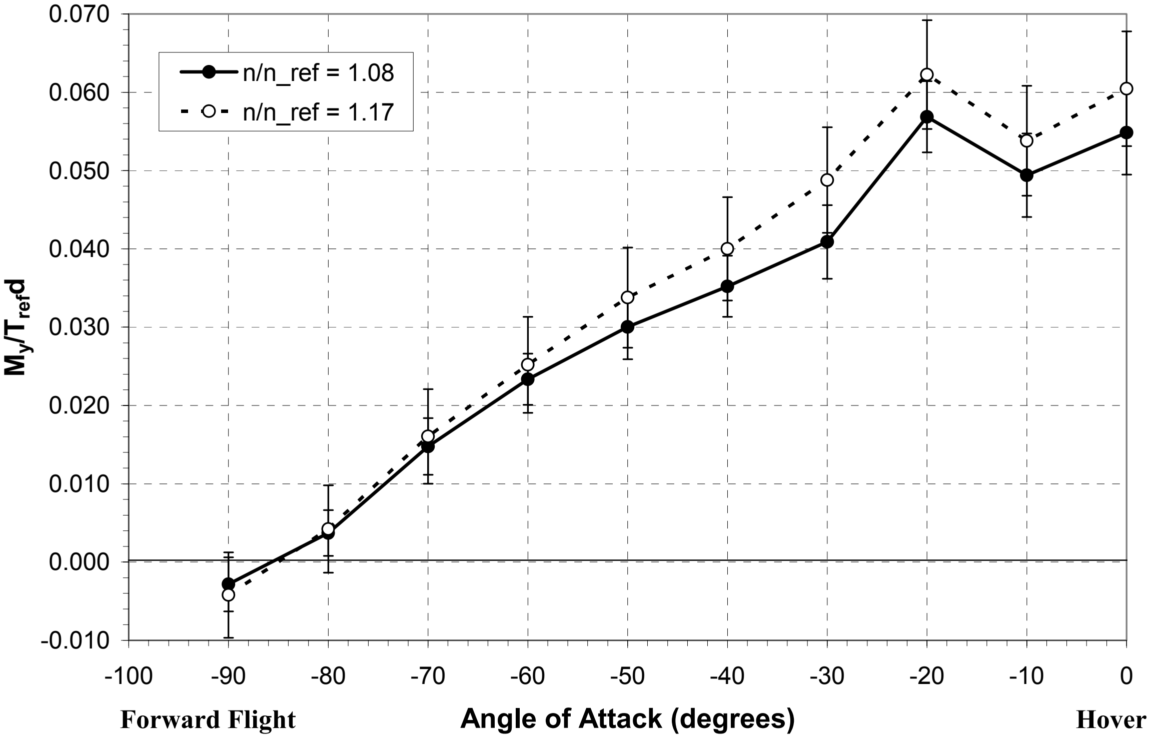

Figure B-6: Replica of Figure 4-13 (30 ft/s tunnel velocity) with error bars added.

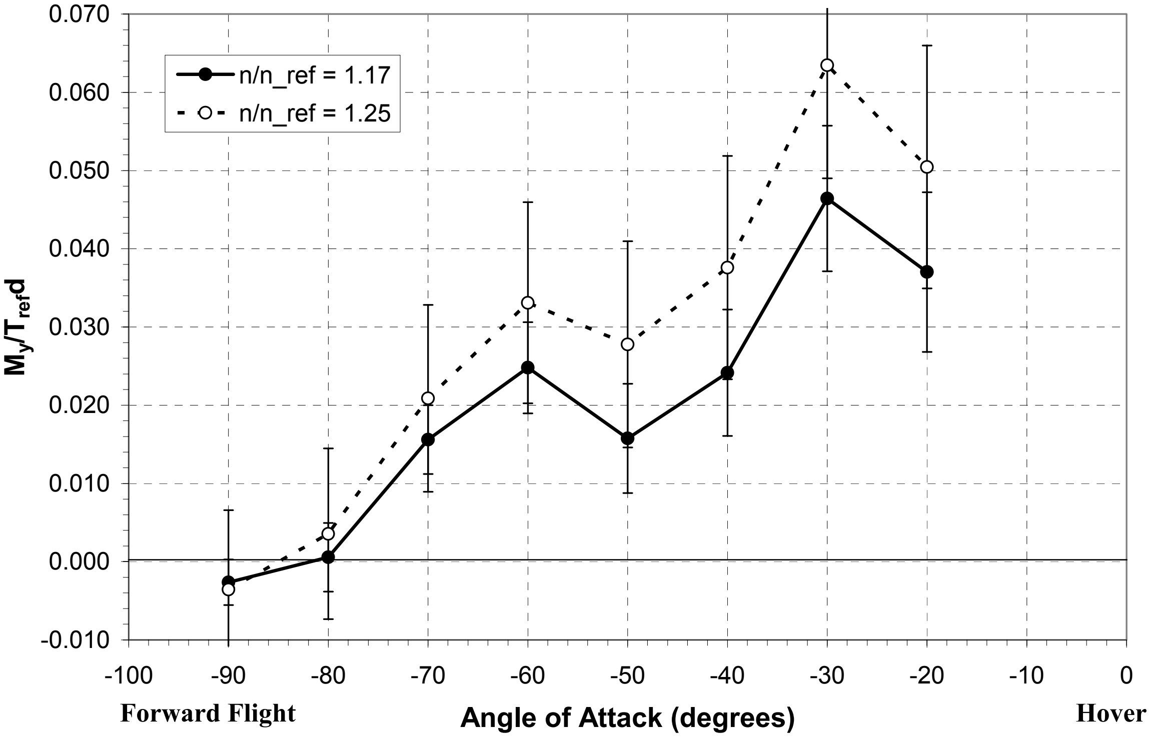

Figure B-7: Replica of Figure 4-14 (60 ft/s tunnel velocity) with error bars added.

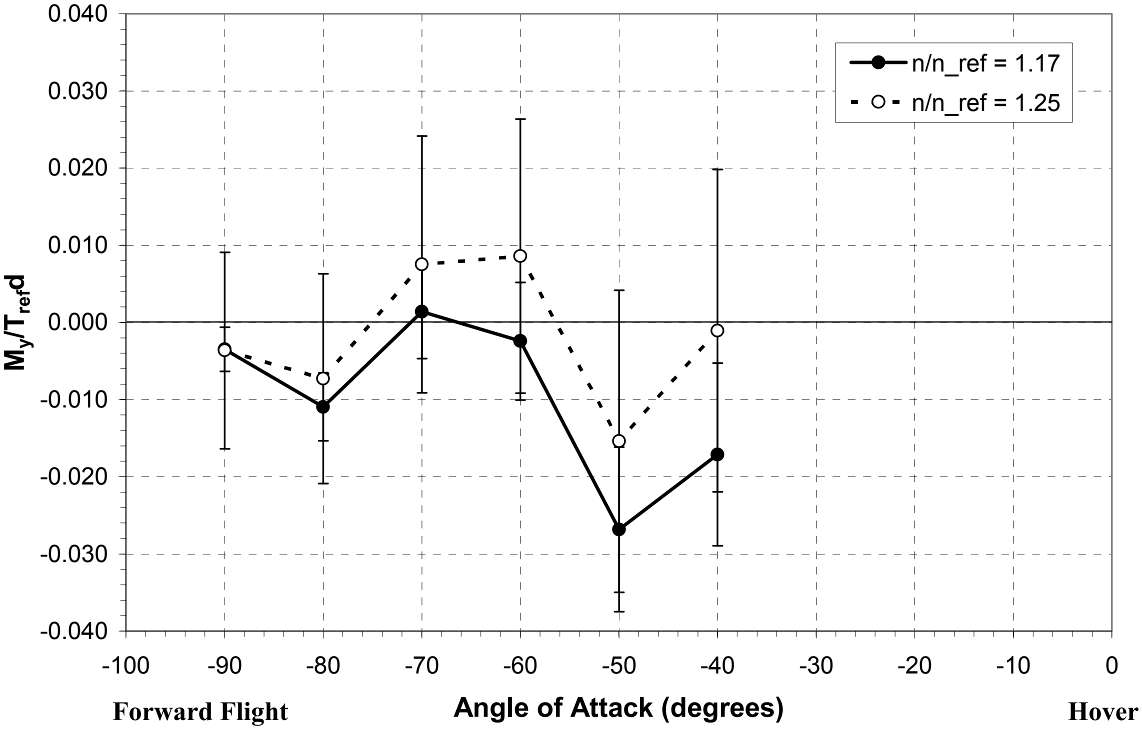

Figure B-8: Replica of Figure 4-15 (85 ft/s tunnel velocity) with error bars added.

Figure B-4 and Figure B-5 show the uncertainties in the pitching moment for the Baseline and Enlarged lips (about $M_y/T_{ref}d$ = ±0.0075), and Figure B-6, Figure B-7, and Figure B-8 show the uncertainties for the Revised lip (about $M_y/T_{ref}d$ = ±0.0053 at 30 ft/s, $M_y/T_{ref}d$ = ±0.0097 at 60 ft/s, and $M_y/T_{ref}d$ = ±0.0121 at 85 ft/s). The uncertainties tend to increase with increasing crosswind velocity, but vary little with a change in angle of attack. At high crosswind velocities and angles of attack approaching 0°, the uncertainties tend to be larger than at other velocities and angles because F_x is larger at those conditions. In general, the uncertainties appear to be larger for the pitching moments than the lift and drag forces because of the extra uncertainty terms from F_x and the moment arm.

Finally, the equation for the center of pressure location is shown in Equation (A-18), and its associated uncertainty equation is shown in Equation (A-19).

$$z_{cp} = \frac{M_y}{-F_x}(12) \tag{A-18}$$

$$\delta z_{cp} = \left(\left(\frac{-12}{F_x} \delta M_y \right)^2 + \left(\frac{12 M_y}{F_x^2} \delta F_x \right)^2 \right)^{1/2} \tag{A-19}$$

The constant value of 12 in Equation (A-18) serves to convert the units from feet to inches. Figure B-9 and Figure B-10 display the uncertainties in the center of pressure location for the Baseline and Enlarged lips (about z_{cp}/d = ±0.024), and Figure B-11, Figure B-12, and Figure B-13 display the uncertainties in the Revised lip (about z_{cp}/d = ±0.023 at 30 ft/s, z_{cp}/d = ±0.019 at 60 ft/s, and z_{cp}/d = ±0.018 at 85ft/s). These uncertainties also show a dependence on the crosswind velocity, but the relationship is opposite that of the pitching moment. As the crosswind velocity increases, the uncertainty in the center of pressure location decreases. Again, there does not appear to be a dependence on the angle of attack. Also note that the uncertainties at low crosswind velocities and angles of attack approaching -90 degrees are much larger than those at other velocities and angles. As with the pitching moment, the culprit is the F_x term. F_x becomes very small at low crosswind velocities and large negative angles of attack, thus inflating the terms with F_x in the denominator. Overall, the uncertainties are large due to the large uncertainties in the pitching moment.

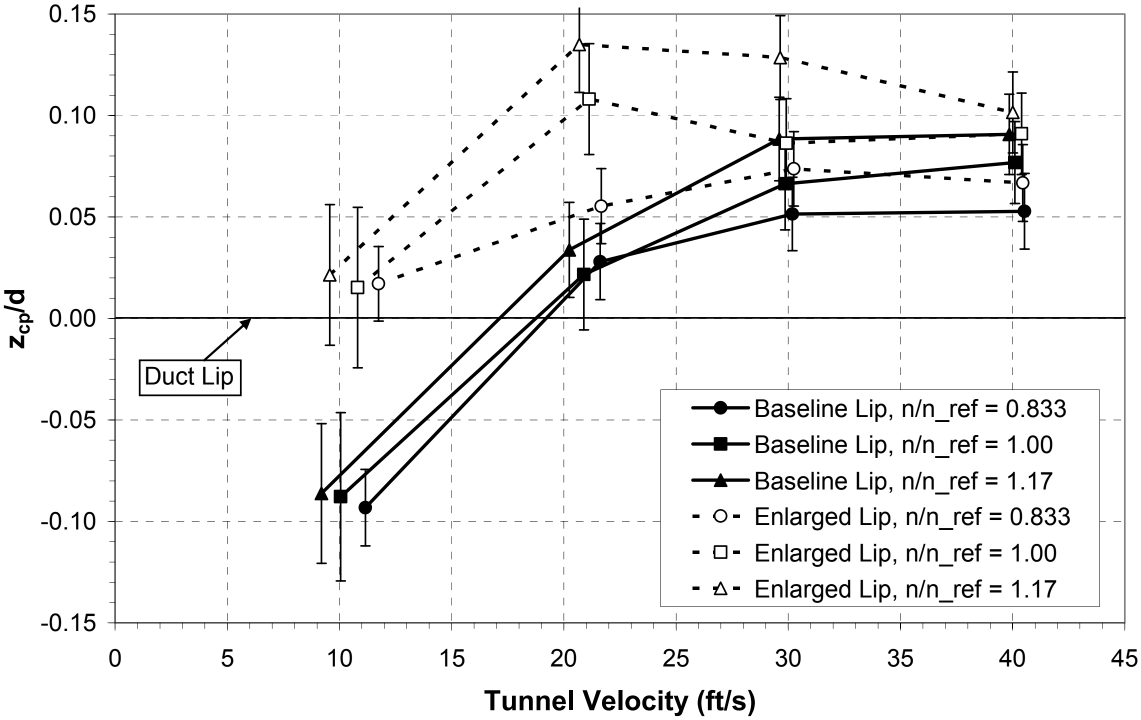

Figure B-9: Replica of Figure 4-16 (0 degrees angle of attack) with error bars added.

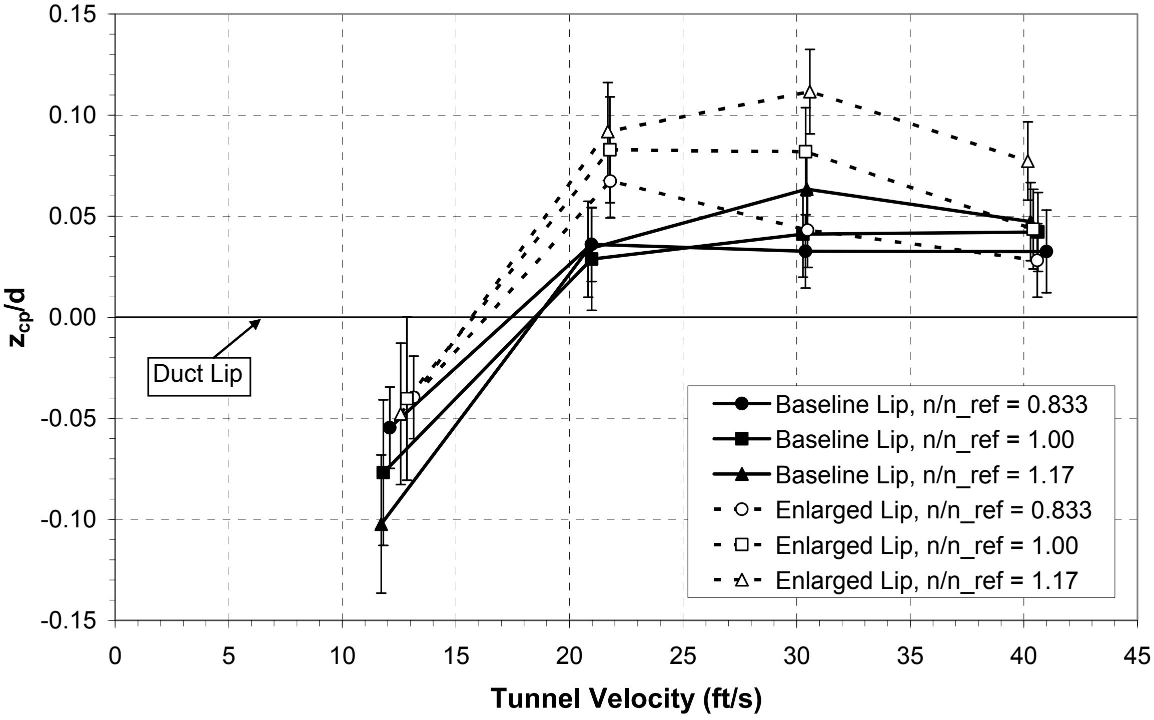

Figure B-10: Replica of Figure 4-17 (-15 degrees angle of attack) with error bars added.

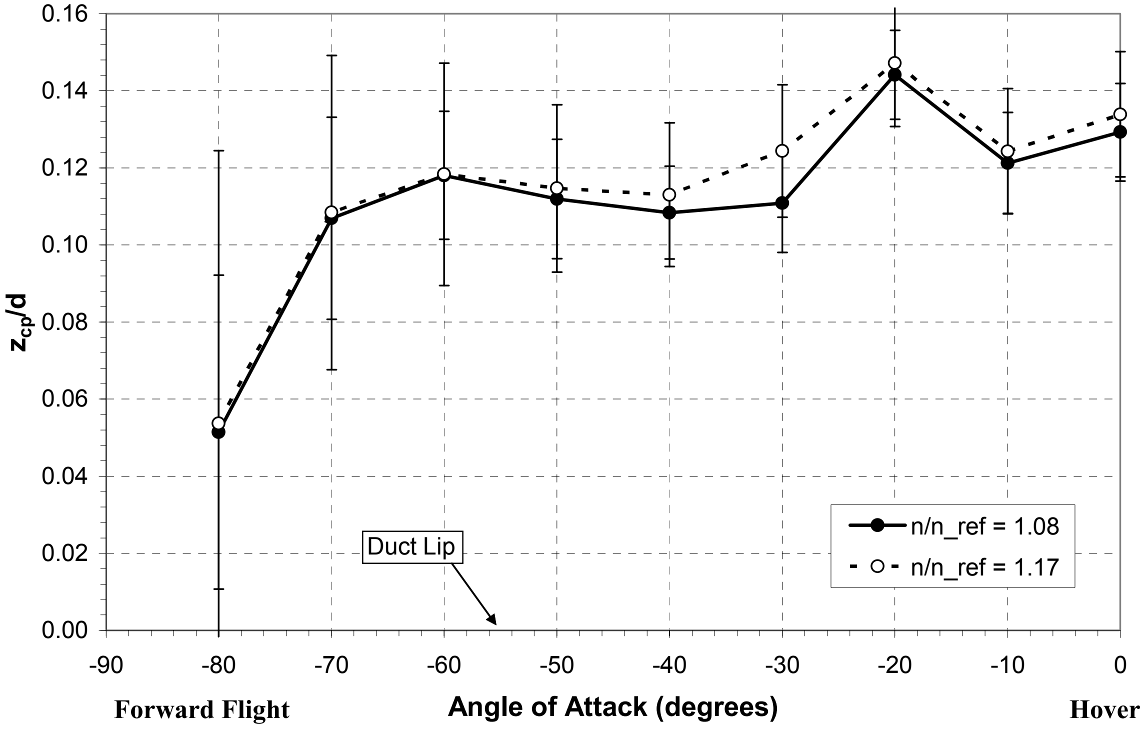

Figure B-11: Replica of Figure 4-18 (30 ft/s tunnel velocity) with error bars added.

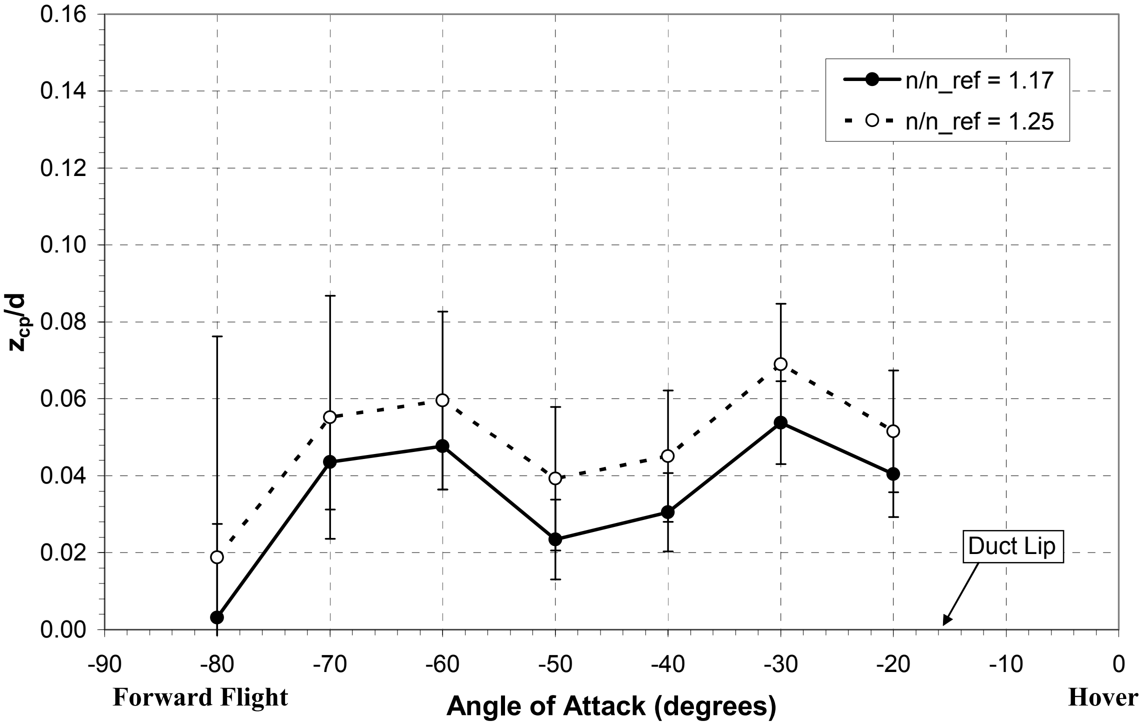

Figure B-12: Replica of Figure 4-19 (60 ft/s tunnel velocity) with error bars added.

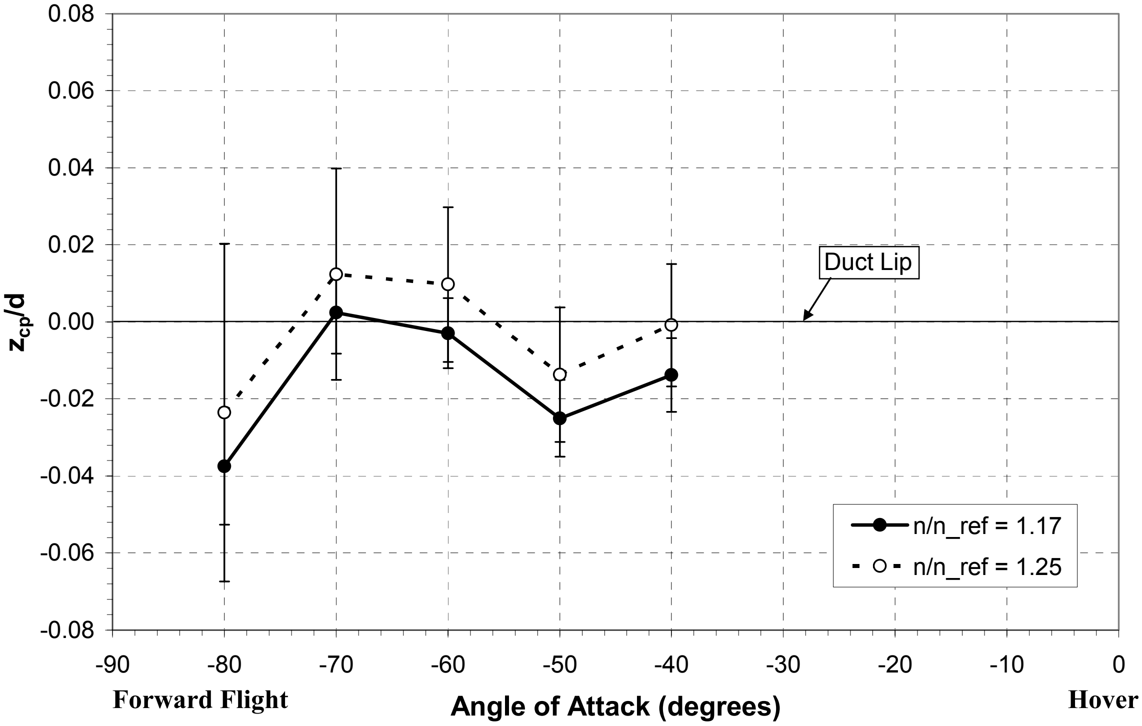

Figure B-13: Replica of Figure 4-20 (85 ft/s tunnel velocity) with error bars added.

The above equations can also be applied to the control vane data, resulting in an average uncertainty in static pitching moment of $M_y/T_{ref}d$ = ±0.003, too small to appear on the plots. However, the uncertainties for the wind tunnel control vane data is a little larger and can be shown on their respective plots, Figure B-14 through Figure B-16. Not only do the uncertainties increase with increase tunnel velocity, but they also increase as the angle of attack progresses towards 0 degrees. Additionally, the uncertainties in pitching moment are larger for the 20-degree deflection case compared to the -20-degree case because the vanes stall at approximately 20 degrees of deflection, whereas when deflected the other direction, they don't stall until around -25 degrees of deflection.

The uncertainty in the control effector data can also be calculated using the equations derived above for lift, drag, pitching moment, and center of pressure location. As is the case for most of the data presented thus far, the uncertainties in the lift and drag are too small to appear on the plots, so their average values are presented in numerical form as L/T_{ref} = 0.005 and D/T_{ref} = 0.017. The uncertainties in pitching moment and center of pressure location are presented in Figure B-17 and Figure B-18, respectively. Unlike some of the previous uncertainty data, these uncertainties remain relatively constant throughout the angle of attack range. Although only one

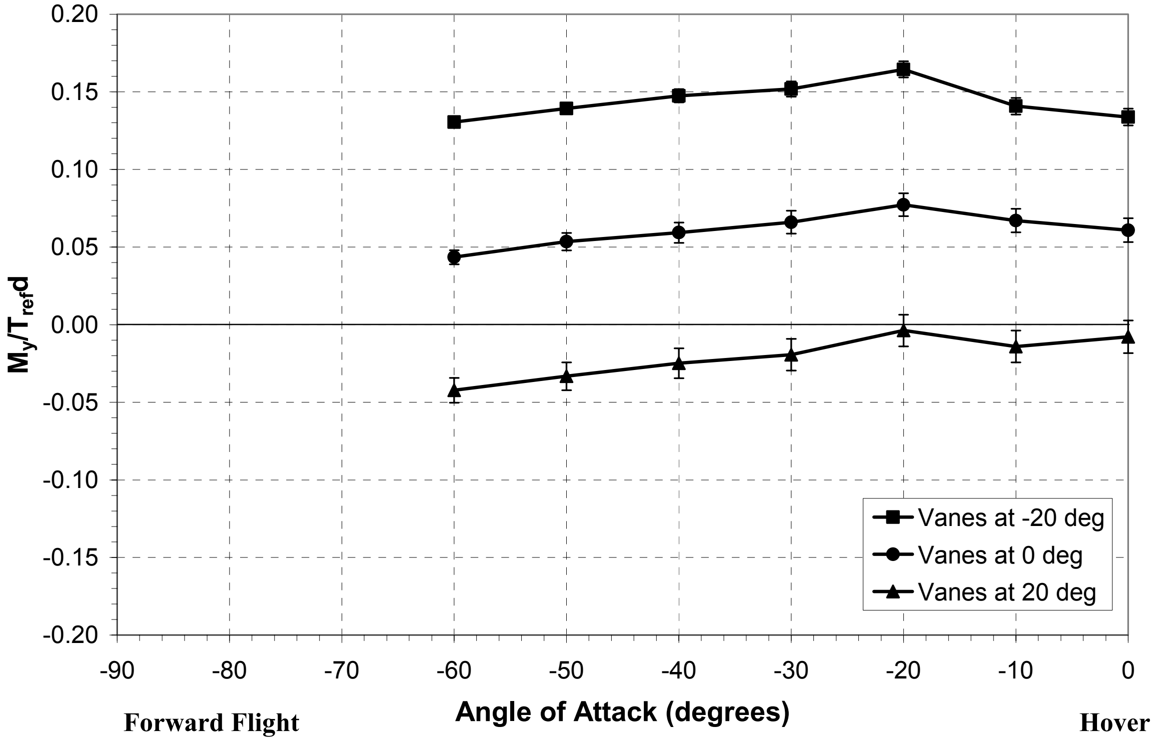

Figure B-14: Replica of Figure 4-25 (30 ft/s tunnel velocity) with error bars added.

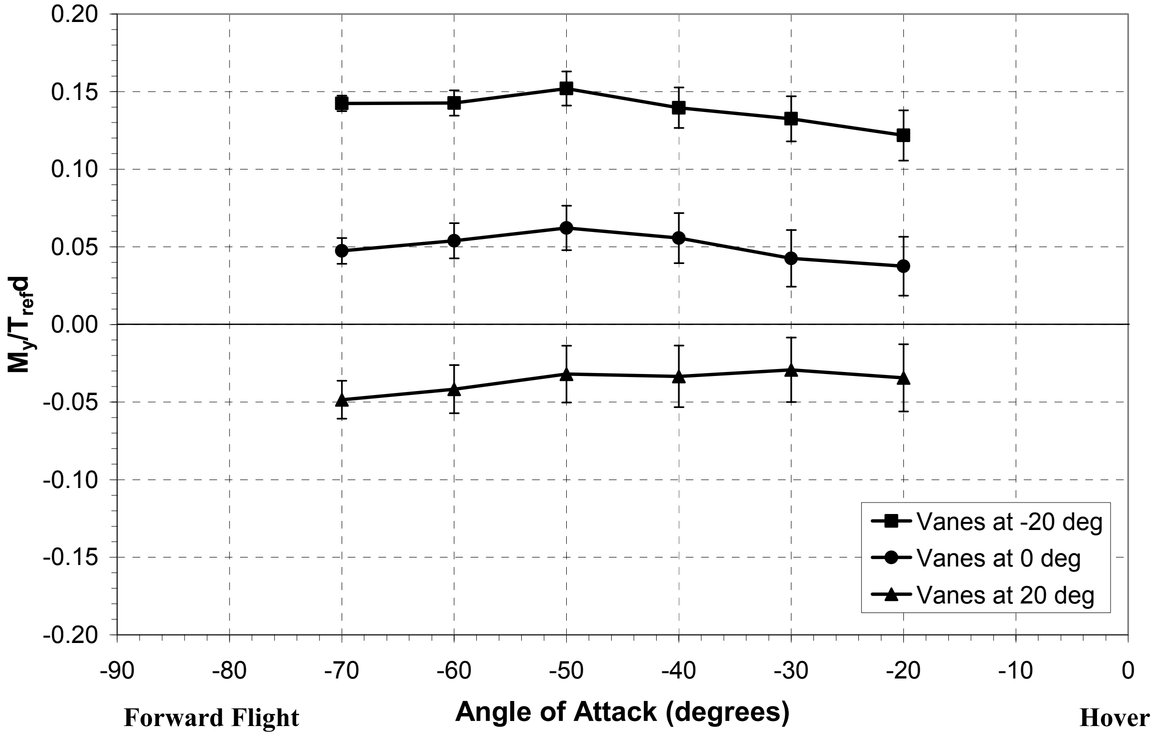

Figure B-15: Replica of Figure 4-26 (60 ft/s tunnel velocity) with error bars added.

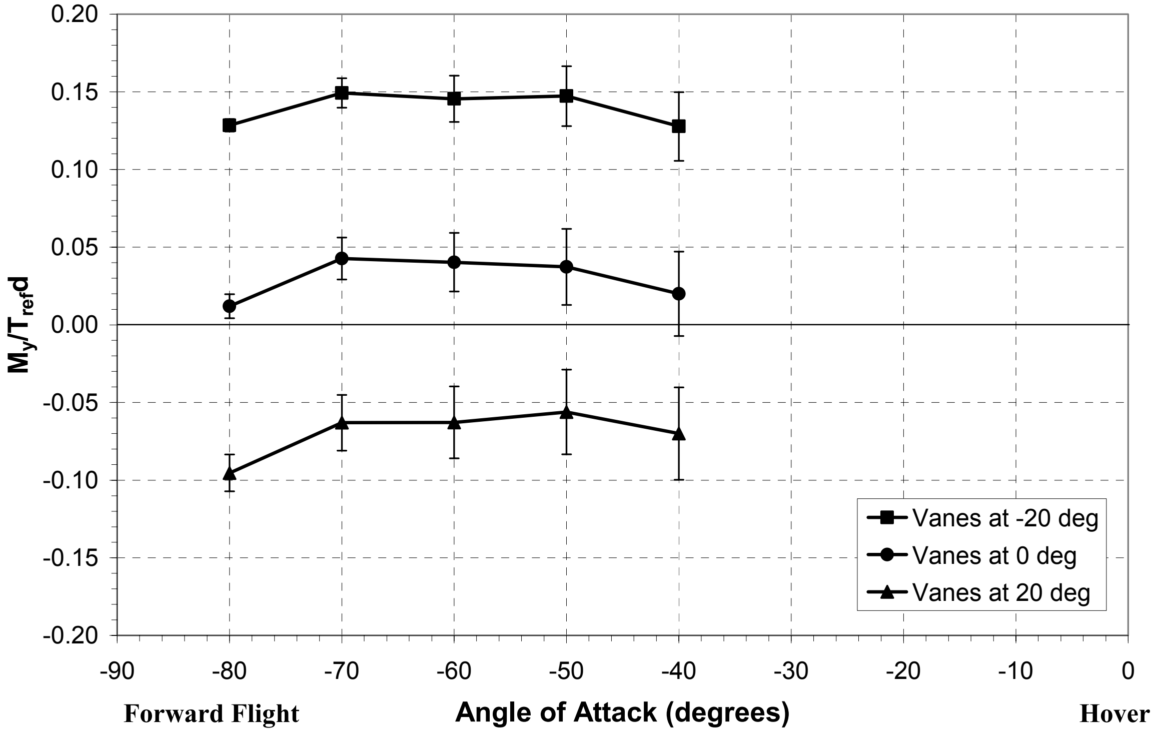

Figure B-16: Replica of Figure 4-27 (85 ft/s tunnel velocity) with error bars added.

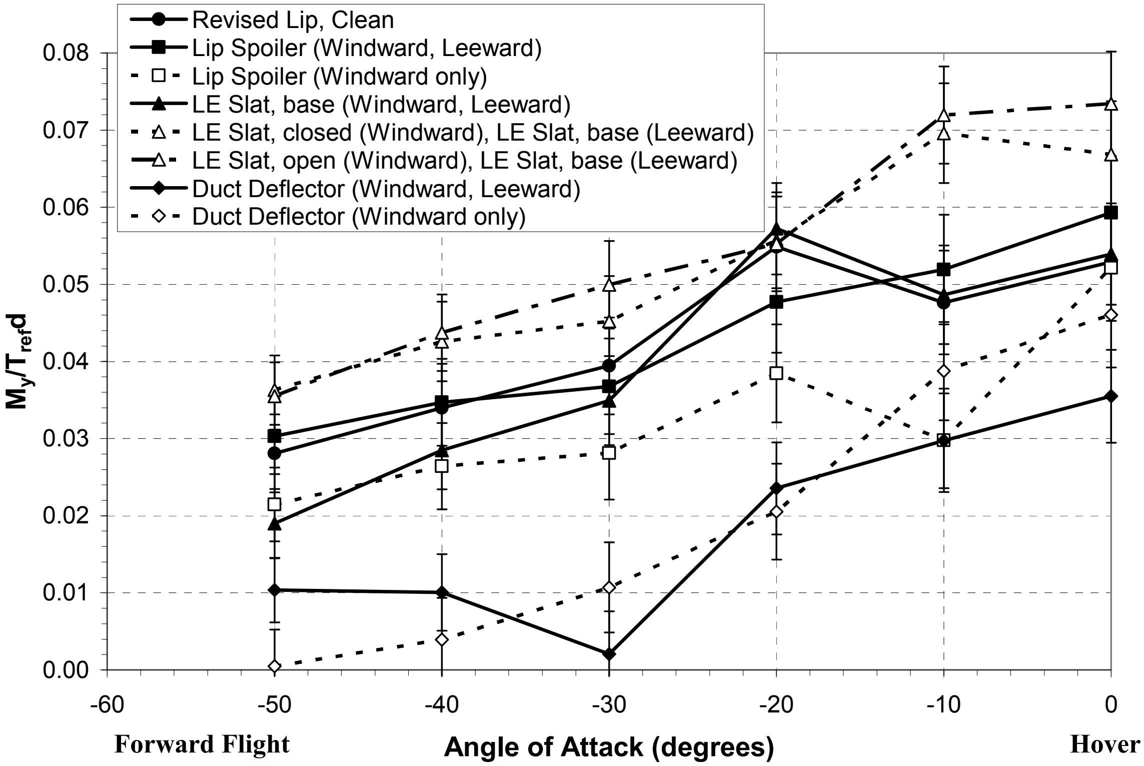

Figure B-17: Replica of Figure 4-32 (30 ft/s tunnel velocity) with error bars added.

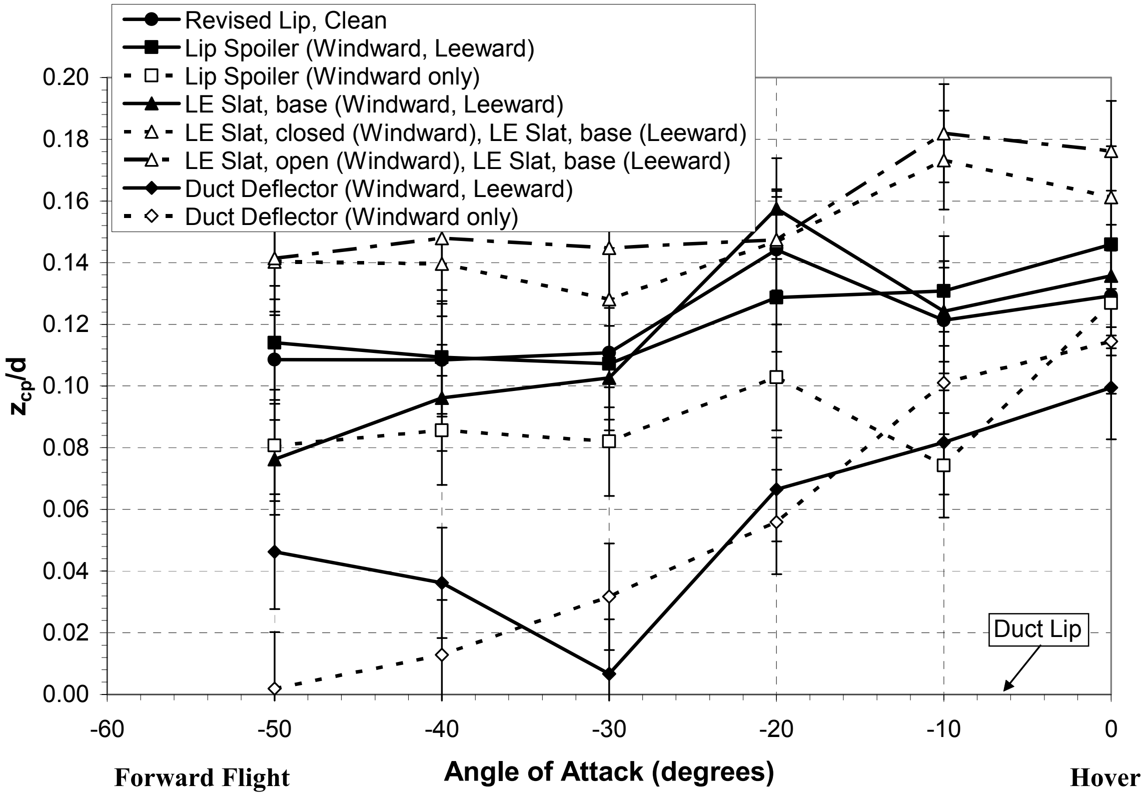

Figure B-18: Replica of Figure 4-34 (30 ft/s tunnel velocity) with error bars added.

tunnel velocity is presented, and the data may begin to show more change in uncertainty at higher tunnel velocities and angles of attack near -90 degrees.

The final set of data presented is that pertaining to the stabilizer vanes, and the pitching moment uncertainties can be seen in Figure B-19 through Figure B-21. Keep in mind that even though the uncertainties look small compared to previously shown pitching moment uncertainty data, the scale of the y-axes of the stabilizer vane data is much larger. Although not as noticeable for the 30-ft/s case, the uncertainties in the stabilizer vane data are slightly larger than those of the case without stabilizer vanes. Also, the uncertainties tend to become larger as the angle of attack progresses towards 0 degrees, where the stabilizer vanes become more effective. The uncertainties in the lift force average $L/T_{ref} = 0.008$ at 30 and 60 ft/s and $L/T_{ref} = 0.006$ at 85 ft/s tunnel velocity. Similarly, the uncertainties in the drag average $D/T_{ref} = 0.018$ at 30 ft/s, $D/T_{ref} = 0.019$ at 60 ft/s, and $D/T_{ref} = 0.017$ at 85 ft/s tunnel velocity.

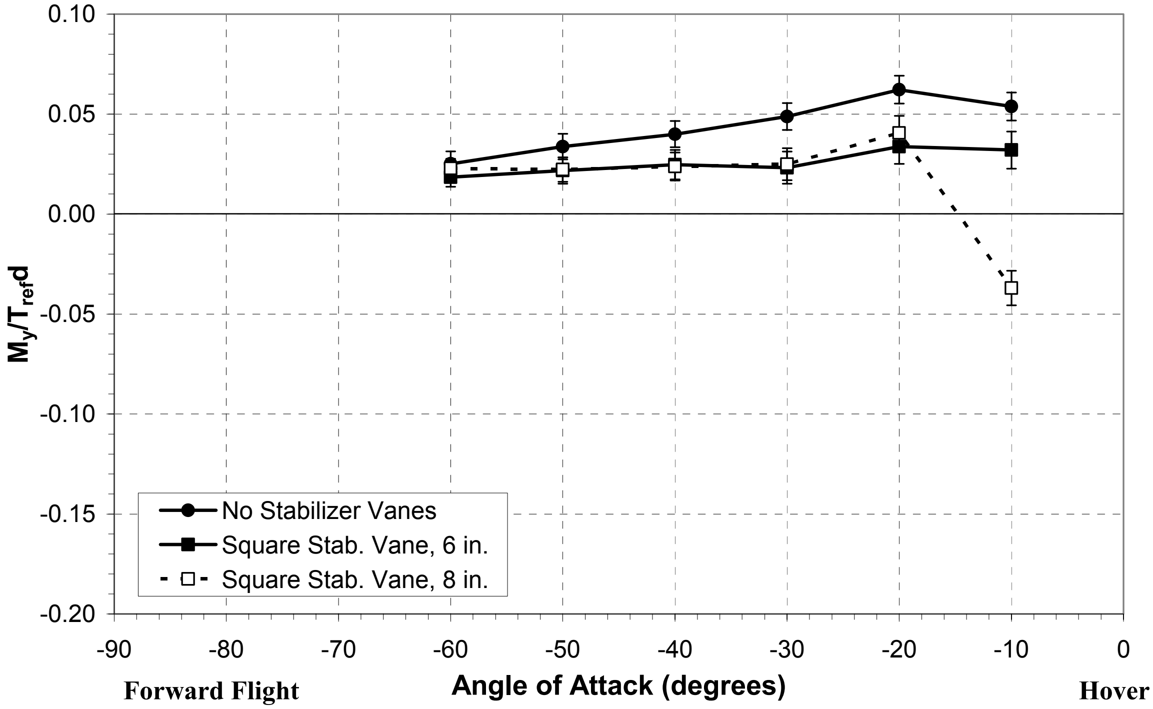

Figure B-19: Replica of Figure 4-37 (30 ft/s tunnel velocity) with error bars added.

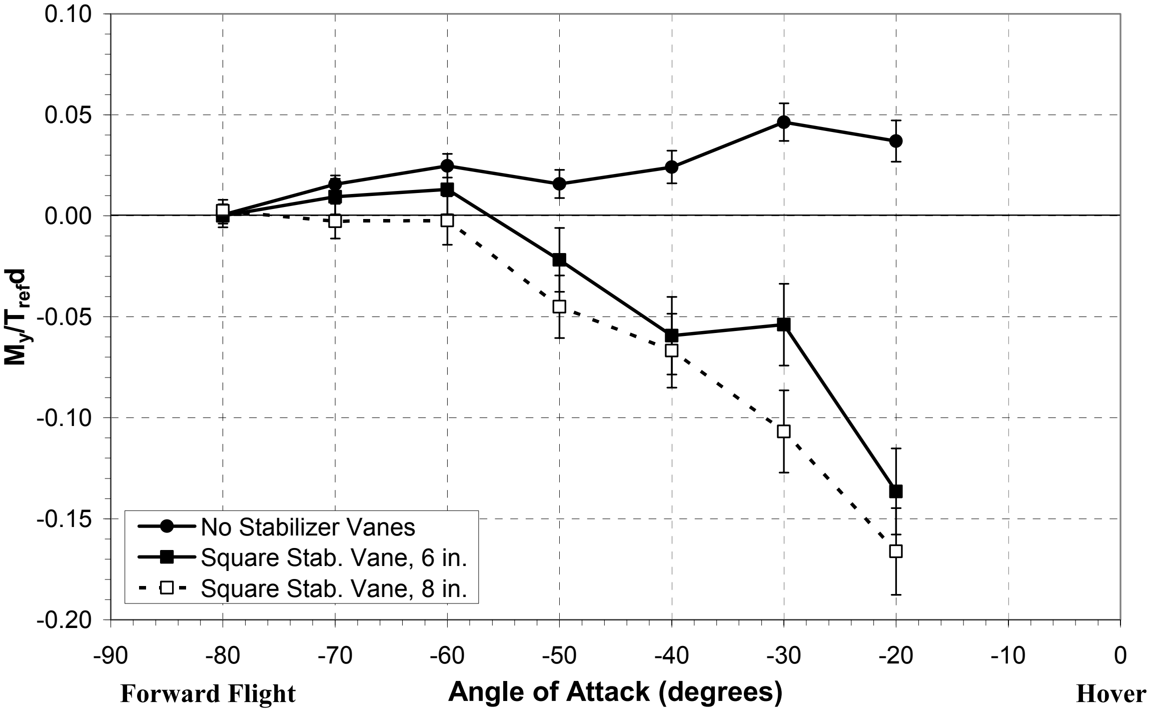

Figure B-20: Replica of Figure 4-38 (60 ft/s tunnel velocity) with error bars added.

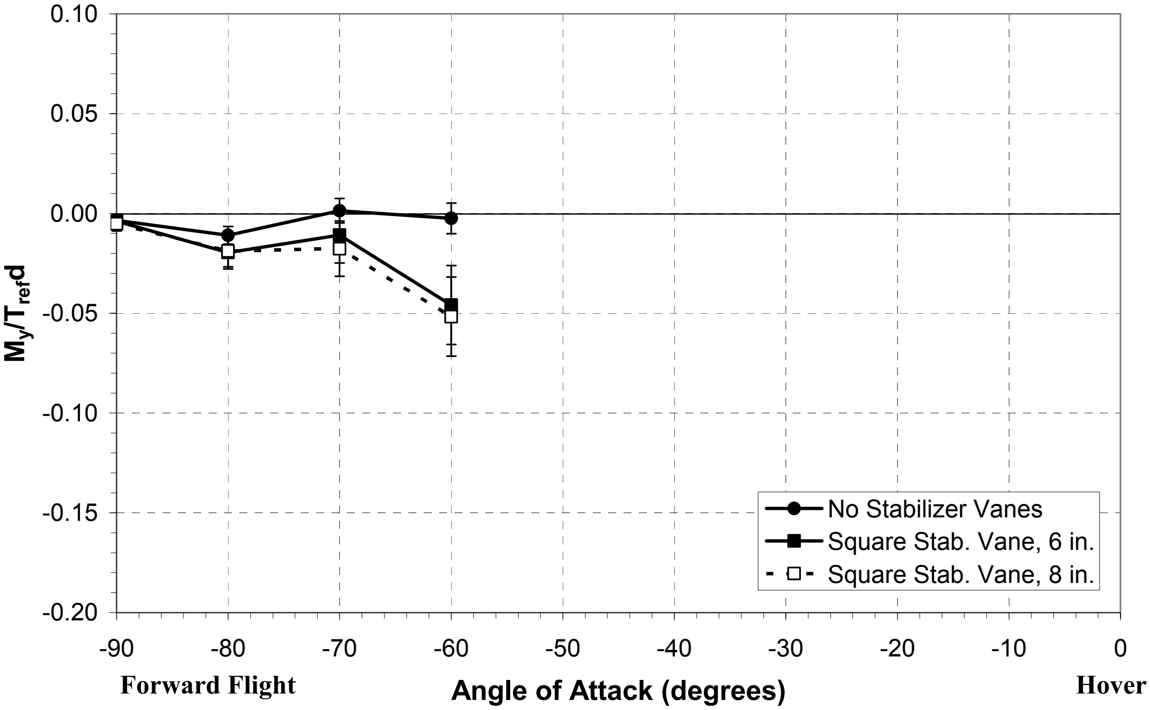

Figure B-21: Replica of Figure 4-39 (85 ft/s tunnel velocity) with error bars added.

Appendix C: Annotated Bibliography

This annotated bibliography is meant to give the reader a better understanding of the prior related research that others have completed. All papers and books described here have previously been listed in the References section and referenced in the body of this report. Topics vary from general research on ducted fans to more specific studies performed on duct lip shape effects.

de Piolenc, F. Marc, Wright, George E., Jr. *Ducted Fan Design*. Vol. 1. West Covina, CA: Mass Flow, 2001.

Primarily intended as a reference for hobbyists desiring to build a ducted fan propulsion system for their radio-controlled model aircraft, the general design features discussed in this book can be applied to a ducted fan VTOL UAV in order to improve efficiency. However, this book does not go into sufficient detail to design a ducted fan VTOL UAV for operation in all regimes. One particularly educational section in this book is the discussion on how ducted fans have been used on aircraft in the distant and recent past. This is where they discuss the Hiller Flying Platform, AROD, and Miller Aerobot among many other aircraft.

Sacks, Alvin H. "The Flying Platform as a Research Vehicle for Ducted Propellers." 26th Annual Meeting of the Institute of the Aeronautical Sciences, New York, January 1958.

As the title of the paper suggests, the author describes how the Hiller Flying Platform can be used as a tool to advance ducted fan research. In particular, he proposes further research into the adverse pitching moment generated when the vehicle is at an angle of attack. Additionally, the author provides theoretical equations for predicting the pitching moment coefficient from the lift coefficient. However, these equations were not put to use in the current research because the pitching moment was measured along with the lift. Finally, this paper briefly discusses the problem of wall interference when testing ducted fans at various angles of attack in the wind tunnel.

Arlowe, H. D. "Airborne Remote Operated Device." AUVS-88, The Fifteenth Annual Technical Symposium and Exhibition of the Association for Unmanned Vehicle Systems, San Diego, CA, June 1988.

This paper covers the design, construction, testing, and operator training for the AROD reconnaissance vehicle for the US Marine Corps. The vehicle was designed to be operated by a small group of soldiers without the need for a large communications van. The paper describes the vehicle, including the propulsion, method of control, and some of the problems the design team faced, such as communications, navigation, station keeping, and tipping over during landing.

White, John E., Phelan, John R. "Stability Augmentations and Control Decoupling for the Airborne Remotely Operated Device." AIAA 87-2453, AIAA Guidance, Navigation, and Control Conference, Monterey, CA, August 1987.

This paper also discusses the AROD UAV but primarily focuses on the control system for the vehicle. The control design issues discussed include design objectives, hardware considerations, dynamic coupling, and aerodynamics. Additionally, linear system dynamics, state space construction, gain determination, robustness and single value analysis, and system performance are discussed. It was determined that a control design based on a simplified linear dynamic model was sufficient to meet the project objectives, and the primary complication involved the gyroscopic coupling between the pitch and yaw axes.

U.S. Patent 4,795,111, January 3, 1989.

This patent describes the physical appearance of the Moller Aerobot in addition to discussing the methods of controlling the vehicle through control vanes and spoilers. Additionally, various missions for the vehicle are proposed ranging from military, such as surveillance and tank destruction, to commercial use, such as remote painting, routine inspection, and simple cleaning.

U.S. Patent 6,450,445, September 17, 2002.

Moller focuses on the control system for the Aerobot in this patent, especially a set of trough-shaped air deflection assemblies at the exit of the duct. The purpose of the troughs is to deflect some of the flow exiting the duct around the trailing edge and up the outside of the duct, thereby affecting the pitching and rolling moment characteristics. The troughs can be rotated to deflect more or less air depending on the flight conditions and what the control system calls for.

Graf, Will, Fleming, Jonathan, Ng, Wing, Gelhausen, Paul. "Ducted Fan Aerodynamics in Forward Flight." AHS International Specialists' Meeting on Unmanned Rotorcraft, Chandler, AZ, January 2005.

This paper was presented near the end of the current research and summarizes some of the results presented here. Additionally, it discusses some of the research performed in conjunction with Honeywell and AVID LLC, particularly the use of AVID OAV, an optimized design code for ducted fan vehicles to predict performance characteristics.

Kruger, W. "On Wind Tunnel Tests and Computations Concerning the Problem of Shrouded Propellers." NACA Technical Memorandum 1202, January 1944.

The effects of the shape of the propeller and the duct lip on the aerodynamic coefficients are examined by Kruger. It was determined that lip shape has a large influence on the aerodynamic characteristics of the vehicle. Particularly, efficiency can be improved by using duct profiles with small chord and thickness, but a small nose radius leads to unfavorable static thrust results. Stator vanes at the exit of the duct were also tested, and it was determined that they were necessary because of the high disk loading on the propeller. Finally, a nose split ring, a small flap extending horizontally outward from the duct lip, was tested to improve the static thrust of the vehicle. This is an excellent resource on ducted fan aerodynamics.

Grunwald, Kalman J., Goodson, Kenneth W. "Division of Aerodynamics Loads on a Semispan Tilting-Ducted-Propeller Model in Hovering and Transition Flight." NASA TN D-1257, NASA Langley, 1962.

This paper investigates the division of aerodynamic loads on a wing-tip-mounted ducted fan. The authors reiterate the fact that the duct provides protection from the spinning propeller and also allows for a reduction in the propeller diameter. It was determined through this research that most of the pitching moment loads were carried by the duct, whereas the propeller and wing contributed little to the pitching moment. Results were also presented showing the gradual stall of the duct lip as the angle of attack increased.

Weir, Robert J. "Aerodynamic Design Considerations for a Free-Flying Ducted Propeller." AIAA 88-4377-CP, AIAA Atmospheric Flight Mechanics Conference, Washington, D.C., 1988.

Another excellent resource on ducted fan aerodynamics, this paper examines the effects of various inlet designs, exit designs, and external appendages, as well as sizing and placement of control vanes. Weir describes in detail the inlet lip aerodynamics and the effects on flight characteristics, including the asymmetric lift in crosswinds and forward flight, flow separation in the inside of the duct lip, and the effects of lip radius on lift and pitching moment. Weir also illustrates the advantages of the ducted fan over an open propeller by discussing its improved safety and higher thrust to power ratio.

McCormick, Barnes W., Jr. *Aerodynamics of V/STOL Flight*. Mineola, New York: Dover Publications, 1999.

In this book, McCormick discusses many aspects of V/STOL flight, including propeller and helicopter aerodynamics, unpowered and powered flaps, wings and propellers at high angles of attack, ducted fans, boundary layer control, and ground effect, for various aircraft configurations. In particular, the ducted fan chapter explains how the duct maintains the loading on the propeller to the tips of the blades, thus increasing its efficiency. Also, the importance of duct shaping is discussed, as well as the adverse pitching moment generated when the duct is at an angle of attack.

Black, Donald M., Wainauski, Harry S., Rohrbach, Carl. "Shrouded Propellers – A Comprehensive Performance Study." AIAA 68-994, AIAA 5th Annual Meeting and Technical Display, Philadelphia, PA, October 1968.

This paper covers many aspects of ducted fan design, including lip shape, chord, exit area ratio, propeller location within the shroud, vanes, propeller blade shape, number of blades, and blade tip clearance. The results substantiate the performance potential of ducted fans in that higher values of thrust per horsepower were obtained for a same diameter propeller. Additionally, it was found that the most influential variable in static performance was the duct exit area ratio, where an increase in exit ratio increased static performance but decreased cruise performance. The authors suggest a variable geometry duct in order to optimize the vehicle for all flight regimes. Also, the research resulted in duct surface pressure distributions for a ducted fan in cruise (thrust vector pointing directly into the wind).

Abrego, Anita I., Bulaga, Robert W. "Performance Study of a Ducted Fan System." American Helicopter Society Aerodynamics, Acoustics, and Test and Evaluation Technical Specialists Meeting, San Francisco, CA, January 2002.

General ducted fan test results are presented in this paper, where several factors were examined, such as duct angle of attack, control vane deflection and chord length, duct chord length, and tip clearance. Flow separation was observed at various angles of attack, which affected the performance of the vehicle. Duct chord length was not found to significantly affect the thrust coefficient, and control vane deflection proved to be an effective method at creating a side force and thus improving vehicle control.

Friend, Carl F. "VTOL Flight – Performance, Stability and Control." ***VTOL Vehicles – Practice and Potential*****. Ed. Dr. C. Ming Wong. Vol. 3. North Hollywood, California: Western Periodicals Co., 1966.**

This is a collection of papers and notes that highlight the issues concerning VTOL aircraft and introduce various aircraft configurations utilizing VTOL propulsion methods.

One issue of particular concern was ground erosion and foreign object damage due to the lifting jets stirring up dust and debris during takeoff and landing. Visibility problems become an issue during takeoff and landing as well. Several solutions were given to avoid this issue, including jet suppression, engine cycle selection, site preparation and maintenance, and personnel shelters. Additionally, VTOL aircraft performance issues were discussed in comparison with conventional aircraft.

Fleming, Jonathan, Jones, Troy, Ng, Wing, Gelhausen, Paul, Enns, Dale. "Improving Control System Effectiveness for Ducted Fan VTOL UAVs Operating in Crosswinds." 2nd AIAA UAV Conference and Workshop & Exhibit, San Diego, CA, September 2003.

This is an excellent source of descriptions of ducted fan aerodynamics and insights into the current research pertaining to improving flight characteristics in crosswinds. The primary goal of the research was to counteract the adverse pitching moment without generating a force in the x-direction. This was accomplished through the use of deflector vanes in the interior of the duct and thrust reversers similar to the Moller Aerobot's troughs. Results showed slight improvements using these devices, and the authors mention additional devices were being tested.

Fleming, Jon. "Developing an Effective Control System for VTOL UAVs in Adverse Winds: An Investigation of Techniques for Improving Ducted Fan Aerodynamic Performance in Crosswinds." Phase I Final Report, Army Contract #DAAH10-03-C-0019, Army Report # USAAMCOM TR 03-D-12, June 2003.

This paper was the final report for the Phase I portion of the project funding the current research. The report gives detailed descriptions of ducted fan aerodynamics, testing procedures, and model attributes. The primary focus of the research was on control effectors to be used in addition to control vanes to improve vehicle control in crosswinds. The control effectors tested included a lip spoiler, lip flow control, lip leading edge extension, interior duct vane, interior duct deflector, trailing edge flap, and thrust reverser. Results showed that most effectors improved flight characteristics somewhat, but the interior duct vane worked the best in conjunction with the control vanes.

Fleming, Jon, Graf, Will. "Wind Tunnel Data Report – Army VTOL Phase II/Honeywell MAV Wind Tunnel Testing Data Release 2.00." Techsburg Internal Document, Blacksburg, VA, August 2004.

This Techsburg internal document summarizes the testing procedures, model description, and data reduction for an early set of testing pertaining to the current research and its associated project. Some preliminary static and wind tunnel results are presented for each type of test completed (thrust tests, pitch sweeps, yaw sweeps, control vane effectiveness studies, etc.). Additionally, equations were provided for conversion from the body-axis coordinate system to the wind-axis coordinate system, as well as equations for advance ratio, thrust coefficient, power coefficient, and figure of merit.

Parlett, Lysle P. "Experimental Investigation of Some of the Parameters Related to the Stability and Control of Aerial Vehicles Supported by Ducted Fans." NASA TN D-616, NASA Langley, November 1960.

Parlett examined the forward flight characteristics of two lip shapes of different leading edge radius and determined that the smaller lip radius produced a smaller pitching moment due to separated flow on the surface of the lip. Additionally, the smaller lip radius required greater power from the motor because of the stalled region of the lip. Various fan configurations were also tested, including 2-bladed, 3-bladed, and 4-bladed propellers

Martin, P. B., Boxwell, D. A. "Design, Analysis, and Experiments on a 10-inch Ducted Rotor VTOL UAV." AHS International Specialists' Meeting on Unmanned Rotorcraft, Chandler, AZ, January 2005.

This paper primarily presents the results of acoustic testing on a ducted fan VTOL UAV model. However, the analysis of tip gap and duct lip effects was performed, which resulted in the conclusion that the lip shape was the most important parameter in ducted fan design. In addition, thrust as a function of power was plotted for each lip shape reflecting the idea that a lip with a smaller leading edge radius requires more power

because of separated flow. Also, a new fan was designed using customized low Reynolds number airfoil sections.

Leishman, J. Gordon. *Principles of Helicopter Aerodynamics*. Cambridge: Cambridge University Press, 2000.

Leishman's book covers all aspects of helicopter aerodynamics, and, although there are major differences between the aerodynamics of ducted fans and open rotors, similarities do exist. Particularly, equations used to calculate disk loading, thrust and power coefficients, and figure of merit remain the same for both configurations. The book is also useful in learning more about general rotor aerodynamics, the knowledge of which can be applied to ducted fans in order to better understand their flow physics.

Martin, Preston, Tung, Chee. "Performance and Flowfield Measurements on a 10-inch Ducted Rotor VTOL UAV." AHS 2004-0264, American Helicopter Society 60th Annual Forum, Baltimore, MD, June 2004.

This paper analyzes a ducted fan VTOL UAV at various angles of attacks and wind speeds up to 120 ft/s. The model was tested with duct only, fan only, and with duct and fan. Fluorescent oil flow visualization on the interior and exterior of the duct provided information on flow separation. Both tip gap and lip shape were varied throughout the testing to determine the effects of each. Results showed that as the tip gap was increased, the thrust decreased significantly. Also, the duct with the smaller leading edge radius provided less thrust but improved the stability in a crosswind. Finally, the powered duct (duct and fan together) stalled at a higher angle of attack than the unpowered duct (duct only), and the powered duct achieved five times the maximum lift coefficient of the unpowered duct.

Mort, Kenneth W., Gamse, Berl. "A Wind-Tunnel Investigation of a 7-Foot-Diameter Ducted Propeller." NASA TN D-4142, NASA Langley, 1967.

Wind tunnel testing of a full-sized ducted fan is discussed in this paper. Power, wind speed, blade angle, and duct angle of attack were varied to define the aerodynamic characteristics. Pressure distributions on the duct surface determined stall boundaries at various angles of attack and power settings. It was found that the windward lip was more prone to stalling than the leeward lip, and stall was more likely to occur at high angles of attack and low fan speeds.

Mort, Kenneth W., Yaggy, Paul F. "Aerodynamic Characteristics of a 4-Foot-Diameter Ducted Fan Mounted on the Tip of a Semispan Wing." NASA TN D-1301, NASA Langley, 1962.

The research presented in this paper focused on the aerodynamics of a ducted fan on the tip of a wing. However, similar results were found in that stall on the windward lip caused a rapid change in the pitching moment and an increase in the power required. It was surmised that this adverse pitching moment would limit the descent rate of a vehicle with this configuration at low horizontal velocities. Additionally, results showed that a ducted fan powered vehicle would require less power if it were supported by a wing and ducted fans than if it were supported by only ducted fans.

Mort, Kenneth W. "Performance Characteristics of a 4-Foot-Diameter Ducted Fan at Zero Angle of Attack for Several Fan Blade Angles." NASA TN D-3122, NASA Langley, 1965.

The focus of this paper is on propulsive efficiency at various advance ratios. The advance ratio was varied by changing the fan speed and wind speed. Because the duct was designed for static conditions, it performed better at wind speeds below 100 knots. However, a different model, designed for higher speeds, was tested, and high speed performance improved. This further enforces the importance of duct shaping in ducted fan design.

Fletcher, Herman S. "Experimental Investigation of Lift, Drag, and Pitching Moment of Five Annular Airfoils." NACA TN 4117, Langley Field, VA, October 1957.

The testing of five annular airfoils is discussed in this paper. Although each had equal projected areas, they had varying chords and diameters, resulting in a range of aspect ratios. Results were compared to plane rectangular airfoils of similar aspect ratio. A tuft grid was utilized to examine the wake flow at various angles of attacks. Similar to wing-tip vortices of plane rectangular airfoils, two vortices developed at the trailing edge of the annular airfoils. Additionally it was found that the center of pressure location remained relatively constant through a large range of angles of attack.

Rabinowicz, Ernest. *An Introduction to Experimentation*. Reading, Massachusetts: Addison-Wesley Publishing Company, 1970.

This is an excellent source for uncertainty analysis and determining errors in calculations. It covers evaluations of experiments, errors of measurement, and evaluation of functional relationships. Statistical analyses involving normal and Poisson distributions are also included in conjunction with the uncertainty analysis equations. This book enhances understanding of experimentation error, thus improving the value of the results.

Vita

Will Edward Graf was born on August 11, 1981 in Del Rio, Texas. Until high school graduation he lived in Del Rio with his parents, David and Candy, older brother, Ben, and younger brother, Luke. After graduation in 1999, he attended Trinity University in San Antonio, Texas in the Engineering Science department. His senior design project consisted of designing and building a radio-controlled aircraft capable of lifting a heavy payload. Throughout his undergraduate career, he held several internships in multiple engineering fields. He spent one summer with Dominion Engineering in Del Rio, Texas as a construction contractor's assistant, two summers with the Texas Department of Transportation in Del Rio acting as an assistant to the highway inspectors, and two summers as an assistant to a manufacturing engineer with Columbia Industries in San Antonio, Texas. Upon graduation from Trinity University in 2003, Will was accepted to Virginia Tech's Aerospace Engineering graduate program in Blacksburg, Virginia, where he studied under Dr. William Mason and Dr. Wing Ng (Mechanical Engineering). While pursuing his M.S. degree, he worked for a local research company, Techsburg, Inc., on projects pertaining to ducted fan UAVs for the Army and Honeywell.